

**Modelling Impacts of Producer Turnover Time and
Elevated Atmospheric Carbon Dioxide on Food Chains**

by

Colleen M. Davies

A thesis submitted in partial fulfillment of the requirements for the degree of

Master of Science

in

Applied Mathematics

Department of Mathematical and Statistical Sciences
University of Alberta

© Colleen M. Davies, 2020

Abstract

Ecological stoichiometry is a framework that allows explicit consideration of nutrient restrictions on growth, and can be used to answer important ecological questions. First, we consider the impact of the turnover rate of producer biomass on ecosystems, since it is usually much faster in aquatic ecosystems than terrestrial. The WKL model uses ecological stoichiometry to describe the flow of phosphorus and carbon through a producer-grazer system, hence varying the model parameters allows for analysis of different ecosystems of this type. Here we explore the impacts of the intrinsic growth rate of the producer and the maximal ingestion rate of the grazer on these dynamics. Simulations show that for low intrinsic growth rate and maximal ingestion rate, the grazer goes extinct; for higher values, coexistence occurs in oscillations. Analyses show that the persistence of terrestrial grazers despite lower turnover times likely relies on additional factors, such as light intensity and grazer loss rate.

Second, we extend the WKL model to allow for consideration of the impacts of elevated atmospheric carbon dioxide concentration on producer-grazer dynamics. Three new models are developed, with varying amounts of system openness to carbon as well as consideration of different impacts of elevated atmospheric carbon dioxide concentration on photosynthesis. The most basic of these models is analysed further using primarily local bifurcation analysis. Overall, these analyses show that increased carbon sequestration and decreased stoichiometric quality of producers would require sufficient amounts of other factors necessary for photosynthesis.

Preface

Parts of Chapter 1 and Chapter 2 of this thesis were produced from an article that has published in the special ICMA-VII issue of the Journal of Biological Dynamics. The article was published with the title “Contrasting stoichiometric dynamics in terrestrial and aquatic grazer-producer systems”. I was responsible for the analysis as well as writing the article. My co-author and supervisor, Dr. Hao Wang, provided the main research question and some guidance on the analysis. He also contributed to edits of the article.

Acknowledgements

I would like to acknowledge the efforts of my supervisor, Dr. Hao Wang, who provided thought-provoking questions which I could address as well as guidance on how to best investigate these important issues. I would also like to thank our research group for all of their suggestions. In particular, I would like to thank Chris Heggerud for helping me with MatCont, and Dr. Jude Kong, who provided me with thoughtful suggestions for the third chapter of my thesis. I also very much appreciate the members of my committee taking time out of their busy lives to assist me in completing my degree.

Additionally, I would like to thank my officemates, who encouraged and supported me throughout the whole process of my degree. Also, I want to express my gratitude to my family and friends, without whom I certainly would not have been able to make it this far.

Table of Contents

1	Introduction	1
1.1	Ecological Stoichiometry	1
1.2	Mathematical Concepts	9
1.2.1	Sensitivity analysis	9
1.2.2	Bifurcation analysis	11
1.3	Outline	14
2	Contrasting terrestrial and aquatic ecosystems	16
2.1	Introduction	16
2.2	Model Formulation	18
2.3	Mathematical Analysis	21
2.3.1	Invariant set	21
2.3.2	Equilibria	22
2.3.3	Stability	27
2.4	Numerical Dynamics	35
2.4.1	Numerical simulations	35
2.4.2	Sensitivity analysis	39
2.4.3	One parameter bifurcation analysis	48

2.4.4	Two parameter bifurcation analysis	54
2.4.5	WKL vs. LKE model	57
2.5	Discussion	58
3	Incorporating atmospheric concentration of carbon dioxide	62
3.1	Introduction	62
3.2	Model Formulation	67
3.2.1	Local closed model	67
3.2.2	Local closed model with PCO	70
3.2.3	Local open model	72
3.2.4	Parameters	73
3.3	Local Closed: Mathematical Analysis	76
3.3.1	Invariant set	76
3.3.2	Equilibria	82
3.3.3	Stability	88
3.4	Numerical Dynamics	120
3.4.1	Numerical simulations comparing models	120
3.4.2	One parameter bifurcation analysis	129
3.4.3	Two parameter bifurcation analysis	143
3.5	Discussion	150
4	Discussion	158
4.1	Conclusions	158
4.2	Future Work	160
	Bibliography	161

Appendix A	167
Appendix B	176

List of Tables

2.1	Parameter values used for WKL model simulations	21
2.2	Bifurcation values for c from stability analysis	34
2.3	Low light sensitivity indices for steady state values	41
2.4	High light sensitivity indices for steady state values	42
2.5	Very high light sensitivity indices for steady state values	43
2.6	Intermediate light sensitivity indices for amplitude	44
2.7	Intermediate light sensitivity indices for period	45
2.8	Summary of normalized forward sensitivity indices	47
2.9	Summary of signs of sensitivity indices for steady states	47
2.10	Summary of signs of sensitivity indices for oscillations	48
3.1	Parameter values used for new model numerical simulations	74

List of Figures

2.1	Sample WKL model dynamics for various r values	37
2.2	Sample WKL model dynamics for various c values	38
2.3	WKL model classifications	40
2.4	r bifurcation diagrams: $K = 0.25$	49
2.5	c bifurcation diagrams: $K = 0.25$	50
2.6	r bifurcation diagrams: $K = 0.75$	51
2.7	c bifurcation diagrams: $K = 0.75$	52
2.8	r bifurcation diagrams: $K = 2.00$	53
2.9	c bifurcation diagrams: $K = 2.00$	53
2.10	Two parameter bifurcation diagrams varying K	56
3.1	Local closed model versus WKL model: very high light	122
3.2	Local closed model special case	126
3.3	Local closed model special case: limiting factors	127
3.4	Local open model special case	128
3.5	K bifurcation diagrams: $T_P = 0.003, T_C = 98.2, \gamma = 0.01023$.	130
3.6	K bifurcation diagrams: $T_P = 0.030, T_C = 98.2, \gamma = 0.0045$. .	132
3.7	K bifurcation diagrams: $T_P = 0.030, T_C = 98.2, \gamma = 0.01023$.	132

3.8	K bifurcation diagrams: $T_P = 0.030, T_C = 98.2, \gamma = 0.021$. . .	133
3.9	K bifurcation diagrams: $T_P = 0.030, T_C = 409.4, \gamma = 0.01023$		134
3.10	T_C bifurcation diagrams: $K = 1.00, T_P = 0.003, \gamma = 0.01023$. .	135
3.11	T_C bifurcation diagrams: $K = 0.25, T_P = 0.030, \gamma = 0.01023$. .	136
3.12	T_C bifurcation diagrams: $K = 1.00, T_P = 0.030, \gamma = 0.01023$. .	137
3.13	T_C bifurcation diagrams: $K = 2.00, T_P = 0.030, \gamma = 0.01023$. .	138
3.14	T_P bifurcation diagrams: $K = 0.25, T_C = 98.2, \gamma = 0.0045$. . .	140
3.15	T_P bifurcation diagrams: $K = 2.00, T_C = 98.2, \gamma = 0.021$. . .	141
3.16	T_P bifurcation diagrams: $K = 0.75, T_C = 409.4, \gamma = 0.021$. . .	142
3.17	Local closed bistable states	144
3.18	K & T_C bifurcation diagrams	145
3.19	K & T_P bifurcation diagrams	148
3.20	T_C & T_P bifurcation diagrams	151

Chapter 1

Introduction

1.1 Ecological Stoichiometry

Ecological stoichiometry is a framework that applies the law of conservation of mass to ecological interactions and studies the balance of the elements that make up life [44]. This approach quantifies relationships between organisms made up of several measurable elements. These elements can be neither created nor destroyed in ordinary chemical reactions, imposing a balance on the amounts in a closed biological system throughout its interactions and processes. Consideration of this balance in mathematical modelling of ecological systems allows for study of the flow of nutrients and energy in these systems.

There are many elements that are required for growth, reproduction, and survival of organisms. Three of the main elements in biological molecules are carbon, nitrogen, and phosphorus, despite their scarcity in the Earth's crust relative to other elements [44]. Carbon provides structure, and its compounds store energy, while nitrogen and phosphorus are crucial constituents of proteins

and nucleic acids [44]. However, due to different biomolecule requirements for structural, metabolic, and reproductive components, the stoichiometric ratios of organisms vary. In general, herbivores are assumed to have more rigid requirements, as well as higher nutrient requirements than the producers they consume. Many models assume that the grazers exhibit strict homeostasis, meaning that they maintain a fixed nutrient to carbon ratio by excreting excess carbon or nutrient ingested due to an elemental imbalance with their food [29, 53]. This nutrient imbalance means that grazers can be limited either by the quantity or quality of their food. This adds a degree of complexity to modelling grazing. There can also be elemental imbalance between a producer and its environment [44], and nutrient limitation in the producer can lead to nutrient limitation in the grazer [6].

A common application of ecological stoichiometry is in the study of producer-grazer systems. Initially, these were modelled using the Lotka-Volterra predator-prey equations [14]:

$$\begin{aligned}\frac{dx}{dt} &= bx - axy, \\ \frac{dy}{dt} &= cxy - dy,\end{aligned}$$

where x and y correspond to the prey and predator respectively, b is the net growth rate of the prey in the absence of predators, d is the net death rate of the predators in the absence of prey, and c/a is the conversion efficiency from prey to predator biomass ($a > c$) [14].

The Lotka-Volterra predator-prey equations have been widely used to model predator-prey and producer-grazer interactions, explaining examples such as

the changes in fishing during World War I that sparked Volterra's interest in the topic, as well as the cycles in lynx and snowshoe hare pelts traded in the 1840s by the Hudson Bay Company [14]. However, there are cases where considering all prey/producers to be identical at the elemental level fails to capture realistic dynamics.

For example, an experiment involving *Daphnia* and a green alga showed that at very high light intensity, the algal population boomed due to increased photosynthetic rate, but the grazer abundance remained low [16, 48]. While the light limited growth of the algae at low light levels and the resulting low grazer abundance can be explained by the Lotka-Volterra equations, the model cannot explain a case where high algal abundance does not result in a high grazer abundance. This is because in any non-stoichiometric form of the Lotka-Volterra equations, increased algal growth can only be beneficial to the grazer. However, as experimentally demonstrated, this is not always true – when there is too much growth of the algae, their more flexible nutrient requirements allow them to become phosphorus-poor, and therefore they can limit grazer growth due to being poor quality food relative to the requirement of the grazer [29].

One model developed using the framework of ecological stoichiometry to deal with this counterexample is the LKE model [29], which is a predator-prey model. In this case, the prey is a primary producer, such as a phytoplankton, and the predator is a zooplankton grazer, such as *Daphnia*. This model tracks only two elements, carbon (C) and phosphorus (P), where all others are assumed to be sufficiently abundant so as to be nonlimiting – that is, there is enough in the environment for the requirements of the organisms considered. Carbon is often included in ecological stoichiometry models, since it can be

used to represent energy or biomass. The producer population is quantified by the density of carbon in the producer, x , and the grazer population by the density of carbon in the grazer, y . In this case, phosphorus was chosen as a focal nutrient since it is often a limiting nutrient in freshwater systems, and it is used in construction of several biological molecules for structure and energy metabolism [29, 44].

The LKE model [29] is

$$\begin{aligned}\frac{dx}{dt} &= bx \left(1 - \frac{x}{\min(K, (P - \theta y)/q)} \right) - f(x)y, \\ \frac{dy}{dt} &= \hat{e} \min \left(1, \frac{(P - \theta y)/x}{\theta} \right) f(x)y - dy,\end{aligned}$$

where x and y are the producer and grazer carbon densities respectively, b is the intrinsic growth rate of the producer, d is the specific loss rate of the grazer (including respiration and death), K is the constant light-dependent carrying capacity of the producer, \hat{e} is the maximal conversation efficiency, $f(x)$ is the ingestion rate of the grazer, q is the minimum phosphorus to carbon ratio (P:C) in the producer, θ is the fixed P:C of the grazer, and P is the total phosphorus in the system [29].

Here Liebig's Law of the Minimum is applied. The Law of the Minimum states that organisms are limited by whatever resource is least available relative to their requirements [44]. We see that in the absence of the grazer, the producer exhibits logistic growth limited either by energy or by the availability of phosphorus [29]. If solar energy is in lower supply relative to the organism's needs, then we will see $K < (P - \theta y)/q$, and the growth rate of the producer (dx/dt) is determined by the light-dependent carrying capacity

K . Conversely, if the intracellular phosphorus of the producer ($P - \theta y$) is in lower supply relative to the producer population's minimal requirement (xq), then $(P - \theta y)/q < K$ and the growth rate of the producers is determined by the availability of phosphorus [29].

We observe that grazer carbon density undergoes exponential decay in the absence of the producer [29]. The growth of the grazer is limited either by food quantity or food quality. That is, by either the amount of producer carbon available or by the amount of producer phosphorus available relative to their needs. Here θ is the fixed P:C ratio grazers must maintain to survive [29]. This in particular allows for the model to exhibit such dynamics in the very high light case as those presented by Elser and Kuang (2002) [16], where abundant light energy caused the algae to become poor quality food for the grazer relative to their needs – $(P - \theta y)/x < \theta$, where $(P - \theta y)/x$ is the P:C ratio of the algae and θ is the homeostatic requirement of the grazer – and thus to limit the grazer abundance.

This model's applications are limited by one of its main assumptions, which states that “all phosphorus in the system is divided into two pools: phosphorus in the grazer and phosphorus in the producer” [29]. This requires immediate recycling of phosphorus and immediate utilization by the producer, and does not allow for any free phosphorus in the medium. The relaxation of this assumption yielded the WKL model [53], which is presented in Section 2.2 and is the basis for this work.

Despite the difficulty in analyzing the nonsmooth LKE model [29], some analysis has been completed. If f and g are assumed to be Holling type I functional responses, then the system has no limit cycles and the internal equi-

librium is globally asymptotically stable [28]. With Holling type II functional responses, bifurcation analysis of the parameter K revealed the potential for bistability and several bifurcations [28]. A global analysis of the LKE model with Holling type II functional responses was also completed, revealing four types of bistability as well as many possible bifurcations [58]. These analyses illuminate the rich and complicated dynamics this relatively simple stoichiometric model can exhibit.

There are several possible applications of ecological stoichiometry, many of which involve extensions of the LKE model [29]. These applications are primarily focussed on looking at the effects of food quality on population dynamics, since explicit consideration of non-carbon nutrients allows nutrient limitations to impact the model dynamics in realistic ways [22]. For example, there are models incorporating the stoichiometric knife edge, which is a theory that there is an ideal nutrient richness, supported by evidence that grazers are affected by both insufficient and excess food nutrient content [36, 37, 60]. There is also a model which considers phosphorus loading of the environment [3]. This topic is globally relevant because of anthropogenic nutrient loading due to agricultural fertilizers and industrial emissions [15, 22].

There is evidence that trophic level elemental imbalances can impact foraging and therefore impact population growth [35]. Ecological stoichiometry has been used to capture this influence through consideration of varied energetic costs of foraging dependent upon food nutrient content. Such models have been used to show that grazers can benefit from compensatory feeding behaviours when consuming non-optimal food [35, 46].

The impacts of seasonal changes in light level were also investigated using a

variant on the LKE model [2]. Seasonal fluctuations in light level were shown to lead to more complicated population dynamics. Whereas the basic LKE model allows for stable equilibria or limit cycles, seasonal forcing produces periodic and quasi-periodic solutions [2]. This analysis provides more insight into the complicated relationship between grazer growth and the nutrient quality of their food.

Additionally, an asexual clonal genotype model was developed following the WKL model, including rapid evolution in order to investigate the impacts of evolution of the grazer's P:C on dynamics [59]. This model together with a quantitative genetic model indicated rapid evolution can destabilize dynamics and prevent extinction of the grazer. The resulting changes in allocation and flux of nutrients in a system could have far reaching impacts in the environment [59].

Another extension of the WKL model to two grazer species was used to study the success of an invasive species of the zooplankton *Daphnia* [52]. Using a microcosm experiment as well as the extended model, the authors found that the invasive species, which was more prone to carbon limitation than nutrient, could be outcompeted by the native species in low light cases, where energy limitation was more likely than nutrient limitation [52]. Such insights allow for better management of invasive species.

An algae only stoichiometric model was used to more specifically clarify the impacts of light and nutrient availability on algal growth [27]. Severe nutrient limitation was found to always cause algal extinction, while sufficient nutrient and any nonzero light intensity allowed persistence of the algae. For this model, there were two possible globally attracting states: an internal equilibrium or

an equilibrium with algal C at its carrying capacity, which is on the boundary of a positively invariant open trapezoid domain [27].

Many developments in ecological stoichiometry focus on consumer homeostasis, mass balance, and trophic transfer efficiency [22]. Additionally, there are many studies on the growth rate hypothesis, which links growth rate, phosphorus content, and RNA content. More broadly, there has been research done on the stoichiometry of pelagic systems in addition to freshwater and estuarine, as well as the impacts of light and carbon dioxide on stoichiometry. All of these developments could be important for environment management given the current extensive anthropogenic impacts on global carbon, phosphorus, and nitrogen cycles [22].

However, despite its global applications, stoichiometry comes with many associated challenges. As with all models, one must balance the realisticness of the model with the ease of analysis. Stoichiometric systems are often nonsmooth, and require consideration of multiple cases due to applications of Liebig's Law of the Minimum [60]. Additionally, data on elemental composition in different species are relatively limited, as are efforts to compile these data [44]. In particular, element explicit data for terrestrial ecosystems are difficult to find, due to the fact that terrestrial experiments are often time-consuming, and determining elemental composition usually involves incinerating specimens.

Some analysis has already been completed for the WKL model [53]. The analysis is focussed around K , the resource carrying capacity determined by light. This particular parameter is controllable in a laboratory setting. However, there are other parameters that remain to be investigated. These pa-

rameters help uniquely define the conditions both within and surrounding the biological interactions we consider.

1.2 Mathematical Concepts

1.2.1 Sensitivity analysis

Here we apply the definition of sensitivity analysis established by Nestorov (1999) [33]; that is, the examination of model responses to either perturbations of the model's quantitative factors, such as parameters, or variations in the model's qualitative features. In particular, in Chapter 2, we investigate the impacts on the system's asymptotic state of perturbing parameters from some baseline values. Sensitivity analysis can provide insight into how robust model predictions are to small errors or uncertainties in parameter values [7].

There are two main categories of methods for sensitivity analysis: local and global [20]. The sensitivity analysis used in Chapter 2 applies a local method, since only one parameter is changed per index computed while other input factors (including the other parameters) are fixed at their baseline values. Comparatively, global methods vary all uncertain input factors simultaneously over the entire input space [20]. Global methods use variance- or sampling-based approaches and allow for study of interactions between inputs, which are likely important for biological systems [47]. Consider, for example, the relationships seen between birth and death rates of species, which tend to be positively correlated. However, despite their limitations, local sensitivity analysis methods are applied here due to their simplicity and the lack of im-

mediately applicable data to determine realistic parameter ranges, especially for terrestrial ecosystems. Local methods are also more directly interpreted.

Local sensitivity methods are limited by their baseline parameter set [20, 47]. Depending upon the system, parameters may vary considerably, and local sensitivity results are only applicable for some narrow subset of all possible parameter regimes. Given the general applicability of the WKL model which is used in Chapter 2, clearly there are natural cases to which our sensitivity results do not apply. However, even global methods require some degree of confidence in realistic parameter ranges, which are difficult to define for terrestrial systems.

In order to determine how impactful individual parameters are on the asymptotic state of our system for several different parameter regimes, sensitivity indices of target quantities to each parameter are computed. In particular, we find the normalized forward sensitivity index, which is the ratio of the relative change in the target value to the relative change in the parameter [7]. Here it is defined as

$$\Upsilon_{\rho}^u \equiv \frac{\partial u}{\partial \rho} \times \frac{\rho}{u},$$

where u is the target quantity and ρ is the parameter [7]. To estimate the partial derivative, a central difference approximation is used:

$$\frac{\partial u}{\partial \rho} = \frac{u(par + h) - u(par - h)}{2h} + O(h^2),$$

where par is the baseline value of the parameter. For the step size, h , 1% of

the baseline parameter value is used.

The absolute values of the indices are then compared between parameters for a specific baseline parameter regime. A larger magnitude of the sensitivity index is indicative of a stronger relative impact of the parameter on the target quantity and thus on the asymptotic state of the system [23]. Conversely, a smaller magnitude means the system is more robust to variation in that parameter. Here the target quantities include the equilibrium values of the variables, and the period and amplitude of oscillations, depending on which asymptotic state the system displays for a particular combination of parameters.

The sign of the indices corresponds to the direction of the relationship between the parameter and the target value. A positive sign means that an increase in the parameter value increases the target value, and a negative sign means an increase in the parameter decreases the target value [23]. Although the relationships between the key parameters and the equilibria values are mostly well known, we briefly discuss the signs since there are some inconsistencies between regimes with different light intensities.

1.2.2 Bifurcation analysis

Bifurcations are changes in the qualitative behaviour of the solutions of a set of equations that occur at certain parameter values, called bifurcation values [18]. For example, if a system with parameter μ tends towards an equilibrium for $\mu < \tilde{\mu}$, and it tends towards a different equilibrium for $\mu > \tilde{\mu}$, then a bifurcation has occurred for this system at bifurcation value $\mu = \tilde{\mu}$.

Consider a system of differential equations with parameter μ given by

$\dot{x} = f_\mu(x)$, $x \in \mathbb{R}^n$, $\mu \in \mathbb{R}^k$. Equilibria satisfy $f_\mu(x) = 0$. An equilibrium (x_0, μ_0) where $D_x f_\mu$ has at least one zero eigenvalue is a point of bifurcation [18]. A bifurcation value of μ is a value for which the flow of the system is not structurally stable [18, 19]. In general, it is theoretically possible to analytically determine these values; however, for models as nonsmooth as those analysed in this thesis, that can be incredibly difficult, if not impossible. Bifurcation softwares such as XPPAUTO and MatCont are commonly used for models like these.

There are many different types of bifurcations. Rigorous classification of a bifurcation point requires one to check several conditions on the differential equations at the bifurcation point. Bifurcations which require changing only one parameter are codimension 1 bifurcations; codimension 2 bifurcations require changing two parameters [17]. Examples of codimension 1 bifurcations include the saddle-node bifurcation, the transcritical bifurcation, the pitchfork bifurcation, and the Hopf bifurcation [18].

A saddle-node bifurcation occurs when equilibrium points are created or destroyed. Typically a saddle-node bifurcation at which two equilibria are created produces an unstable saddle and a stable node. This bifurcation is also called a fold bifurcation [19]. An example of a saddle-node bifurcation is the one that occurs at $\mu = 0$ for the differential equation $\dot{x} = \mu - x^2$ [18].

A transcritical bifurcation occurs when changing the parameter value causes an existing equilibrium to change its stability. For example, at $\mu = 0$ there is a transcritical bifurcation for $\dot{x} = \mu x - x^2$ [18].

A pitchfork bifurcation occurs when an equilibrium changes its stability and two new equilibria appears with the opposite stability [19]. There are two

types of pitchfork bifurcation [18]. At a supercritical pitchfork bifurcation, an equilibrium changes its stability from stable to unstable, and two new equilibria appear and are stable. At a subcritical pitchfork bifurcation, an equilibrium changes its stability from unstable to stable, and two new equilibria appear and are unstable [19]. An example of a supercritical pitchfork bifurcation occurs at $\mu = 0$ for $\dot{x} = \mu x - x^3$, and a subcritical pitchfork bifurcation occurs at $\mu = 0$ for $\dot{x} = \mu x + x^3$ [19].

A Hopf bifurcation occurs where an equilibrium changes its stability, and a limit cycle with opposite stability appears. For the following system, there is a Hopf bifurcation at $\mu = 0$ [18]:

$$\begin{aligned}\dot{x} &= -y + x(\mu - (x^2 + y^2)), \\ \dot{y} &= x + y(\mu - (x^2 + y^2)).\end{aligned}$$

There are five types of codimension 2 bifurcations: Bogdanov-Takens, Zero-Hopf, double-Hopf, cusp point, and Generalized Hopf point [17]. The first three are determined by the Jacobian. If it has a double-zero eigenvalue with geometric multiplicity one, the point is a Bogdanov-Takens bifurcation; if it has zero eigenvalue and a conjugate pair of pure imaginary eigenvalues, the point is a Zero-Hopf bifurcation; and if it has two conjugate pairs of pure imaginary eigenvalues, the point is a double-Hopf. A cusp point is found on a fold curve (a bifurcation curve in two-parameter space where a real eigenvalue crosses the imaginary axis) where $0 = p^T G_{xx}^0 q$, with G_x equal to the Jacobian of the system and with p, q the left and right singular vectors of G_x , normalized such that $\langle p, q \rangle = \langle q, q \rangle = 1$. A Generalized Hopf point occurs where the first

Lyapunov value vanishes on a Hopf curve. See [17] for more details.

All of the above pertains to the local bifurcation properties of the system. Theoretical classifications of local bifurcations require coordinate transformations into normal forms, which can be classified using the Taylor series at a point [18]. Global bifurcation analysis involve changes in global aspects of flows, including homoclinic orbits. These analyses cannot be reduced to studying the vector field of a neighborhood of an equilibrium or closed curve, unlike local bifurcation analysis. More information on global bifurcation analysis can be found in [18].

1.3 Outline

In Chapter 2, we will contrast terrestrial and aquatic ecosystems using the WKL model [53]. It is known that the average turnover rate of producer biomass in terrestrial ecosystems is much lower than in aquatic ecosystems [42]. Two parameters in the WKL model, the intrinsic growth rate of the producer (r) and the maximal ingestion rate of the grazer (c), are major factors in determining this turnover rate. Although some analysis has been completed for the WKL model, it is focussed on the producer's light-dependent carrying capacity, K . To our knowledge, no prior bifurcation analysis has been completed for r and c . In addition, we analyze the stability of the equilibria for Holling type II functional responses in the WKL model, where before Holling type I responses were assumed for stability analysis [53]. We find that for sufficiently low values of r and c , grazer extinction is always observed. This suggests terrestrial grazer populations should not persist. However, this

is likely because other parameters may differ between terrestrial and aquatic ecosystems, such as the constant grazer loss rate, \hat{d} , which has a strong impact on grazer persistence.

In Chapter 3, we will extend the WKL model by incorporating carbon limitation of producer growth, since carbon dioxide is required for photosynthesis and climate change models have predicted a drastic increase in atmospheric carbon dioxide concentration. Three models will be developed. The first, the local closed model, will incorporate carbon limitation of producer growth and consider the system as closed to carbon in addition to phosphorus, rather than completely open to carbon. The second model will build on the first by including the reduction in photorespiration rate due to competitive inhibition of oxygenation by carbon dioxide. The third model will allow for some level of transfer of carbon between the system and its exterior. All three models will be briefly compared. The local closed model will be analyzed more extensively, including exploration of an invariant set, separate stability analyses for Holling type I and type II functional responses, and both one- and two-parameter bifurcation analyses for the light-dependent carrying capacity (K), the total phosphorus in the system (T_P) and the total carbon in the system (T_C). A general trend is observed due to sequential limitation, with the nutrient in lowest supply determining whether the system approaches the grazer extinction equilibrium, a coexistence equilibrium, or a stable limit cycle. The models suggest that increased carbon sequestration and decreased stoichiometric quality of producers due to elevated atmospheric concentration of carbon dioxide would require sufficient light and nutrients, as expected given the application of Liebig's Law of the Minimum.

Chapter 2

Contrasting terrestrial and aquatic ecosystems

2.1 Introduction

Earth has many diverse habitats. One of the most fundamental dichotomies in the biosphere is between aquatic- and terrestrial-based ecosystems. These two groups vary greatly in average scale, both spatially and temporally. For example, consider the difference between an acacia tree, which grows at a rate of 44.2 cm per year [38] and feeds giraffes with an average individual ingestion rate of 16.6-19.0 kg per day [39], and a microscopic phytoplankton species which supports zooplankton grazers, both of which cannot be individually discerned by the naked human eye. These two systems also vary in time scale, particularly in the rate of turnover of the producer species at the base of these food chains. While a cyanobacteria bloom on the surface of a lake can appear in a matter of days or weeks, some trees take years to reach maturity. We

apply ecological stoichiometry to compare these seemingly opposite systems at the elemental level.

This chapter intends to compare the dynamics in a terrestrial ecosystem versus those in an aquatic ecosystem by specifically focussing on two parameters: r and c . The maximal growth rate of producers, r , tends to be higher in aquatic systems than in terrestrial [42]. Similarly, the maximum ingestion rate of grazer's, c , tends to be higher in aquatic producer-grazer systems than terrestrial. There is evidence that producer biomass can be consumed at a rate four times higher by aquatic grazers than terrestrial [42]. Comparison of the life cycle of an acacia tree to that of a phytoplankton clearly exemplifies this phenomenon. Investigating these parameters can allow us to rigorously compare such terrestrial and aquatic ecosystems, despite the extensive biological differences.

Another related contrast in parameter values lies in the tradeoff between r and c . Often, prey species must “choose” between investing energy into their growth, increasing r , or into their defences against predation, decreasing c [21, 52]. For example, undefended Caribbean coral reef sponges have been found to exhibit higher growth rates than those of defended species when predation is prevented by cages [26]. Therefore, we expect to naturally see systems with low r and low c , and systems with high r and high c . This is similar to the above contrast between terrestrial and aquatic ecosystems. Thus, the investigative efforts within this paper can also allow for comparison between organisms' survival and reproductive strategies.

2.2 Model Formulation

The WKL model tracks the amounts of carbon and phosphorus in the producer and the grazer [53]. Let x be the density of carbon in the producer and y be the density of carbon in the grazer, both measured in (mg C)/l. For phosphorus contents measured in (mg P)/l, we use p for the density of phosphorus in the producer and P for the density of free phosphorus in the medium. Hence, p/x is the phosphorus to carbon ratio (P:C) of the producer.

The resulting equations are [53]

$$\begin{aligned}
 \frac{dx}{dt} &= \underbrace{rx \left(1 - \frac{x}{\min\{K, p/q\}} \right)}_{\text{producer growth limited by nutrient \& light}} - \underbrace{f(x)y}_{\text{uptake by grazers}}, \\
 \frac{dy}{dt} &= \underbrace{\hat{e} \min \left\{ 1, \frac{p/x}{\theta} \right\} f(x)y}_{\text{grazer growth limited by food quality \& quantity}} - \underbrace{\hat{d}y}_{\text{grazer death and respiration loss}}, \\
 \frac{dp}{dt} &= \underbrace{g(P)x}_{\text{P uptake by producer}} - \underbrace{\frac{p}{x} f(x)y}_{\text{P loss due to grazing}} - \underbrace{dp}_{\text{P loss due to producer recycling}}, \\
 \frac{dP}{dt} &= \underbrace{-g(P)x}_{\text{P uptake by producer}} + \underbrace{dp}_{\text{P recycling from producer}} + \underbrace{\theta \hat{d}y}_{\text{P recycling from dead grazer}} \\
 &\quad + \underbrace{\left(\frac{p}{x} - \hat{e} \min \left\{ \theta, \frac{p}{x} \right\} \right) f(x)y}_{\text{P recycling from grazer feces}}.
 \end{aligned}$$

The model uses two major assumptions. The first is that “the total mass of phosphorus in the entire system is fixed” [53], i.e., the system is closed to phosphorus but open to carbon. The second is that the producer P:C varies, but never falls below a fixed minimum q ((mg P)/(mg C)); the grazer P:C is equal to a constant, denoted by θ ((mg P)/(mg C)), which is known as strict

homeostasis [44, 53]. Note that due to assumption 2, we do not directly track the phosphorus content in the grazers – the instantaneous phosphorus content in the grazer is simply θy .

From assumption 1, the total phosphorus T in the system is constant, i.e.,

$$\frac{dT}{dt} = 0$$

for $T = p + P + \theta y$. Thus, we can write $P = T - p - \theta y$, and we can reduce the system to three equations [53]:

$$\frac{dx}{dt} = rx \left(1 - \frac{x}{\min\{K, p/q\}} \right) - f(x)y, \quad (2.1)$$

$$\frac{dy}{dt} = \hat{e} \min \left\{ 1, \frac{p/x}{\theta} \right\} f(x)y - \hat{d}y, \quad (2.2)$$

$$\frac{dp}{dt} = g(T - p - \theta y)x - \frac{p}{x}f(x)y - dp. \quad (2.3)$$

The parameters are r , the producer intrinsic growth rate (day^{-1}); K , the producer light-dependent carrying capacity ($(\text{mg C})/l$); q , the minimal producer P:C ($(\text{mg P})/(\text{mg C})$); \hat{e} , the grazer maximal conversion rate; θ , the constant grazer P:C ($(\text{mg P})/(\text{mg C})$); \hat{d} , the grazer loss rate (day^{-1}); and d , the producer phosphorus loss rate (day^{-1}) [53]. Due to the second law of thermodynamics, $\hat{e} < 1$, and in reality, $\theta \gg q$ [53]. Therefore, we assume herein that $\theta > q$.

The model also uses two functions: $f(x)$, which is the rate at which the grazers ingest producer biomass, and $g(P)$, which is the per capita phosphorus

uptake rate of the producers [53]. If we assume $f(x)$ and $g(P)$ take the form of the Holling type II functional response, then we have

$$f(x) = \frac{cx}{a+x},$$

$$g(P) = \frac{\hat{c}P}{\hat{a}+P}.$$

In general, f and g are assumed to be bounded smooth functions that are zero at zero ($f(0) = 0$), strictly increasing ($f'(x) > 0$ for $x \geq 0$), and concave down ($f''(x) \leq 0$ for $x \geq 0$) [53]. For the Holling type II functional responses chosen here, let c be the maximal rate of ingestion of producer biomass by the grazers (day^{-1}); \hat{c} be the producer maximal phosphorus uptake rate ((mg P)/(mg C)/ day); a be the grazer carbon half-saturation constant ((mg C)/l); and \hat{a} be the producer phosphorus half-saturation constant((mg P)/l) [53].

For analyses, parameter values from Wang, Kuang, and Loladze (2008) [53] are used, as shown in Table 2.1. The baseline values used for r and c are 0.93 day^{-1} and 0.75 day^{-1} respectively. Therefore, we consider values ranging from 0.1 up to 2.00 for these two parameters, which includes a maximum value more than double the realistic parameters used previously. Within these analyses, all other parameters are assumed to be equal between terrestrial and aquatic ecosystems, which clearly limits the applicability of the results somewhat. The model was originally parametrized for a freshwater system. Hence, we consider the parameter values for r and c less than the specified baseline values representative of terrestrial ecosystems, and those greater than or equal to the baselines representative of aquatic ecosystems.

Table 2.1: The parameter (P) values (V) used for simulations [53].

P	Description	V
r	Producer intrinsic growth rate	0.1-2.0 day ⁻¹
K	Producer light-dependent carrying capacity	0.25-2 (mg C)/l
c	Grazer maximal ingestion rate	0.1-2.0 day ⁻¹
\hat{c}	Producer maximal phosphorus uptake rate	0.2 (mg P)/(mg C)/day
a	Grazer carbon half-saturation constant	0.25 (mg C)/l
\hat{a}	Producer phosphorus half-saturation constant	0.008 (mg P)/l
\hat{e}	Grazer maximal conversion rate	0.74
\hat{d}	Grazer loss rate (death and respiration)	0.22 day ⁻¹
d	Producer phosphorus loss rate	0.05 day ⁻¹
θ	Constant grazer P:C ratio	0.04 (mg P)/(mg C)
q	Minimal producer P:C ratio	0.004 (mg P)/(mg C)
T	Total system phosphorus	0.03 (mg P)/l

2.3 Mathematical Analysis

2.3.1 Invariant set

Wang et al. (2008) [53] presented the following theorem for positive invariance.

Theorem 1. *Solutions with initial conditions in the set*

$$\Omega = \{(x, y, p) : 0 < x < \min\{K, T/q\}, 0 < y, 0 < p, p + \theta y < T\}$$

remain there for all forward times.

This is proven by way of contradiction. The full proof was provided by Wang et al. (2008) [53], but in brief, one considers a solution $X(t)$ with initial condition in Ω , then assumes there is a time t_1 such that $X(t)$ touches or crosses the boundary of the closure of Ω for the first time. Then one considers cases for different segments of the boundary and reaches a contradiction in each case.

The invariant set is biologically meaningful. Densities of elements cannot be negative and therefore positivity is required. Also, growth of the producer is limited either by light (K) or by the maximum phosphorus availability relative to their needs (T/q). This is Liebig's Law of the Minimum – the resource which is least abundant relative to an organism's needs becomes limiting [44]. Hence, the bounds on x in Ω make sense. The bounds on phosphorus levels are also realistic: the phosphorus contained in the producers and grazers ($p + \theta y$) cannot exceed what is available in the system (T).

For the purposes of this chapter, this set should be kept in mind when considering stability. Equilibria outside of this set cannot be globally attracting, since no solution starting in this set will ever leave it. Also, for numerical simulations, once a solution enters this set, we know the general location of the solution for all forward times.

2.3.2 Equilibria

Wang et al. (2008) [53] found the equilibria for the model when f and g are Holling type I functions, then analyzed the stability of the boundary steady states. For this simplified case, there were two boundary equilibria: the ex-

tinction equilibrium $E_0 = (0, 0, 0)$, and the grazer extinction equilibrium E_1 where the form depends on if light or nutrients are limiting for the producer [53]. E_1 is given by

$$\begin{cases} \left(K, 0, \frac{TK}{K+d/\alpha} \right), & K < \frac{T}{q} - \frac{d}{\alpha}, \\ \left(\frac{T}{q} - \frac{d}{\alpha}, 0, q \left(\frac{T}{q} - \frac{d}{\alpha} \right) \right), & K > \frac{T}{q} - \frac{d}{\alpha}, \end{cases}$$

where $f(x) = \beta x$ and $g(P) = \alpha P$ [53].

As stated in Section 2.2, for the model, f and g are always assumed to be bounded smooth functions that are zero at zero, strictly increasing, and concave down. While the Holling type I functional responses used in Wang et al. (2008) [53] do satisfy this requirement, they are not realistic. Holling type I requires the assumption that there are no physical limits to the amount of food the grazer can consume. Clearly metabolic restrictions make this unrealistic. Thus, while Holling type I makes mathematical analysis more manageable, it limits applicability of the results.

For the numerical analyses, we assume that f and g are Holling type II functions. Hence, we find equilibria that will match our numerical analyses.

Then, any equilibrium $(\bar{x}, \bar{y}, \bar{p})$ satisfies

$$0 = \bar{x} \left(r \left(1 - \frac{\bar{x}}{\min\{K, \bar{p}/q\}} \right) - \frac{c\bar{y}}{a + \bar{x}} \right) \equiv \bar{x}F(\bar{x}, \bar{y}, \bar{p}), \quad (2.4)$$

$$0 = \bar{y} \left(\hat{e} \min \left\{ 1, \frac{\bar{p}/\bar{x}}{\theta} \right\} \frac{c\bar{x}}{a + \bar{x}} - \hat{d} \right) \equiv \bar{y}G(\bar{x}, \bar{y}, \bar{p}), \quad (2.5)$$

$$0 = \frac{\hat{c}(T - \bar{p} - \theta\bar{y})\bar{x}}{\hat{a} + (T - \bar{p} - \theta\bar{y})} - \frac{c\bar{p}\bar{y}}{a + \bar{x}} - d\bar{p} \equiv H(\bar{x}, \bar{y}, \bar{p}). \quad (2.6)$$

To find the equilibria, we split into cases based on the minimum functions included in $F(\bar{x}, \bar{y}, \bar{p})$ and $G(\bar{x}, \bar{y}, \bar{p})$, given by

1. $\bar{p} < Kq$ and $\bar{p} < \theta\bar{x}$: producer is nutrient limited and grazer is limited by food quality;
2. $\bar{p} < Kq$ and $\bar{p} > \theta\bar{x}$: producer is nutrient limited and grazer is limited by food quantity;
3. $\bar{p} > Kq$ and $\bar{p} < \theta\bar{x}$: producer is light limited and grazer is limited by food quality;
4. $\bar{p} > Kq$ and $\bar{p} > \theta\bar{x}$: producer is light limited and grazer is limited by food quantity.

All four cases have between one and three boundary equilibria: the extinction equilibrium $E_0 = (0, 0, 0)$, and the grazer extinction equilibrium/a E_1 . As with the Holling type I case, the form of E_1 depends on what resource is limiting for the producer, i.e., it is the same for Case 1 as Case 2, and the same for Case 3 as Case 4. When the producer is nutrient limited, E_1 is

$$\left(\frac{dq(\hat{a} + T) - \hat{c}T}{q(dq - \hat{c})}, 0, \frac{dq(\hat{a} + T) - \hat{c}T}{dq - \hat{c}} \right).$$

Note that for the above, $\bar{x} = \bar{p}/q$. Also, for the given baseline parameter values

for the WKL model, this equilibrium is non-negative and thus biologically feasible ($E_1 = (7.4980, 0, 0.0300)$). When the producer is light limited, E_1 actually has two possible values of \bar{p} , both of which are positive:

$$\left(K, 0, \frac{(\hat{a}d + dT + \hat{c}K) \pm \sqrt{(\hat{a}d + dT + \hat{c}K)^2 - 4\hat{c}dKT}}{2d} \right).$$

For Cases 1 and 3, we also have an additional mathematically possible boundary equilibrium if we assume quality is limiting:

$$\left(0, -\frac{ad}{c}, \frac{a\hat{d}\theta}{\hat{c}} \right).$$

However, this is not biologically feasible. All parameters are assumed to be positive and thus for this equilibrium $\bar{y} < 0$, which is not realistic since we cannot observe negative carbon densities. Also, this equilibrium would not satisfy the quality limitation condition if we multiply the terms within the minimum by $f(\bar{x})$, since $f(0) = 0 < ((c\bar{p})/(a\theta)) = \hat{d}/\hat{c}$.

For the parameter values used in the numerical simulations, $K < (T/q) = 7.50$ for all K in 0.25-2.00. Also, for $K < 7.5$, $Kq < \bar{p}$ for either form of the grazer extinction equilibrium. Thus for the range of K we consider and the values of T and q used, we will never have $Kq > \bar{p}$ and thus these equilibria will always fall in the producer light limited region of the phase space. Hence we are restricted to Cases 3 and 4 for the parameters given in Table 2.1. For the condition that distinguishes Case 3 from Case 4, we note that $\bar{x}\theta = K\theta$. Also, since \bar{p} does not depend on r or c , we can fix r and c at their baseline values and check the condition only varying K . Therefore, we only need to

check the sign of $\bar{p} - \theta\bar{x}$ for our various values of K , and for both of the grazer extinction equilibria (varying \bar{p}). For the version of \bar{p} that uses the plus sign, we observe that $\bar{p} - \theta\bar{x} > 0$ for all $K \in (0, 2]$. Hence this boundary equilibrium is always in Case 4. On the other hand, the equilibrium applying the negative sign has $\bar{p} - \theta\bar{x} > 0$ until a value of K between 0.74 and 0.75, when it becomes negative. Hence this equilibrium is in Case 4 until approximately $K = 0.75$, at which point it switches to Case 3. We also note that our grazer extinction equilibria will never be in the invariant set presented in Section 2.3.1, since the set does not include $y = 0$ or $x = K$.

Observe that in all cases, the forms of the biologically feasible boundary equilibria have no explicit dependence on either r or c . Given our assumption that all other parameters are the same between terrestrial and aquatic ecosystems, this means that the value of the boundary equilibria will not depend on whether the ecosystem is terrestrial or aquatic. However, the asymptotic state of the system will still depend on r and c , since they will determine which equilibria are stable.

Lastly, there may exist coexistence equilibria which satisfy

$$\begin{aligned} 0 &= r \left(1 - \frac{\bar{x}}{\min\{K, \bar{p}/q\}} \right) - \frac{c\bar{y}}{a + \bar{x}}, \\ 0 &= \hat{e} \min \left\{ 1, \frac{\bar{p}/\bar{x}}{\theta} \right\} \frac{c\bar{x}}{a + \bar{x}} - \hat{d}, \\ 0 &= \frac{\hat{c}(T - \bar{p} - \theta\bar{y})\bar{x}}{\hat{a} + (T - \bar{p} - \theta\bar{y})} - \frac{c\bar{p}\bar{y}}{a + \bar{x}} - d\bar{p}, \end{aligned}$$

i.e., $F(\bar{x}, \bar{y}, \bar{p}) = 0$, $G(\bar{x}, \bar{y}, \bar{p}) = 0$, and $H(\bar{x}, \bar{y}, \bar{p}) = 0$. Clearly there is likely to be an explicit dependence on r and c for coexistence equilibria, although

analytically determining the explicit dependence is incredibly time consuming and may be impossible due to extensive nonlinearity.

The results of this section are summarized in the following theorem.

Theorem 2. *Equations (2.1)-(2.3) with Holling type II functional responses yield the trivial extinction equilibrium $E_0 = (0, 0, 0)$, at most two grazer extinction equilibria E_1 , and may have coexistence equilibria, where the grazer extinction equilibria satisfy the following:*

(i) *If $\bar{p} < Kq$, then there is one grazer extinction equilibrium*

$$E_1 = \left(\frac{dq(\hat{a} + T) - \hat{c}T}{q(dq - \hat{c})}, 0, \frac{dq(\hat{a} + T) - \hat{c}T}{dq - \hat{c}} \right);$$

(ii) *If $\bar{p} > Kq$, then there are two grazer extinction equilibria*

$$E_1 = \left(K, 0, \frac{(\hat{a}d + dT + \hat{c}K) \pm \sqrt{(\hat{a}d + dT + \hat{c}K)^2 - 4\hat{c}dKT}}{2d} \right).$$

2.3.3 Stability

For the extinction equilibrium, Wang et al. (2008) [53] proved a stability theorem for the extinction steady state. Here we improve upon the theorem, using a very similar proof:

Theorem 3. *The extinction steady state $E_0 = (0, 0, 0)$ in Equations (2.1)-(2.3) is globally asymptotically stable if $d > \tilde{m}g(T)$, where $\tilde{m} = \min\{x(0)/p(0), [1 + d/r]/q\}$.*

Proof: Let $u = x/p$, then applying quotient rule as well as Equations (2.1) - (2.3)

$$\begin{aligned}
\frac{du}{dt} &= \frac{d}{dt} \frac{x}{p} \\
&= \frac{(dx/dt)p - x(dp/dt)}{p^2} \\
&= \frac{dx/dt}{p} - x \frac{dp/dt}{p^2} \\
&= \frac{1}{p} \left(rx \left(1 - \frac{x}{\min\{K, p/q\}} \right) - f(x)y \right) - \frac{x}{p^2} \left(g(T - p - \theta y)x - \frac{p}{x} f(x)y - dp \right) \\
&= \frac{rx}{p} \left(1 - \frac{x}{\min\{K, p/q\}} \right) - \frac{f(x)y}{p} - \frac{x^2}{p^2} g(T - p - \theta y) + \frac{f(x)y}{p} + \frac{dx}{p} \\
&= ru \left(1 - \frac{x}{\min\{K, p/q\}} \right) - \frac{f(x)y}{p} - u^2 g(T - p - \theta y) + \frac{f(x)y}{p} + du \\
&= ru \left(1 - \frac{x}{\min\{K, p/q\}} \right) - u^2 g(T - p - \theta y) + du.
\end{aligned}$$

Since $g(0) = 0$ and $g'(P) > 0$, $-u^2 g(T - p - \theta y) \leq 0$. We observe that

$$\min\{K, p/q\} \leq p/q \iff \frac{1}{p/q} \leq \frac{1}{\min\{K, p/q\}} \iff -\frac{1}{\min\{K, p/q\}} \leq -\frac{1}{p/q}.$$

Therefore, we can bound the first term in du/dt with $ru(1 - x/(p/q))$.

Thus

$$\frac{du}{dt} \leq ru \left(1 - \frac{x}{p/q} \right) + du = ru(1 - qu) + du.$$

Then,

$$\frac{du}{dt} \leq ru(1 + d/r - qu).$$

Therefore, $u \leq \min\{x(0)/p(0), [1 + d/r]/q\} \equiv \tilde{m}$. From Equation (2.3)

$$\begin{aligned}\frac{dp}{dt} &= g(T)x - \frac{p}{x}f(x)y - dp \\ &\leq g(T)x - dp \\ &\leq g(T)\tilde{m}p - dp \\ &= (g(T)\tilde{m} - d)p,\end{aligned}$$

since $u = x/p$, and $u \leq \tilde{m}$. Since we assume $d > \tilde{m}g(T)$, and this implies $g(T)\tilde{m} - d < 0$, then $p \rightarrow 0$ as $t \rightarrow \infty$.

Now, consider Equation (2.1)

$$\begin{aligned}\frac{dx}{dt} &= rx \left(1 - \frac{x}{\min\{K, p/q\}}\right) - f(x)y \\ &\leq rx \left(1 - \frac{x}{p/q}\right) = rx \left(1 - \frac{qx}{p}\right).\end{aligned}$$

Therefore, $\limsup_{t \rightarrow \infty} x(t) \leq p/q$. Since $p \rightarrow 0$ as $t \rightarrow \infty$, then this implies $x \rightarrow 0$ as $t \rightarrow \infty$. Then as $t \rightarrow \infty$ in Equation (2.2), the first term goes to 0 and thus $y \rightarrow 0$.

Thus, if $d > \tilde{m}g(T)$, then the extinction steady state is globally asymptotically stable.

The original theorem from Wang et al. (2008) [53] had $d > mg(T)$ with $m = \min\{x(0)/p(0), [1 + (d + f'(0)T/\theta)/r]/q\}$. Since we assume f is strictly increasing and all parameters are assumed to be positive, then $f'(0)T/\theta > 0$, and thus

$$[1 + (d + f'(0)T/\theta)/r]/q > [1 + d/r]/q.$$

Therefore, $m \geq \tilde{m}$, and hence there is a potentially larger range of values of d for which the extinction equilibrium is stable if we use \tilde{m} instead of m .

This theorem was proven for the general form of f and g , and thus applies for Holling type II functional responses. We observe the possible dependence on r and c . However, for the parameter regimes considered here, this condition requires $m = x(0)/p(0) < 0.3167$, which is highly unrealistic as it requires the initial P:C of the producer to exceed 3.1579. Still, this condition is not necessary, and we may observe stability of the extinction steady state within this parameter regime.

It remains to investigate the stability of the other boundary equilibria. The Jacobian matrix is

$$A = \begin{bmatrix} F + xF_x & xF_y & xF_p \\ yG_x & G + yG_y & yG_p \\ H_x & H_y & H_p \end{bmatrix}.$$

Let A_{kk} be the determinant of the matrix produced by removing row k and column k from matrix A . By the Routh-Hurwitz criterion, all eigenvalues of A have strictly negative real parts if the following conditions hold [53]: $\text{tr}A < 0$; $\det A < 0$; and $\det A - (\text{tr}A)(\sum_{k=1}^3 A_{kk}) > 0$.

We compute the Jacobian by finding the partial derivatives of F and G (as defined in equations (2.4)-(2.6)), as well as the appropriate sums for the Jacobian:

$$\begin{aligned}
\frac{\partial F}{\partial x} &= -\frac{r}{\min\{K, p/q\}} + \frac{cy}{(a+x)^2}, & F + xF_x &= \begin{cases} r - \frac{2rx}{K} - \frac{acy}{(a+x)^2}, & K < p/q, \\ r - \frac{2r qx}{p} - \frac{acy}{(a+x)^2}, & K > p/q, \end{cases} \\
\frac{\partial F}{\partial y} &= -\frac{c}{a+x}, & xF_y &= -\frac{cx}{a+x}, \\
\frac{\partial F}{\partial p} &= \begin{cases} 0, & K < p/q, \\ \frac{r qx}{p^2}, & K > p/q, \end{cases} & xF_p &= \begin{cases} 0, & K < p/q, \\ \frac{r qx^2}{p^2}, & K > p/q, \end{cases} \\
\frac{\partial G}{\partial x} &= \begin{cases} \frac{ac\hat{e}}{(a+x)^2}, & 1 < \frac{p/x}{\theta}, \\ -\frac{c\hat{e}p}{\theta(a+x)^2}, & 1 > \frac{p/x}{\theta}, \end{cases} & yG_x &= \begin{cases} \frac{ac\hat{e}y}{(a+x)^2}, & 1 < \frac{p/x}{\theta}, \\ -\frac{c\hat{e}py}{\theta(a+x)^2}, & 1 > \frac{p/x}{\theta}, \end{cases} \\
\frac{\partial G}{\partial y} &= 0, & G + yG_y &= \begin{cases} \frac{c\hat{e}x}{a+x} - \hat{d}, & 1 < \frac{p/x}{\theta}, \\ \frac{c\hat{e}p}{\theta(a+x)} - \hat{d}, & 1 > \frac{p/x}{\theta}, \end{cases} \\
\frac{\partial G}{\partial p} &= \begin{cases} 0, & 1 < \frac{p/x}{\theta}, \\ \frac{c\hat{e}}{\theta(a+x)}, & 1 > \frac{p/x}{\theta}, \end{cases} & yG_p &= \begin{cases} 0, & 1 < \frac{p/x}{\theta}, \\ \frac{c\hat{e}y}{\theta(a+x)}, & 1 > \frac{p/x}{\theta}. \end{cases}
\end{aligned}$$

Similarly, for H ,

$$\begin{aligned}
\frac{\partial H}{\partial x} &= \frac{\hat{c}(T-p-\theta y)}{\hat{a}+(T-p-\theta y)} + \frac{cpy}{(a+x)^2}, \\
\frac{\partial H}{\partial y} &= -\frac{\hat{a}\hat{c}\theta x}{(\hat{a}+T-p-\theta y)^2} - \frac{cp}{a+x}, \\
\frac{\partial H}{\partial p} &= -\frac{\hat{a}\hat{c}x}{(\hat{a}+T-p-\theta y)^2} - \frac{cy}{a+x} - d.
\end{aligned}$$

Therefore for the four cases described in Section 2.3.2, we have different Jacobian matrices for E_1 .

CASE 1: $\bar{p} < Kq$ and $\bar{p} < \theta\bar{x}$: $E_1 = (\bar{p}/q, 0, \bar{p})$,

$$A_1 = \begin{bmatrix} -r & -\frac{c\bar{p}}{aq + \bar{p}} & \frac{r}{q} \\ 0 & \frac{c\hat{e}\bar{p}q}{\theta(aq + \bar{p})} - \hat{d} & 0 \\ \frac{\hat{c}(T - \bar{p})}{\hat{a} + T - \bar{p}} & -\frac{\hat{a}\hat{c}\theta\bar{p}}{q(\hat{a} + T - \bar{p})^2} - \frac{c\bar{p}q}{aq + \bar{p}} & -\frac{\hat{a}\hat{c}\bar{p}}{q(\hat{a} + T - \bar{p})^2} - d \end{bmatrix}.$$

CASE 2: $\bar{p} < Kq$ and $\bar{p} > \theta\bar{x}$: $E_1 = (\bar{p}/q, 0, \bar{p})$,

$$A_2 = \begin{bmatrix} -r & -\frac{c\bar{p}}{aq + \bar{p}} & \frac{r}{q} \\ 0 & \frac{c\hat{e}\bar{p}}{aq + \bar{p}} - \hat{d} & 0 \\ \frac{\hat{c}(T - \bar{p})}{\hat{a} + T - \bar{p}} & -\frac{\hat{a}\hat{c}\theta\bar{p}}{q(\hat{a} + T - \bar{p})^2} - \frac{c\bar{p}q}{aq + \bar{p}} & -\frac{\hat{a}\hat{c}\bar{p}}{q(\hat{a} + T - \bar{p})^2} - d \end{bmatrix}.$$

CASE 3: $\bar{p} > Kq$ and $\bar{p} < \theta\bar{x}$: $E_1 = (K, 0, \bar{p})$,

$$A_3 = \begin{bmatrix} -r & -\frac{cK}{a + K} & 0 \\ 0 & \frac{c\hat{e}\bar{p}}{\theta(a + K)} - \hat{d} & 0 \\ \frac{\hat{c}(T - \bar{p})}{\hat{a} + T - \bar{p}} & -\frac{\hat{a}\hat{c}\theta K}{(\hat{a} + T - \bar{p})^2} - \frac{c\bar{p}}{a + K} & -\frac{\hat{a}\hat{c}K}{(\hat{a} + T - \bar{p})^2} - d \end{bmatrix}.$$

CASE 4: $\bar{p} > Kq$ and $\bar{p} > \theta\bar{x}$: $E_1 = (K, 0, \bar{p})$,

$$A_4 = \begin{bmatrix} -r & -\frac{cK}{a + K} & 0 \\ 0 & \frac{c\hat{e}K}{a + K} - \hat{d} & 0 \\ \frac{\hat{c}(T - \bar{p})}{\hat{a} + T - \bar{p}} & -\frac{\hat{a}\hat{c}\theta K}{(\hat{a} + T - \bar{p})^2} - \frac{c\bar{p}}{a + K} & -\frac{\hat{a}\hat{c}K}{(\hat{a} + T - \bar{p})^2} - d \end{bmatrix}.$$

To determine the stability of E_1 for Case i ($i \in \{1, 2\}$) we need to find the trace and determinant of A_i . However, this is not particularly illuminat-

ing mathematically – determining conditions such that A_1 and A_2 satisfy the Routh-Hurwitz criterion seems very complicated (see Appendix A). The eigenvalues are similarly non-illuminating, other than demonstrating that stability does not depend on K for Case 1, and it does not depend on K or θ for Case 2. However, for Cases 3 and 4, we can explicitly compute the determinant of $A - \lambda I$. For either case, a cofactor expansion along the third column yields the product of $A_i^{33} - \lambda$, and the determinant of a 2 x 2 upper triangular matrix. Thus, the eigenvalues of A_i are along the main diagonal for $i \in \{3, 4\}$. For both Case 3 and 4, we have two eigenvalues which are always negative:

$$\begin{aligned}\lambda_1 &= -r, \\ \lambda_2 &= -\frac{\hat{a}\hat{c}K}{(\hat{a} + T - \bar{p})^2} - d.\end{aligned}$$

Thus, stability of a grazer extinction equilibrium is determined by the sign of the eigenvalue A_i^{22} for $i \in \{3, 4\}$. Since all parameters are positive, then E_1 is a stable node for

$$\hat{d} > \frac{c\hat{e}\bar{p}}{\theta(a + K)}$$

for Case 3, and

$$\hat{d} > \frac{c\hat{e}K}{a + K}$$

for Case 4. When the inequalities are reversed, then E_1 is a saddle with a one-dimensional unstable manifold and a two-dimensional stable manifold.

We can find the value of c such that \hat{d} is equal to the right hand side in the above conditions. The values are in Table 2.2. We observe that the minimum condition for stability of our equilibria for this parameter regime involves a

low maximal ingestion rate, which suggests that terrestrial systems would be more likely to trend towards the grazer extinction equilibria based purely on r and c .

Table 2.2: The value of c for the appearance of a zero eigenvalue for Cases 3 and 4. Note that there are two possible values of \bar{p} for Case 3 and the bifurcation value depends on \bar{p} , thus there is a row for each of these equilibria.

Case	K=0.25	K=0.75	K=1.00	K=2.00
3+	0.0059	0.0040	0.0037	0.0033
3-	0.1998	0.3975	0.4965	0.8928
4	0.5946	0.3964	0.3716	0.3345

Recall that when the producer is light limited, there are two grazer extinction equilibria. To decide which, if either, is stable, we use the following theorem:

Theorem 4. *The grazer extinction equilibria $E_1 = (\bar{x}, 0, \bar{p})$ for (2.1)-(2.3) satisfy the following when $\bar{p} > Kq$.*

(i) *If $\bar{p} < \theta\bar{x}$, a grazer extinction equilibrium has a bifurcation at*

$$\hat{d} = \frac{c\hat{e}\bar{p}}{\theta(a + K)}.$$

The equilibrium is a stable node for \hat{d} greater than this bifurcation value, and a saddle for \hat{d} less than this bifurcation value.

(ii) *If $\bar{p} > \theta\bar{x}$, a grazer extinction equilibrium has a bifurcation at*

$$\hat{d} = \frac{c\hat{e}K}{a + K}.$$

The equilibrium is a stable node for \hat{d} greater than this bifurcation value, and

a saddle for \hat{d} less than this bifurcation value.

2.4 Numerical Dynamics

2.4.1 Numerical simulations

Using MATLAB, the system was simulated using the parameter values in Table 2.1. Since the model is nonsmooth, ode45 was not reliable for certain combinations of parameters. A singularity produced negative densities, thus ode23s was used instead since it is a stiff solver. The initial condition was always held at $(x_0, y_0, p_0) = (0.3, 0.3, 0.01)$, which is not in the invariant set from Section 2.3.1 but is at least biologically feasible and orbits starting here can still enter the set in time. This initial condition was selected since it was the one used in the paper where the model was presented.

First the simulations were run for t ranging from 0 to 50 days, varying one of the two focal parameters at a time. For each $K \in \{0.25, 0.75, 1.00, 2.00\}$, the system was numerically simulated for $r \in \{0.1, 0.2, \dots, 2.0\}$, with c held constant at the baseline value 0.75. Then the process was repeated with r held constant at 0.93 and $c \in \{0.1, 0.2, \dots, 2.0\}$. The lower values of r and c were used to represent the slower average turnover rate of terrestrial systems, and the higher parts of the ranges were used for the faster average turnover rate of aquatic systems.

For the intrinsic growth rate of the producer (r), we see that as r increases with K held at the following level:

- $K=0.25$: grazers benefit; producers harmed until they plateau; coexis-

tence at a steady state.

- $K=0.75, 1.00$: oscillations appear and then replaced by coexistence at a steady state.
- $K=2.00$: grazers benefit; producers harmed until a point where grazers go extinct.

For the maximal ingestion rate of the grazer (c), we see that as c increases with K held at the following level:

- $K=0.25, 0.75, 1.00$: grazers benefit and producers harmed until oscillations appear.
- $K=2.00$: grazers benefit until the carbon density curves intersect and the system trends toward oscillations.

Figures 2.1 and 2.2 show the shifts in dynamics described above.

Then the simulations were run for t in 0 to 200, varying both of the focal parameters. The time limit was extended since there appeared to be some dynamics that had not completely ‘settled’ by $t = 50$. The values of the focal parameters were selected based on the previous simulations to align with where shifts in dynamics occurred. Thus the simulations were run for all possible combinations of $K \in \{0.25, 0.75, 1.00, 2.00\}$, $r \in \{0.1, 0.5, 1.0, 1.5, 2.0\}$, and $c \in \{0.1, 0.5, 1.0, 1.5, 2.0\}$, again using `ode23s` in MATLAB. The behaviour at $t = 200$ was then classified according to the possible dynamics seen in prior papers [29, 53]. The dynamics were classified as either grazer extinction; coexistence at a nonzero steady state; coexistence with oscillations; or coexistence with oscillations with decreasing amplitude, leading to coexistence at a steady state. Examples of the above dynamics are shown in Figure 2.3. These observed dynamics were then used to develop classifications for two parameter

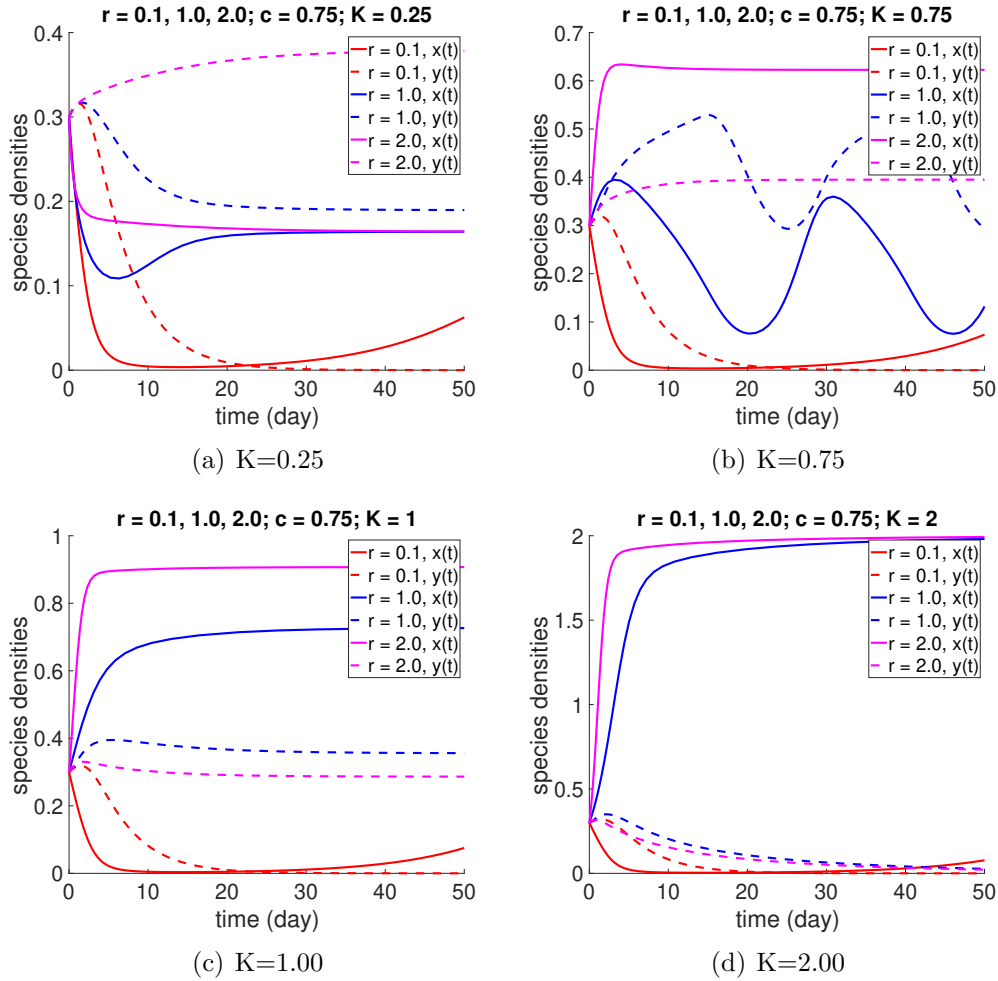


Figure 2.1: Sample dynamics for various r values, $r = 0.1, 1.0, 2.0$, for $K = 0.25, 0.75, 1.00, 2.00$ and baseline c (as well as all other parameters). For low to intermediate light, we observe that increasing r in general increases the carbon densities for both producers and grazers. In the high and very high light cases, increasing r to 2.0 is detrimental to the grazer, likely due to nutrient limitation of grazer growth.

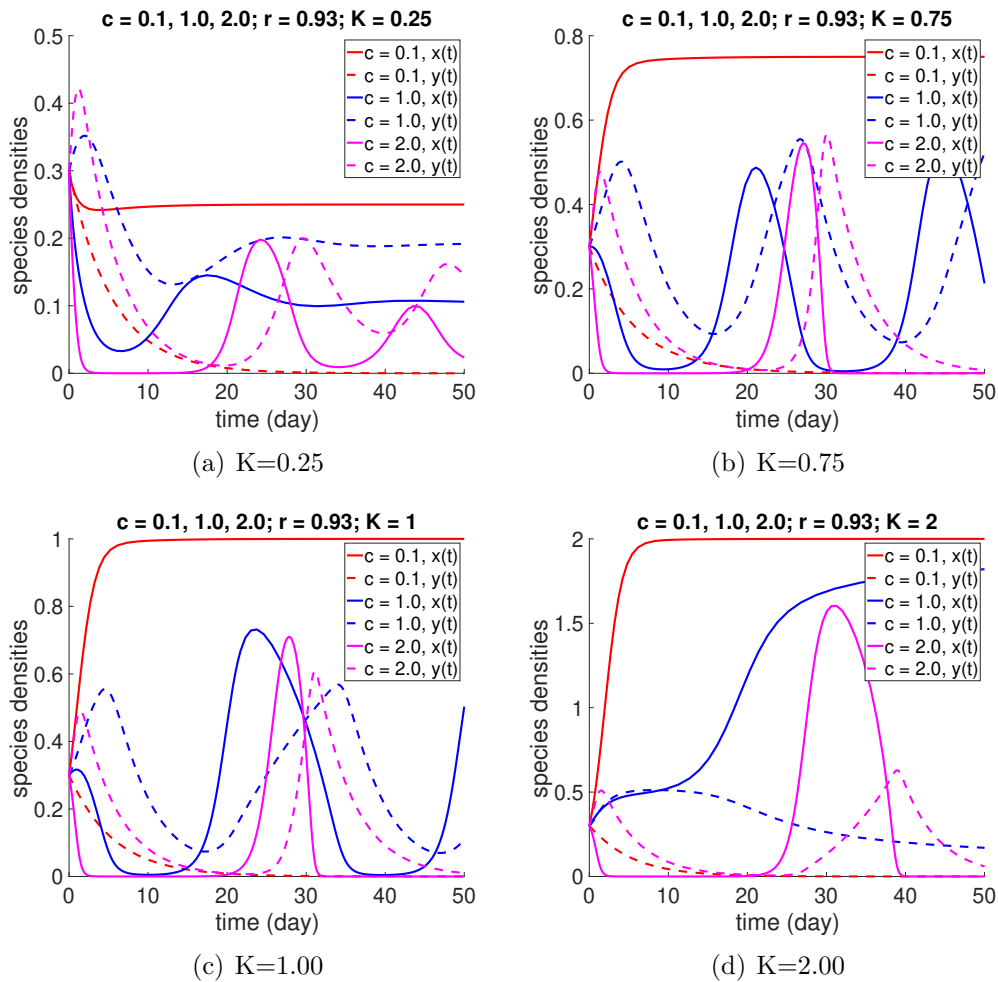


Figure 2.2: Sample dynamics for various c values, $c = 0.1, 1.0, 2.0$, for $K = 0.25, 0.75, 1.00, 2.00$ and baseline r (as well as all other parameters). In general, increasing c is detrimental to the producer population, and beneficial for the grazer in all cases except low light.

bifurcation diagrams and expectations for what dynamics may be produced.

2.4.2 Sensitivity analysis

Local sensitivity analysis was completed with various light intensities. For $K = 0.25, 1.00,$ and $2.00,$ the baseline parameters produce a solution which tends to an equilibrium. After visually assessing the dynamics for each of the required parameter combinations using a plot in MATLAB, the variables selected for sensitivity analysis for these K values were $x, y,$ and p at $t = 200$ days. The normalized forward sensitivity indices for $x(200), y(200)$ and $p(200)$ for all parameters were computed using the formula

$$\Upsilon_{\rho}^u \equiv \frac{\partial u}{\partial \rho} \times \frac{\rho}{u},$$

where u is the variable and ρ is the parameter [7]. To estimate the partial derivative, a central difference approximation was used:

$$\frac{\partial u}{\partial \rho} = \frac{u(\text{par} + h) - u(\text{par} - h)}{2h} + O(h^2),$$

where u is the variable, ρ is the parameter, and par is the baseline value of the parameter, as given in Table 2.1. For the parameters that vary between simulations, $r = 0.93$ and $c = 0.75$ were used for the baseline values. To approximate the values of $x(200), y(200),$ and $p(200)$ for $\text{par} + h$ and $\text{par} - h,$ `ode23s` was used, with all other parameters set at baseline values except the one for which the index was calculated. The step size h was taken to be one percent of the baseline value. The results for $K = 0.25$ are shown in Table

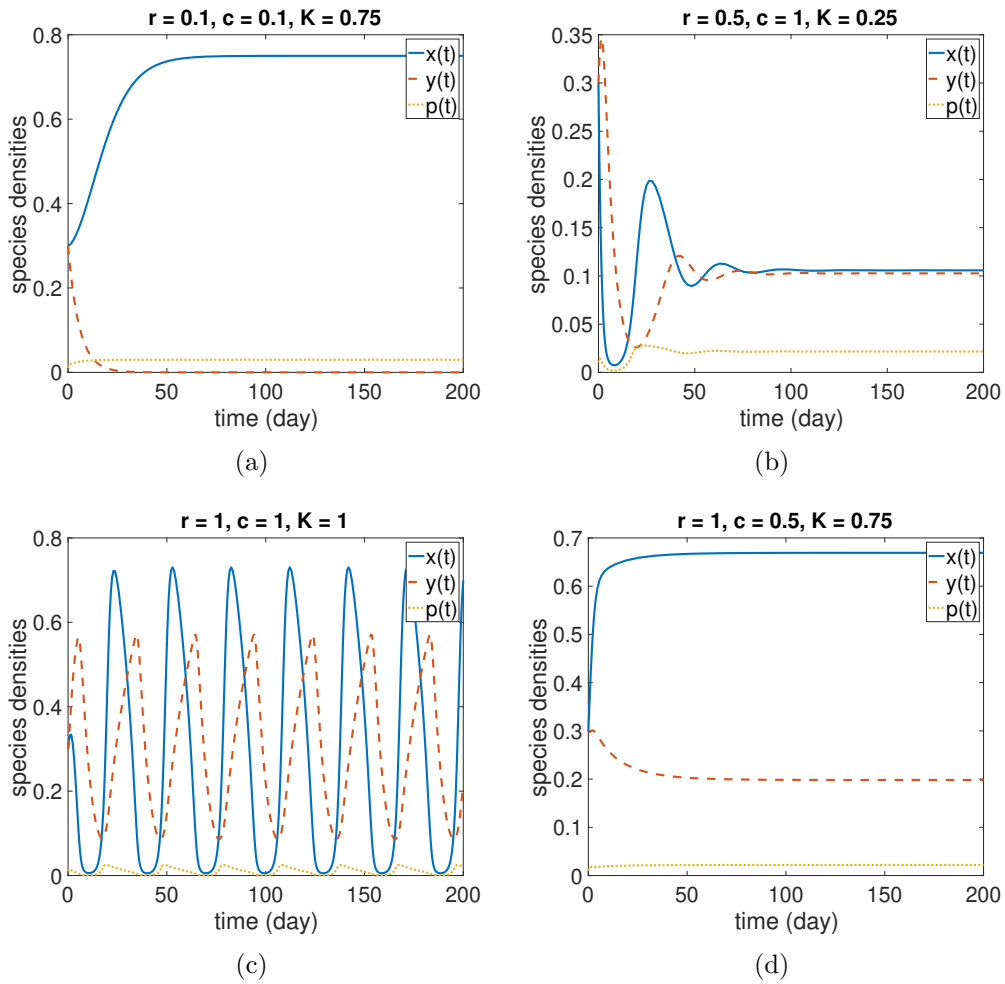


Figure 2.3: Sample dynamics: (a) grazer extinction (terrestrial r and c); (b) coexistence oscillations to coexistence steady state (mixed r and c); (c) coexistence oscillations (aquatic r and c); (d) coexistence at a steady state (mixed r and c).

2.3. This process was repeated for $K = 1.00$ and $K = 2.00$, with the results shown in Table 2.4 and Table 2.5 respectively.

Table 2.3: The sensitivity of variables to the parameters, sorted from largest to smallest absolute value, for low light ($K = 0.25$).

Strength	P	S.I. $x(200)$	P	S.I. $y(200)$	P	S.I. $p(200)$
1	\hat{e}	-1.6572	\hat{e}	2.5140	\hat{e}	-1.3297
2	c	-1.6572	\hat{d}	-2.5130	\hat{d}	1.3294
3	\hat{d}	1.6568	K	1.9132	T	1.2674
4	a	1.000	c	1.5148	c	-1.0321
5	r	4.4438e-10	r	1.0000	K	-0.7885
6	K	2.1687e-10	a	-0.9130	a	0.6225
7	T	-1.7783e-10	T	6.54054e-11	r	-0.4121
8	\hat{c}	-1.3844e-10	\hat{c}	4.8559e-11	θ	-0.2979
9	\hat{a}	1.1039e-10	\hat{a}	-3.7830e-11	\hat{c}	0.1321
10	θ	8.0970e-11	θ	-2.9463e-11	\hat{a}	-0.1015
11	d	-3.9728e-13	d	-1.5743e-12	d	-0.0179
12	q	0	q	0	q	0

For $K = 0.75$ (intermediate light), the baseline parameters produce a limit cycle. Accordingly, local sensitivity indices were computed for the amplitude and period of the oscillations in the variables, using the same formulas to estimate the partial derivatives and the normalized forward sensitivity indices. Each of the necessary simulations was run using ode23s, and the time span $[0, 200]$ was determined to be adequate to capture the settled behaviour. The period of the oscillations was estimated to be between 25 and 30 days, and in order to make sure that enough troughs and crests existed in the tail for each

variable, the tail used was $[\geq 140, 200]$, i.e., roughly the last 60 days, depending on the intervals selected by ode23s. Amplitude was determined by finding the maximum and minimum values in the tail for the variable. The period was determined by first finding places where the sign of the difference in the variable value from one element of the array to the next changed, then finding the time difference between the last and third last such point. The resulting sensitivity indices are shown in Table 2.6 and Table 2.7 for the amplitude and period respectively.

Table 2.4: The sensitivity of variables to the parameters, sorted from largest to smallest absolute value, for high light ($K = 1.00$).

Strength	P	S.I. $x(200)$	P	S.I. $y(200)$	P	S.I. $p(200)$
1	K	3.2753	θ	-4.0834	θ	3.3279
2	θ	3.2020	T	4.0779	c	-3.3247
3	c	-3.1968	c	3.0786	K	2.3832
4	T	-3.1953	K	-2.1853	T	-2.3250
5	r	1.6325	\hat{d}	-2.0146	\hat{d}	2.1432
6	\hat{d}	1.5715	\hat{e}	2.0145	\hat{e}	-2.1430
7	\hat{e}	-1.5715	r	-1.0892	r	1.1878
8	a	0.8625	a	-0.8336	a	0.8999
9	\hat{c}	-0.0357	\hat{c}	0.0458	\hat{c}	-0.0260
10	\hat{a}	0.0343	\hat{a}	-0.0440	\hat{a}	0.0250
11	d	0.0050	d	-0.0064	d	0.0036
12	q	0	q	0	q	0

Table 2.5: The sensitivity of variables to the parameters, sorted from largest to smallest absolute value, for very high light ($K = 2.00$).

Strength	P	S.I. $x(200)$	P	S.I. $y(200)$	P	S.I. $p(200)$
1	K	1.0014	\hat{d}	-40.3478	T	0.9945
2	\hat{d}	0.0018	θ	-34.2900	\hat{d}	0.0066
3	c	-0.00157	T	34.1587	K	0.0058
4	θ	0.00156	c	33.4886	c	-0.00551
5	T	-0.00155	\hat{e}	33.0903	θ	0.00547
6	\hat{e}	-0.0015	K	-29.3316	\hat{e}	-0.0054
7	a	1.7753e-04	a	-3.7990	d	-0.0010
8	r	7.5568e-05	r	-0.6150	\hat{c}	9.9984e-04
9	\hat{c}	-2.1494e-06	\hat{c}	0.0473	\hat{a}	-9.9613e-04
10	\hat{a}	2.1034e-06	\hat{a}	-0.0463	a	6.2477e-04
11	d	1.5530e-06	d	-0.0243	r	1.0118e-04
12	q	0	q	0	q	0

For $K = 0.25$ (Table 2.3), we see that the intrinsic growth rate of the producer, r , ranks fifth for $x(200)$ and $y(200)$, and seventh for $p(200)$. For $K = 0.75$ (Tables 2.6 and 2.7), it ranks sixth for the amplitude of producer carbon oscillations and seventh for the amplitude of grazer carbon and producer phosphorus oscillations; it ranks third, fourth, and second respectively for the periods of oscillations of x , y , and p . For $K = 1.00$ (Table 2.4), it ranks fifth for $x(200)$, and seventh for both $y(200)$ and $p(200)$. For $K = 2.00$ (Table 2.5), it ranks eighth for $x(200)$ and $y(200)$, and eleventh for $p(200)$.

Table 2.6: The sensitivity of the amplitude of oscillations to the parameters, sorted from largest to smallest absolute value, for intermediate light ($K = 0.75$).

Strength	P	S.I. x amp	P	S.I. y amp	P	S.I. p amp
1	c	3.9124	c	4.2797	c	5.7681
2	a	-3.6197	T	4.0362	T	5.1911
3	θ	-3.3473	θ	-3.9980	a	-4.1941
4	T	3.3446	a	-2.9970	θ	-4.0400
5	\hat{d}	-2.0498	\hat{e}	2.4612	\hat{d}	-3.0475
6	r	-2.0058	\hat{d}	-2.4329	\hat{e}	2.9610
7	\hat{e}	1.5260	r	-2.0534	r	-2.7508
8	K	1.3498	K	0.2578	K	0.1410
9	\hat{c}	0.1715	\hat{c}	0.2078	\hat{a}	-0.1270
10	\hat{a}	-0.1544	\hat{a}	-0.1908	\hat{c}	0.0372
11	d	-0.0094	d	-0.0108	d	-0.0118
12	q	0	q	0	q	0

Comparatively, the grazer ingestion rate c ranks second, fourth, and fourth for $K = 0.25$ for x , y , and p respectively. It ranks first for all amplitudes of oscillation for $K = 0.75$, and fifth, fifth, and sixth for the periods. For $K = 1.00$, c ranks third, third, and second. Finally, for $K = 2.00$, c ranks third, fourth, and fourth for x , y , and p respectively.

The local sensitivity rankings of the intrinsic growth rate of the producer, r , and the maximal grazer ingestion rate, c , out of the twelve parameters are summarized in Table 2.8. Also, the signs of the sensitivity indices are in Table 2.9 for steady states and Table 2.10 for amplitude and period.

Table 2.7: The sensitivity of the period of oscillations to the parameters, sorted from largest to smallest absolute value, for intermediate light ($K = 0.75$).

Strength	P	S.I. x pd	P	S.I. y pd	P	S.I. p pd
1	θ	1.2673	K	1.2723	K	1.2832
2	K	1.2498	θ	0.9735	r	-1.0029
3	r	1.2461	T	-0.6442	θ	0.9537
4	\hat{d}	-1.1570	r	0.6073	\hat{d}	-0.8080
5	c	-0.6355	c	-0.5824	T	-0.6410
6	T	-0.5347	\hat{e}	-0.3794	c	-0.5695
7	\hat{e}	-0.4139	a	-0.3253	\hat{e}	-0.3749
8	a	0.1283	\hat{a}	-0.0576	a	-0.2894
9	\hat{a}	-0.0867	\hat{c}	0.0570	\hat{a}	-0.0558
10	\hat{c}	0.0852	\hat{d}	-0.0314	\hat{c}	0.0553
11	d	0.0019	d	0.0019	d	0.0019
12	q	0	q	0	q	0

In particular, we see that increasing r consistently increases the steady state producer carbon density, indicated by the positive sign of the index; for low light, it increases the steady state grazer carbon density and decreases the steady state producer phosphorus density, and vice versa for (very) high light. This suggests that increasing the intrinsic growth rate of the producer is consistently good for the producer carbon density, while it is only good for the grazer at low light and harmful for higher light conditions. This is likely due to the resulting decrease in nutrient quality of the producer with higher growth rates but limited phosphorus resources. At intermediate light, increasing r

decreases the amplitude of oscillations in all three variables, while it increases the period for carbon but decreases the period for producer phosphorus. This suggests that overall r has a dampening effect on oscillations. In this case, increasing K consistently increases both amplitude and period of oscillations.

Comparatively, increasing c consistently decreases the equilibrium values for the producer, and increases them for the grazer. This is the relationship we expect, given that a higher ingestion rate of producer biomass would correspond to a decrease in their population. For intermediate light, increasing c increases the amplitudes of oscillations and decreases the periods. Thus, c appears to have an amplifying effect on oscillations.

Overall, we notice that the system is more sensitive to the grazer ingestion rate than to the intrinsic growth rate of the producer. Therefore, the grazer's impact on the turnover time is more influential in the contrast between terrestrial and aquatic ecosystems than the producer's. In general, the sensitivity rank of r decreases as light intensity increases, and the system is overall more sensitive to c for intermediate to high light levels.

Given this is local sensitivity analysis, it is entirely dependent on the baseline parameters. Note that for the parameters used, the systems with $K = 0.25$ and $K = 1.00$ approach a coexistence equilibrium; $K = 0.75$ produces coexistence oscillations; and $K = 2.00$ approaches a grazer extinction equilibrium. Since we explicitly know the forms of the grazer extinction equilibria, the sensitivity results for $K = 2.00$ are not unexpected. However, the results for $K = 0.25$ and $K = 1.00$ give us insight into a coexistence equilibrium that was not solved for explicitly.

Table 2.8: The rankings of r and c among the twelve parameters for the sensitivity indices. For $K = 0.75$, the rankings are amplitude first, then period.

K	r S.I. x	r S.I. y	r S.I. p	c S.I. x	c S.I. y	c S.I. p
0.25	5th	5th	7th	2nd	4th	4th
0.75	6th/3rd	7th/4th	7th/2nd	1st/5th	1st/5th	1st/6th
1.00	5th	7th	7th	3rd	3rd	2nd
2.00	8th	8th	11th	3rd	4th	4th

Table 2.9: The signs of the normalized forward sensitivity indices among the twelve parameters. The three signs correspond to the cases of $K = 0.25, K = 1.00$ and $K = 2.00$ respectively. q had index 0 for all quantities, so no sign could be selected.

P	S.I. $x(200)$	S.I. $y(200)$	S.I. $p(200)$
r	+ / + / +	+ / - / -	- / + / +
K	+ / + / +	+ / - / -	- / + / +
c	- / - / -	+ / + / +	- / - / -
\hat{c}	- / - / -	+ / + / +	+ / - / +
a	+ / + / +	- / - / -	+ / + / +
\hat{a}	+ / + / +	- / - / -	- / + / -
\hat{e}	- / - / -	+ / + / +	- / - / -
\hat{d}	+ / + / +	- / - / -	+ / + / +
d	- / + / +	- / - / -	- / + / -
θ	+ / + / +	- / - / -	- / + / +
q	0 / 0 / 0	0 / 0 / 0	0 / 0 / 0
T	- / - / -	+ / + / +	+ / - / +

Table 2.10: The signs of the normalized forward sensitivity indices among the twelve parameters for $K = 0.75$. The first three columns correspond to amplitude, and the last three correspond to period. q had index 0 for all quantities.

P	S.I. x amp	S.I. y amp	S.I. p amp	S.I. x pd	S.I. y pd	S.I. p pd
r	-	-	-	+	+	-
K	+	+	+	+	+	+
c	+	+	+	-	-	-
\hat{c}	+	+	+	+	+	+
a	-	-	-	+	-	-
\hat{a}	-	-	-	-	-	-
\hat{e}	+	+	+	-	-	-
\hat{d}	-	-	-	-	-	-
d	-	-	-	+	+	+
θ	-	-	-	+	+	+
T	+	+	+	-	-	-

2.4.3 One parameter bifurcation analysis

Bifurcation analysis was performed using MatCont [10]. For all one parameter bifurcation diagrams, a solid blue curve represents a stable equilibrium point; a magenta dashed curve is an unstable equilibrium point; and a cyan dotted curve represents the minimum/maximum of a stable limit cycle.

In Figure 2.4, we see that the boundary equilibria are unstable for all $r \in (0, 2]$. Therefore, the coexistence equilibrium is always stable for $K = 0.25, r \in (0, 2]$, and c held at its baseline value. There is a neutral saddle

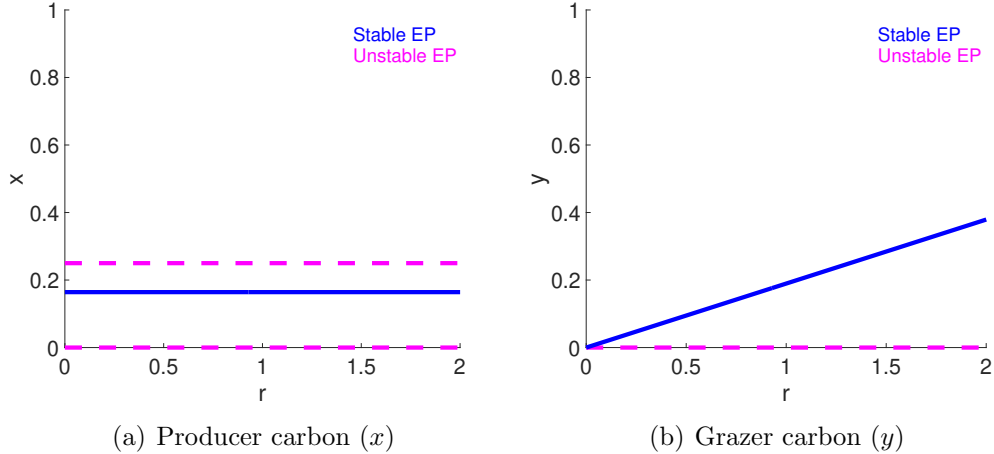


Figure 2.4: One parameter bifurcation diagrams for r with low light ($K = 0.25$); c is held at its baseline value. x is on the left and y is on the right. There are no bifurcations. The coexistence equilibrium is stable throughout.

equilibrium that occurs at $r = 0.0575$, as well as a branch point, a Hopf point, and another branch point which occur at values that are essentially 0 and are too small to continue in the two parameter diagrams.

In Figure 2.5, for $K = 0.25$, we see that there is a transcritical bifurcation, which occurs at $c = 0.594560$. At this bifurcation, the grazer extinction equilibrium becomes unstable and the coexistence equilibrium becomes stable. Note that before this bifurcation point, the coexistence equilibrium is not biologically feasible. In Section 2.3.3, we found that the determinant of the Jacobian evaluated at the grazer extinction equilibrium changed signs at $c = 0.5946$, since $K = 0.25$ falls under Case 4. This validates our result.

As shown in Figure 2.6, the complete extinction equilibrium and the grazer extinction equilibrium are both unstable for the full range of r values for

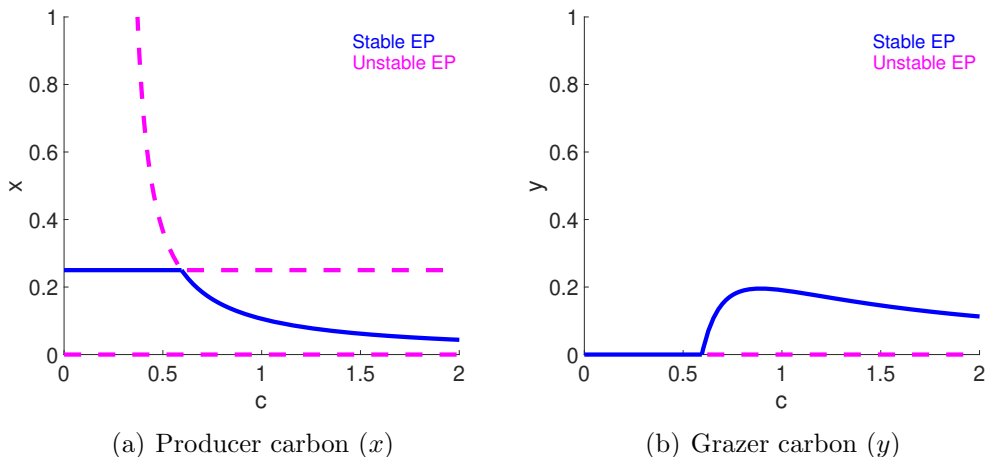


Figure 2.5: One parameter bifurcation diagrams for c with low light ($K = 0.25$); r is held at its baseline value. x is on the left and y is on the right. There is a transcritical bifurcation around $c = 0.59$. For $c < 0.59$, we observe a stable grazer extinction equilibrium; for $c > 0.59$, the coexistence equilibrium is stable.

$K = 0.75$. However, there are several bifurcations. There is a saddle-node bifurcation at $r = 1.151380$, where an unstable saddle coexistence equilibrium collides with a stable node coexistence equilibrium. There is a Hopf bifurcation at $r = 1.23910$, where a stable limit cycle disappears, and a branch of the coexistence equilibrium becomes stable. Then there is another saddle-node bifurcation at $r = 1.23951$, at which this stable branch of the coexistence equilibrium collides with an unstable branch. Note that this interval of stability is too small to see in the diagram. Between $r = 1.23910$ and $r = 1.23951$ there may be bistability between two equilibrium points. There is also a neutral saddle equilibrium point, and a branch point at a very low parameter value.

From Figure 2.7, for $K = 0.75$, the grazer equilibrium is stable until the transcritical bifurcation at $c = 0.397464$, where the coexistence equilibrium be-

comes biologically feasible and stable. There are two saddle-node bifurcations: the first is at $c = 0.62783$ and the second is at $c = 0.650870$. Note that only the second is clearly visible in Figure 2.7. Also, a stable limit cycle appears with an increasing amplitude at a Hopf bifurcation around $c = 0.62800$. As with the bifurcation diagram for r , there is clearly an interval of bistability between the Hopf bifurcation and the second saddle-node bifurcation, and there may be an interval of bistability with two equilibria for $c \in [0.62783, 0.62800]$. In Section 2.3.3, we found that the determinant of the Jacobian evaluated at the grazer extinction equilibrium changed signs at $c = 0.3975$, since $K = 0.75$ is in Case 3. This agrees with the transcritical bifurcation point observed here.

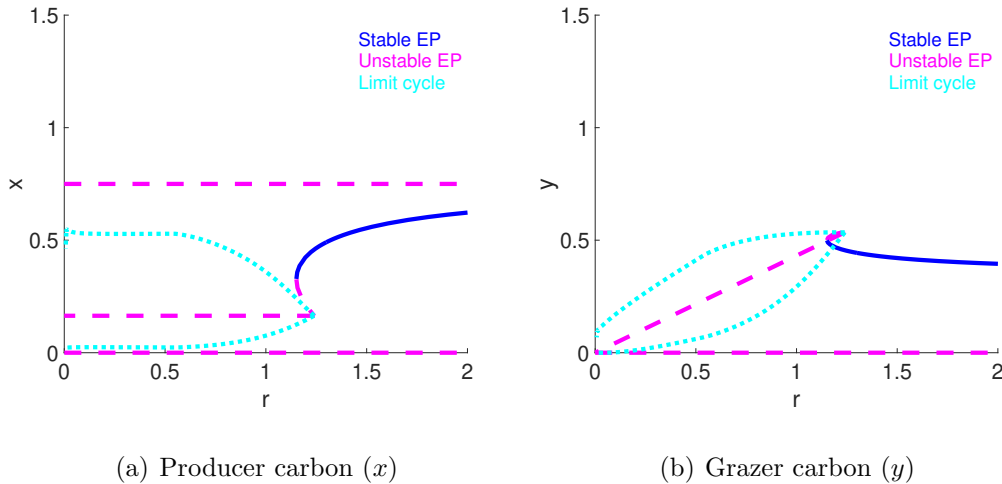


Figure 2.6: One parameter bifurcation diagrams for r with intermediate light ($K = 0.75$). There is a saddle-node bifurcation around $r = 1.15$, a Hopf bifurcation around 1.23910 , and another saddle-node bifurcation around $r = 1.23951$. For $r < 1.23910$, there is a stable limit cycle; for $r > 1.15$, there is a stable coexistence equilibrium. There may be bistability between a coexistence equilibrium and a limit cycle for $r \in (1.15, 1.23910)$.

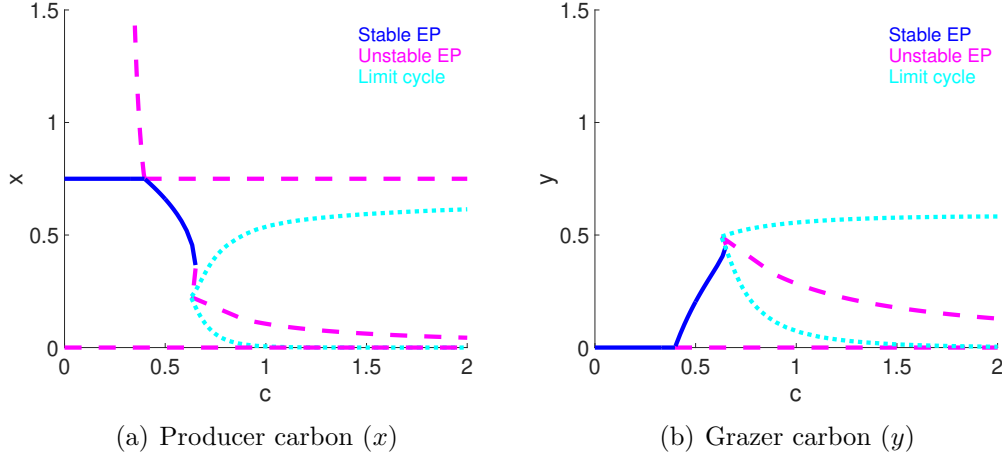


Figure 2.7: One parameter bifurcation diagrams for c with intermediate light ($K = 0.75$). There is a transcritical bifurcation at $c = 0.40$, saddle-node bifurcations at $c = 0.62783, 0.65$, and a Hopf bifurcation at $c = 0.62800$. For $c < 0.40$, grazer extinction is stable; for $0.40 < c < 0.65$, coexistence; and for $c > 0.62800$, oscillations.

For all values of r for $K = 2.00$, the grazer extinction equilibrium is stable, as shown in Figure 2.8. A possible explanation for this result is that the baseline value of c is insufficient for the grazers to consume enough phosphorus to balance their death rate given the poor quality of the producer as food.

For $K = 2.00$ and c , the grazer extinction equilibrium is stable until the coexistence equilibrium becomes biologically feasible and stable at $c = 0.892787$, which matches the value found in Section 2.3.3 (Figure 2.9). There is also a saddle-node bifurcation at $c = 1.302372$, and a neutral saddle equilibrium at $c = 0.698479$. Based on the dynamics, there should be another saddle-node bifurcation and a Hopf bifurcation between the unstable coexistence equilibrium and the stable limit cycle (as in Figure 2.7), but they could not be found using MatCont. Period doubling happens at the left end of the oscillations.

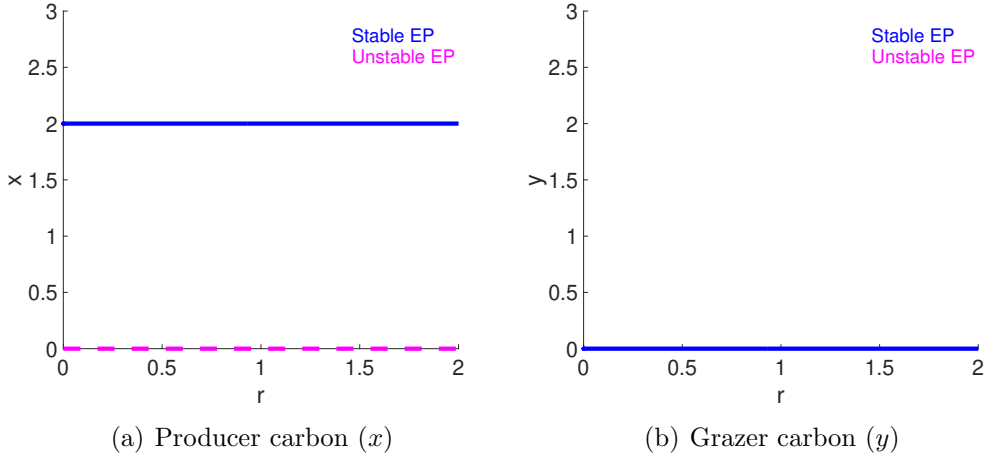


Figure 2.8: One parameter bifurcation diagrams for r with very high light ($K = 2.00$). There are no bifurcation points. The grazer extinction equilibrium is stable throughout.

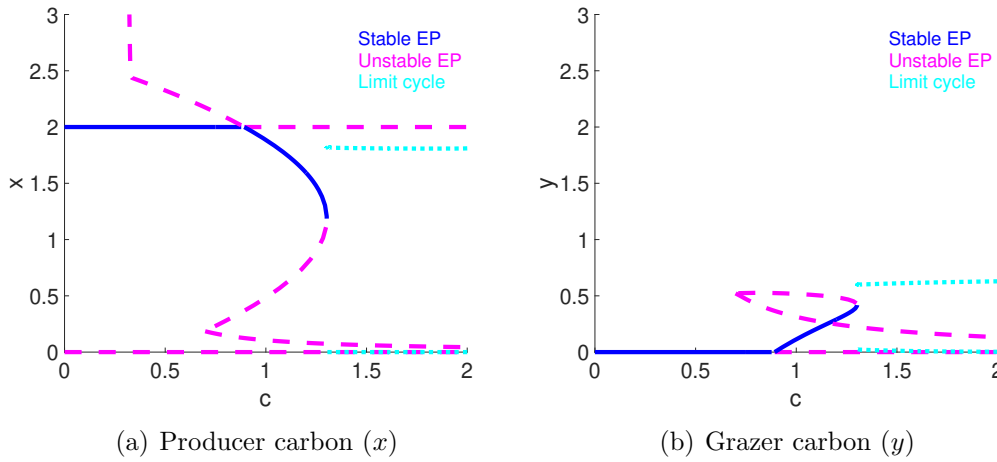


Figure 2.9: One parameter bifurcation diagrams for c with very high light ($K = 2.00$). There is a transcritical bifurcation around $c = 0.89$ and a saddle-node bifurcation at $c = 1.30$. Grazer extinction is stable for $c < 0.89$; then coexistence for $0.89 < c < 1.30$; then oscillations for $c > 1.30$.

2.4.4 Two parameter bifurcation analysis

For Figure 2.10 (a), the vertical line is the transcritical bifurcation. The stable behaviours in the regions are: (1) grazer extinction equilibrium; and (2) coexistence equilibrium.

For Figure 2.10 (b), the vertical line is the transcritical bifurcation and the diagonal line corresponds to the saddle-node bifurcation along the coexistence equilibria curve. There is a cusp point where the two curves intersect. Note that from the one parameter analysis, we know there should also be a Hopf branch, but it could not be continued in two parameters using MatCont. There should also be another saddle-node curve. There is probably a region of bistability missing from this diagram, but the saddle-node bifurcation likely provides a decent approximation of the transition between a stable coexistence equilibrium and stable coexistence oscillations. The regional stable behaviours are: (1) grazer extinction equilibrium; (2) coexistence equilibrium; and (3) coexistence oscillations.

For Figure 2.10 (c), we see the similar curves and regions to Figure 2.10 (b). This is due to the smaller difference between $K = 0.75$ and $K = 1.00$ relative to the other increments in K . However, the shift in the saddle-node curve is sufficient to justify the different behaviours observed at baseline for $K = 0.75$ and $K = 1.00$ by Wang et al. (2008) [53].

For Figure 2.10 (d), the vertical line is the transcritical bifurcation. The magenta curve is from the saddle-node bifurcation along the coexistence equilibria curve. The point where the curves intersect is a cusp point. As in the one parameter bifurcation analysis, there is likely a missing Hopf curve and a miss-

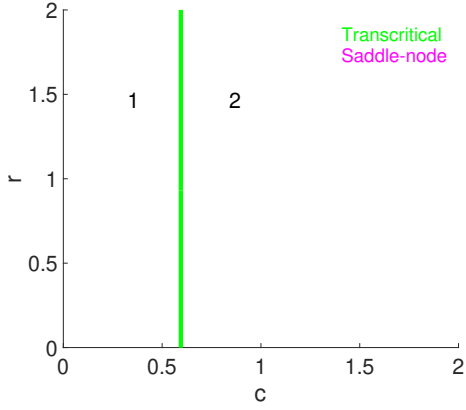
ing saddle-node curve. However, these curves could not be located properly to be extended in the two parameter diagrams. The regional stable behaviours are: (1) grazer extinction equilibrium; (2) coexistence equilibrium; (3) coexistence oscillations; and (4) coexistence oscillations. Note that the lower part of the saddle-node branch does not appear as a limit point when one parameter bifurcation diagrams are created for r , using $c = 1.00$ or $c = 2.00$.

We assumed that all parameters other than r and c are the same between terrestrial and aquatic ecosystems. Since the baseline values for r and c (0.93 and 0.75 respectively), were for an aquatic system, then we consider roughly the lower left hand corner of the diagrams to represent terrestrial ecosystems and the opposite to represent aquatic. Thus, in low light conditions, we expect either grazer extinction or coexistence at an equilibrium for terrestrial ecosystems, and coexistence at equilibrium for aquatic (Figure 2.10 (a)). For intermediate to high light levels, we would expect to see a variety of possible dynamics for terrestrial systems including grazer extinction, coexistence at equilibrium, and coexistence oscillations; for aquatic, these results suggest coexistence would occur in some form (Figure 2.10 (b)-(c)). Lastly, for very high light levels, achievable only in a laboratory setting, we expect the terrestrial grazer to die out completely, and the aquatic system to exhibit some form of coexistence (Figure 2.10 (d)).

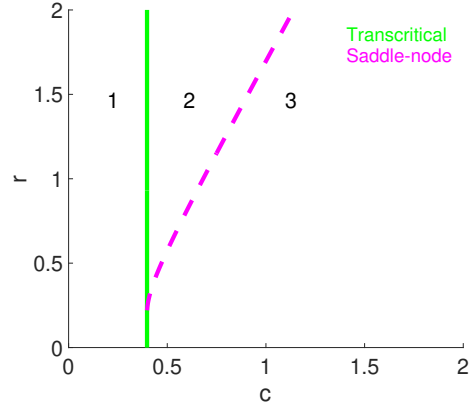
We observe that from the grazer equation with Holling type II functions

$$\frac{dy}{dt} = y * \left(\hat{e} \min \left\{ 1, \frac{p/x}{\theta} \right\} \left(\frac{cx}{a+x} \right) - \hat{d} \right) < y * (\hat{e}c - \hat{d}).$$

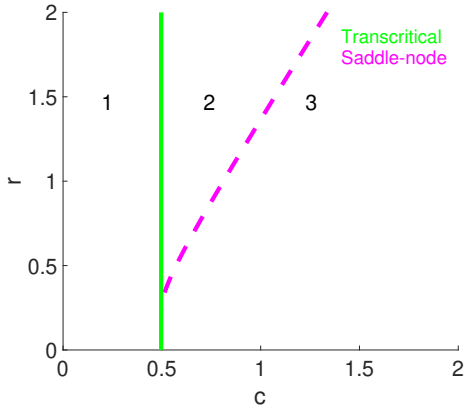
Since $y \geq 0$ biologically, then this means that for $c < \hat{d}/\hat{e} = 0.2973$, the



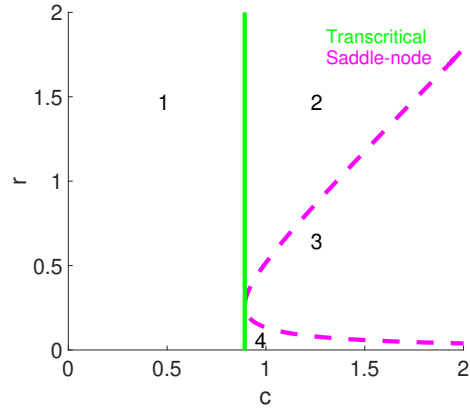
(a) $K=0.25$



(b) $K=0.75$



(c) $K=1.00$



(d) $K=2.00$

Figure 2.10: Two parameter bifurcation diagrams, varying K . Green solid curves correspond to transcritical bifurcations, and magenta dashed curves to saddle-node bifurcations. For regional stable behaviour, (1) corresponds to the grazer extinction equilibrium, (2) to a coexistence equilibrium, (3) to coexistence oscillations, and (4) to coexistence oscillations.

grazer's population density is decreasing, regardless of the size of the producer population or the light intensity. Therefore, for low c , we can only ever see extinction of the grazer, as found in the bifurcation diagrams. Given that terrestrial grazer populations persist, this would seem to suggest that the value of c must be above this threshold, even in terrestrial ecosystems. This may also suggest that the grazer's loss rate should also be lower in terrestrial populations than in aquatic.

2.4.5 WKL vs. LKE model

Wang et al. (2008) [53] found that solutions of the WKL model are almost identical to those of the LKE model for small or large K , while they slightly differ for intermediate K . However, when K is near the homoclinic bifurcation point ($K = 0.95$), they are completely different.

To investigate if there are any other differences between the two models as r and c vary, simulations were completed using ode23s for the WKL and the LKE models for all possible combinations of $K \in \{0.25, 0.75, 2.00, 0.95\}$, $r \in \{0.1, 1.0, 2.0\}$, and $c \in \{0.1, 1.0, 2.0\}$.

The two differ slightly quantitatively for

- $K = 0.25 : r = 1, c = 2; r = 2, c = 2.$
- $K = 0.75 : r = 1, c = 1; r = 1, c = 2; r = 2, c = 1; r = 2, c = 2.$
- $K = 2.00 : r = 1, c = 1; r = 1, c = 2; r = 2, c = 2.$
- $K = 0.95 : r = 1, c = 1; r = 1, c = 2; r = 2, c = 1; r = 2, c = 2.$

We notice that there are never discernible differences for $r = 0.1$ or $c = 0.1$. Thus for very low intrinsic growth rate and grazer ingestion rate, there is no noticeable difference between the two models, regardless of the value of K . For none of the simulated combinations were there completely different dynamics as there were for $K = 0.95$ with the baseline values of r and c . This indicates that the bifurcation point in K shifts for different values of r and c .

The differences between the WKL and LKE model relate to the relaxation of the assumption that there is no free phosphorus in the medium. Given the above, we can conclude that this assumption matters more for aquatic ecosystems with intermediate to high turnover rates than for terrestrial ecosystems. This is likely because at very low values of c , the nutritional quality of the producer is less likely to be the controlling factor in the grazer's population density since the inability to balance their loss rate is more important.

2.5 Discussion

Multiple mathematical models have been developed to study the flow of nutrients and energy through a producer-grazer system. In particular, the WKL model tracks carbon and phosphorus while allowing for free phosphorus in the medium. The impacts of changing the light-dependent carrying capacity of the producer on the dynamics of this system have been studied in the past. However, other parameters are also of interest.

In particular, the intrinsic growth rate of the producer (r) and the maximal ingestion rate of the grazer (c) vary between aquatic and terrestrial ecosystems, particularly for terrestrial systems with large producers and herbivores. In

general, both rates are lower in terrestrial ecosystems than aquatic, resulting in a lower turnover rate for producer biomass in terrestrial-based than aquatic-based ecosystems. Here, all other parameters were assumed to be the same, regardless of whether the system was terrestrial or aquatic.

For very low r and c , extinction of the grazer is observed numerically; for very high r and c , oscillatory coexistence or coexistence at a steady state is observed, depending on the value of K . This suggests that aquatic ecosystems are more prone to exhibiting coexistence than terrestrial ecosystems.

Overall, local sensitivity analysis implies that r and c are not the most important parameters in determining the asymptotic behaviour of the system. Other parameters have more influence over the results for this particular parameter regime, and these parameters may differ in general between aquatic and terrestrial ecosystems. Generally c has more influence than r , and changing K has more of an impact on the sensitivity of the system to r than to c . We also observe that the grazer loss rate is more influential for intermediate to high light levels, and that the system becomes more sensitive to the light intensity dependent carrying capacity as it increases. Note that this is likely because at (very) high light levels and these parameter values, the system reaches the grazer extinction equilibrium, where the prey population is at their light intensity dependent carrying capacity.

Part of the reason that the analysis indicates that terrestrial populations should not persist could be due to additional parameters that should differ. As mentioned in the bifurcation analysis, the grazer's loss rate is likely to have a strong impact, which is supported by the fact that it was one of the parameters the system was the most sensitive to at extreme values of K and the

observation that it is part of the stability condition of the grazer extinction equilibrium. Light intensity likely also differs considerably between terrestrial and aquatic ecosystems, and we see that the grazer extinction region shrinks with increasing K until a point and then grows again. Intermediate light levels in some terrestrial ecosystems may explain the persistence of grazer populations observed naturally, while a lower grazer loss rate may explain terrestrial grazer persistence in low light conditions (e.g., in the shade of a dense rainforest canopy). In addition, the elemental imbalance between the grazer and the producer is larger in terrestrial than in aquatic systems because plants are more reliant on carbon rich structural matter than phytoplankton [5, 22]. This seems to suggest that q , the minimal P:C ratio of the producer, may be lower in terrestrial ecosystems than aquatic. However, rather than explaining the persistence of terrestrial grazers, this change would only further emphasize the grazer extinction observed here. Also, sensitivity analysis indicated q did not have an impact on the asymptotic target values.

Future work could include examination of larger parameter ranges. During bifurcation analysis, bifurcations were observed at higher values of the parameters in some cases, but were not included due to the *a priori* parameter restrictions. It also bears mentioning that the baseline values used for r and c , which lie in the middle of the investigated parameter ranges, are for an aquatic system. Further investigation of data to determine other parameter regimes to test would help to more definitively contrast these ecosystems. Data could also validate our hypothesis that there are other parameters that differ largely between these systems and contribute to the results observed naturally. Given the system's sensitivity to grazer loss rate, further explicit consideration of

this parameter in addition to those examined here may also help explain the unrealistic results implying that land grazers cannot persist. Global stability and sensitivity analyses focussing on r and c also have yet to be completed.

Most stoichiometric models, including the ones mentioned here – LKE and WKL [29, 53] – assume strict homeostasis for heterotrophs, that is, that the grazer in the system must maintain a specific, fixed nutrient ratio within its tissues, regardless of the nutrient availability in its food [44]. This is in contrast to the larger variation in chemical content in the organisms it consumes. However, this assumption is not completely realistic. It has been shown to be reasonable when the variability is sufficiently narrow, independent of variation in their food source, and to be not valid for herbivores with small mortality rates [55]. Therefore, in the case that explicit consideration of grazer loss rate is taken into account, a model may need to be used that relaxes or removes this assumption [54].

Chapter 3

Incorporating atmospheric concentration of carbon dioxide

3.1 Introduction

Since the Industrial Revolution, Earth's atmosphere has been experiencing an unprecedented rate of increase in carbon dioxide [34]. Climate change models have predicted that atmospheric concentrations of carbon dioxide may surpass 700 ppm by 2100 from the current ambient level of approximately 390 ppm [34]. Such a substantial change will likely have far-reaching impacts on the environment and all life on earth. Changes in the global carbon cycle may also influence the global phosphorus and nitrogen cycles due to their coupling through biological interactions [22]. The main mechanisms by which ecosystems are directly impacted by increased atmospheric carbon dioxide concentration are changes in photosynthesis, transpiration and respiration [12]. However, there are also indirect impacts.

According to Elser et al. (2010) [15], the three possible scaling links between atmospheric concentration of carbon dioxide and producer stoichiometry are: stimulation of plant photosynthesis, potentially leading to increased carbon sequestration subject to soil resource constraints; increased plant root:shoot ratios and leaf area, impacting photosynthetic capacity and nutrient requirements; and reduction in Rubisco production due to increased efficiency, allowing for reallocation of nitrogen. The increased rate and efficiency of photosynthesis in C_3 plants occur due to changes in the light-independent reactions.

Photosynthesis is divided into two main components: the light-dependent reactions, and the light-independent reactions. The light-dependent reactions use solar energy as well as water to produce the energy compound ATP and the electron carrier NADPH. The light-independent reactions, also known as the Calvin Cycle, use these two products to fix carbon dioxide into glucose. Specifically, in the carbon fixation step of the Calvin Cycle, the enzyme ribulose-1,5-bisphosphate carboxylase/oxygenase (Rubisco) catalyzes the carboxylation reaction, in which the carbon dioxide molecule combines with a five-carbon acceptor molecule, ribulose-1,5-bisphosphate (RubP). The resulting 6-carbon molecule then undergoes several other reactions to ultimately either make glucose or regenerate the RubP acceptor molecule [45].

However, Rubisco can also catalyse the oxygenation of RubP, which begins the “photosynthetic carbon oxidation or photorespiratory pathway (PCO), which decreases the net efficiency of photosynthesis by 20-50%” [12]. Carbon dioxide (CO_2) competitively inhibits the oxygenation reaction, causing a increase in both Rubisco- and RubP-limited net photosynthesis [12]. This decrease in oxygenation along with the fact that Rubisco is not CO_2 -saturated

at the current atmospheric concentration of CO_2 in some plants are thought to be the reasons that increased concentrations of atmospheric CO_2 have been shown to increase the rate of photosynthesis in C_3 plants, which have no mechanisms in place to reduce photorespiration [1]. According to Ainsworth and Rogers (2007) [1], we know that at room temperature, approximately 23% of fixed carbon is lost due to photorespiration, and that with all oxygenation reactions replaced with carboxylation reactions, uptake of carbon dioxide would be increased by around 53%.

The meta-analysis of terrestrial plants completed by Du et al. (2019) [13] showed that elevated carbon dioxide stimulates photosynthesis, causing an increase in plant carbon (C) and carbon to nitrogen ratio (C:N), and a decrease in plant nitrogen (N), phosphorus (P), and nitrogen to phosphorus ratio (N:P). Thus elevated atmospheric carbon dioxide has a larger impact on levels of N than P, likely due to the fact that a large proportion (approximately 25%) of the nitrogen in a leaf is in Rubisco [12]. Notably, the slight increase in C:P was not statistically significant, despite the relatively large sample size [13]. An alternative explanation for the differences between nitrogen and phosphorus could consider the growth-rate hypothesis [13]: increased growth rate is related to the decrease in N:P because phosphorus-rich RNA is required by plant organs for rapid protein synthesis [44].

There is also evidence that increasing atmospheric carbon dioxide concentration also increases the rate of photosynthesis in non-vascular plants. Experimentally, Urabe, Togari and Elser (2003) [49] found that increased atmospheric concentration of carbon dioxide also increases the partial pressure of carbon dioxide in water, resulting in the stimulation of algal growth. The

saturation level of algal abundance was higher in the increased CO₂ treatments, suggesting that growth of algae in the control was limited by carbon dioxide. Also, there was a significantly lower final algal cellular quota (P:C) for the elevated carbon dioxide treatments compared to the control treatment.

Although the major direct impacts on ecosystems of atmospheric carbon dioxide concentration are related to the producer at the base of the food chain, there are also indirect impacts on the grazer. Since herbivores tend to have more rigid, higher nutrient requirements, their food can become less than optimal if the nutrient content of their food falls below their requirement [44]. Hence, the decrease in algal P:C that may result from increased atmospheric carbon dioxide concentration can result in a decrease in growth of the grazer [49]. Additional experiments conducted by Urabe et al. (2003) [49] confirmed that the decrease in grazer growth they observed was due to the decreased algal P:C, and not due to a direct impact of carbon dioxide on the grazer or to excessive food levels interfering with feeding activities.

Due to dissolved organic carbon from terrestrial ecosystems being mineralized by bacteria into CO₂, lakes are often carbon dioxide sources, not sinks [50]. In natural lakes, the partial pressure of CO₂ can vary over four orders of magnitude and is impacted by environmental perturbations [49]. If algae species have carbon concentration mechanisms (CCMs) that allow them to use dissolved bicarbonate ions (HCO₃⁻) in photosynthesis efficiently, increased partial pressure of carbon dioxide in their lake (pCO₂) would have a reduced impact on their growth, since in most lakes pCO₂ is much lower than the concentration of HCO₃⁻ [32, 49]. However, CCMs appear to operate less efficiently under light or nutrient limitation [49]. Therefore, an increase in atmospheric

carbon dioxide may have a larger impact in natural lakes where both nutrient and light are not sufficiently abundant [49]. Note that the rate of exchange of carbon dioxide between water and the air above is directly proportional to the concentration gradient of carbon dioxide across the water's surface [32]. The proportionality constant, which is known as the gas exchange transfer velocity, is hard to determine due to its relationship with wind speed, which differs globally and temporally [56].

Despite the direct relationship between the exchange rate of carbon dioxide and the concentration gradient of the gas across the boundary, water bodies are rarely equilibrated with the atmosphere [32, 50]. They can either be carbon sources, such as in many freshwater lakes, or sinks, as in many oceans [32]. This is determined primarily by the amount of terrestrial carbon that enters the water [50]. However, in their experiments, Urabe et al. (2003) [49] found that when algal biomass reached saturated levels in the elevated carbon dioxide treatments, the carbon dioxide in the water decreased to levels not significantly different from the control treatment. Hence, the amount of algae in the water can also impact the concentration of dissolved carbon dioxide, since their uptake rate of carbon dioxide can exceed the diffusion rate from the atmosphere [49]. Additional factors that can determine carbon dioxide concentration in ocean surface waters include mixing, temperature, salinity, respiration, and calcification [4].

Models such as the WKL model track the flow of carbon and phosphorus through a producer-grazer system [53]. However, these stoichiometric models assume that the system is open to carbon, given the prevalence in the atmosphere and relatively rapid dissolution of carbon dioxide into water. Thus, the

intention of this chapter is to expand the WKL model to explicitly incorporate atmospheric carbon dioxide concentration, by considering a local system which is closed to carbon, with and without the impacts of photorespiration, and by considering a local system with some degree of exchange with the atmosphere. The three models will be analyzed mathematically and/or numerically, with the intention of addressing the potential impact of elevated atmospheric carbon dioxide concentration on the absolute and relative amounts of nutrient in the producer, and moreover, the impact of this change on the persistence of the grazer population.

3.2 Model Formulation

3.2.1 Local closed model

The first model used to investigate the impacts of elevated atmospheric concentration of CO_2 on a producer-grazer system is a completely closed form of the WKL model from Section 2.2, with an additional carbon-dependent carrying capacity ($h(C)$) for producer growth.

This model assumes that in the immediate area of the system, there is some fixed total amount of carbon. Here C is the free carbon in the medium. The producer's growth follows Liebig's Law of the Minimum, where the growth rate is now either limited by some light-dependent carrying capacity (K), the amount of phosphorus in the producer (p/q), or a carrying capacity dependent on availability of carbon in the medium ($h(C)$). All three factors are assumed to be independently colimiting. Independent colimitation between

light and phosphorus was assumed for the WKL model [53], as well as for the LKE model from which it was derived [29]. Also, data were fit for the algae *Chlamydomonas acidophila* to four different Monod-type models for phosphorus and carbon limitation, and dependent colimitation was rejected in favour of independent colimitation between these two factors [43]. However, there is no strong evidence for classification of colimitation between light and carbon, and independence was assumed for simplicity of modelling.

The equations are

$$\frac{dx}{dt} = \underbrace{rx \left(1 - \frac{x}{\min\{K, p/q, h(C)\}}\right)}_{\text{producer growth limited by nutrient, light, \& carbon}} - \underbrace{f(x)y}_{\text{uptake by grazers}} - \underbrace{l_x x}_{\text{respiration}}, \quad (3.1)$$

$$\frac{dy}{dt} = \underbrace{\hat{e} \min\left\{1, \frac{p/x}{\theta}\right\} f(x)y}_{\text{grazer growth limited by food quality \& quantity}} - \underbrace{\hat{d}y}_{\text{grazer death}} - \underbrace{l_y y}_{\text{respiration}}, \quad (3.2)$$

$$\frac{dp}{dt} = \underbrace{g(P)x}_{\text{P uptake by producer}} - \underbrace{\frac{p}{x} f(x)y}_{\text{P loss due to grazing}} - \underbrace{dp}_{\text{P loss due to producer recycling}}, \quad (3.3)$$

$$\begin{aligned} \frac{dP}{dt} = & \underbrace{-g(P)x}_{\text{P uptake by producer}} + \underbrace{dp}_{\text{P recycling from producer}} + \underbrace{\theta \hat{d}y}_{\text{P recycling from dead grazer}} \\ & + \underbrace{\left(\frac{p}{x} - \hat{e} \min\left\{\theta, \frac{p}{x}\right\}\right) f(x)y}_{\text{P recycling from grazer feces}} + \underbrace{\theta l_y y}_{\text{P recycling from grazer respiration}}, \end{aligned} \quad (3.4)$$

$$\begin{aligned} \frac{dC}{dt} = & \underbrace{l_x x}_{\text{producer respiration}} + \underbrace{l_y y}_{\text{grazer respiration}} - \underbrace{rx \left(1 - \frac{x}{\min\{K, p/q, h(C)\}}\right)}_{\text{C uptake by producer}} \\ & + \underbrace{\left(1 - \hat{e} \min\left\{1, \frac{p/x}{\theta}\right\}\right) f(x)y}_{\text{C recycling from grazer feces}} + \underbrace{\hat{d}y}_{\text{C recycling from dead grazer}}. \end{aligned} \quad (3.5)$$

To make the system closed to carbon, terms specifically representing respiration have been added to the equations. Now Equation (3.1) includes a term for producer respiration, where the rate of respiration is given by l_x . Equation (3.2) also includes a term for loss of carbon due to grazer respiration, where the rate of respiration is given by l_y . Note that whereas in the WKL model \hat{d} included grazer death and respiration loss, now \hat{d} is only for loss due to grazer death. Due to the assumption of strict homeostasis for the grazers, a term for compensatory loss of phosphorus due to respiration is now incorporated in Equation (3.4). Lastly, Equation (3.5), which is for the free carbon in the medium, includes producer respiration, grazer respiration, uptake by the producer via photosynthesis, recycling from grazing, and then degradation/decomposition of dead grazers which is assumed to be instantaneous. As in the WKL model, all parameters are assumed to be positive.

As aforementioned, $h(C)$ is the carbon-dependent carrying capacity of the producer. This term captures the limitation of carbon fixation by insufficient available carbon dioxide, since Rubisco is not CO_2 -saturated at the current atmospheric concentration in some C_3 plants [1, 12]. In general, we assume that $h(C)$ is non-decreasing, and that $h(0) = 0$. The most basic choice for $h(C)$ is a scalar multiple of C , although it is likely $h(C)$ should plateau at some threshold value of C .

Recall that the system is assumed to be closed to both phosphorus and carbon. Let T_P be the total phosphorus in the system, and T_C be the total carbon in the system. Using Equations (3.1)-(3.5), it can be shown that $dT_P/dt = 0 = dT_C/dt$. Note that $T_P = p + P + \theta y$, and $T_C = x + y + C$. Hence, we can write $P = T_P - p - \theta y$ and $C = T_C - x - y$. Thus, through the

Law of Conservation of Mass, we can reduce the dimensionality of the system:

$$\frac{dx}{dt} = rx \left(1 - \frac{x}{\min\{K, p/q, h(T_C - x - y)\}} \right) - f(x)y - l_x x, \quad (3.6)$$

$$\frac{dy}{dt} = \hat{e} \min \left\{ 1, \frac{p/x}{\theta} \right\} f(x)y - \hat{d}y - l_y y, \quad (3.7)$$

$$\frac{dp}{dt} = g(T_P - p - \theta y)x - \frac{p}{x} f(x)y - dp. \quad (3.8)$$

3.2.2 Local closed model with PCO

The second model developed is an extension of the local closed model:

$$\frac{dx}{dt} = \underbrace{rx \left(1 - \frac{x}{\min\{K, p/q, h(C)\}} \right)}_{\text{producer growth limited by nutrient, light, \& carbon}} - \underbrace{f(x)y}_{\text{uptake by grazers}} - \underbrace{\rho(C)l_x x}_{\text{respiration}}, \quad (3.9)$$

$$\frac{dy}{dt} = \underbrace{\hat{e} \min \left\{ 1, \frac{p/x}{\theta} \right\} f(x)y}_{\text{grazer growth limited by food quality \& quantity}} - \underbrace{\hat{d}y}_{\text{grazer death}} - \underbrace{l_y y}_{\text{respiration}}, \quad (3.10)$$

$$\frac{dp}{dt} = \underbrace{g(P)x}_{\text{P uptake by producer}} - \underbrace{\frac{p}{x} f(x)y}_{\text{P loss due to grazing}} - \underbrace{dp}_{\text{P loss due to producer recycling}}, \quad (3.11)$$

$$\begin{aligned} \frac{dP}{dt} = & \underbrace{-g(P)x}_{\text{P uptake by producer}} + \underbrace{dp}_{\text{P recycling from producer}} + \underbrace{\theta \hat{d}y}_{\text{P recycling from dead grazer}} \\ & + \underbrace{\left(\frac{p}{x} - \hat{e} \min \left\{ \theta, \frac{p}{x} \right\} \right) f(x)y}_{\text{P recycling from grazer feces}} + \underbrace{\theta l_y y}_{\text{P recycling from grazer respiration}}, \end{aligned} \quad (3.12)$$

$$\begin{aligned} \frac{dC}{dt} = & \underbrace{l_x x}_{\text{producer respiration}} + \underbrace{l_y y}_{\text{grazer respiration}} - \underbrace{rx \left(1 - \frac{x}{\min\{K, p/q, h(C)\}} \right)}_{\text{C uptake by producer}} \\ & + \underbrace{\left(1 - \hat{e} \min \left\{ 1, \frac{p/x}{\theta} \right\} \right) f(x)y}_{\text{C recycling from grazer feces}} + \underbrace{\hat{d}y}_{\text{C recycling from dead grazer}}. \end{aligned} \quad (3.13)$$

In addition to incorporating the fact that Rubisco is not carbon dioxide saturated at ambient atmospheric concentrations, this model also includes the reduction in photorespiration rate due to competitive inhibition of the oxygenation reaction in Equation (3.9). Here $\rho(C)$ is a decreasing function of C which allows for the reduction of photorespiration at higher carbon levels. We observe that $\rho(C)$ should not tend towards 0 as $C \rightarrow \infty$ since the total respiration term should also include mitochondrial/cellular respiration.

The net respiration of the producer can be modelled using [51]

$$\text{Net respiration} = \frac{2\Gamma_* V_{cmax}}{C_c + K_c(1 + O/K_o)} + R_d,$$

where C_c is the CO₂ partial pressure at the reaction site (μbar); Γ_* is the CO₂ partial pressure at which the carboxylation rate is equal to half the oxygenation rate (μbar); V_{cmax} is the maximal carboxylation rate ($\mu\text{mol m}^{-2}\text{s}^{-1}$); K_c is the CO₂ Michaelis Menten constant (μbar); O is the O₂ partial pressure at the reaction site (mbar); K_o is the O₂ Michaelis Menten constant (mbar); and R_d is the cellular respiration in light not associated with the PCO pathway ($\mu\text{mol m}^{-2}\text{s}^{-1}$). Note that some of these parameters vary between autotroph species. Values were selected from [51].

This equation produces a respiration rate in $\mu\text{molm}^{-2}\text{s}^{-1}$. In Equation (3.9), $\rho(C)$ is a dimensionless quantity. However, the above formula can be used to find approximate values of the net respiration rate which can be rescaled such that $\rho(C) = 1$ at ambient carbon dioxide concentration. These values can then be used to find appropriate parameters for a function of the form $\rho(C) = \eta + \zeta e^{-\xi C}$. This form was selected to reduce the number of parameters

and the complexity of estimating these quantities.

Once again, the system is closed locally to both carbon and phosphorus. Therefore, we can reduce the dimensionality of the system as in Section 3.2.1.

3.2.3 Local open model

The third model extends the local closed model by allowing for some degree of openness in the system for carbon (Equation (3.18)):

$$\frac{dx}{dt} = \underbrace{rx \left(1 - \frac{x}{\min\{K, p/q, h(C)\}} \right)}_{\text{producer growth limited by nutrient, light, \& carbon}} - \underbrace{f(x)y}_{\text{uptake by grazers}} - \underbrace{l_x x}_{\text{respiration}}, \quad (3.14)$$

$$\frac{dy}{dt} = \underbrace{\hat{e} \min \left\{ 1, \frac{p/x}{\theta} \right\} f(x)y}_{\text{grazer growth limited by food quality \& quantity}} - \underbrace{\hat{d}y}_{\text{grazer death}} - \underbrace{l_y y}_{\text{respiration}}, \quad (3.15)$$

$$\frac{dp}{dt} = \underbrace{g(P)x}_{\text{P uptake by producer}} - \underbrace{\frac{p}{x} f(x)y}_{\text{P loss due to grazing}} - \underbrace{dp}_{\text{P loss due to producer recycling}}, \quad (3.16)$$

$$\begin{aligned} \frac{dP}{dt} = & \underbrace{-g(P)x}_{\text{P uptake by producer}} + \underbrace{dp}_{\text{P recycling from producer}} + \underbrace{\theta \hat{d}y}_{\text{P recycling from dead grazer}} \\ & + \underbrace{\left(\frac{p}{x} - \hat{e} \min \left\{ \theta, \frac{p}{x} \right\} \right) f(x)y}_{\text{P recycling from grazer feces}} + \underbrace{\theta l_y y}_{\text{P recycling from grazer respiration}}, \end{aligned} \quad (3.17)$$

$$\begin{aligned} \frac{dC}{dt} = & \underbrace{l_x x}_{\text{producer respiration}} + \underbrace{l_y y}_{\text{grazer respiration}} - \underbrace{rx \left(1 - \frac{x}{\min\{K, p/q, h(C)\}} \right)}_{\text{C uptake by producer}} \\ & + \underbrace{\left(1 - \hat{e} \min \left\{ 1, \frac{p/x}{\theta} \right\} \right) f(x)y}_{\text{C recycling from grazer feces}} + \underbrace{\hat{d}y}_{\text{C recycling from dead grazer}} + \underbrace{\alpha(\beta - C)}_{\text{C exchange}}. \end{aligned} \quad (3.18)$$

In this model there is an additional term for the exchange of carbon dioxide through the boundary of the system: $\alpha(\beta - C)$. Here β is the carbon density in the external medium, which is assumed to be constant; that is, the system has no impact on the external source of carbon dioxide. Hence, the rate of exchange of carbon dioxide is proportional to the gradient across the boundary, as in the literature [32]. The parameter α is the rate of exchange between the system and the external environment, also known as the transfer velocity [56]. A higher value of α means the system is more “open”. Note that for $\alpha = 0$, we have the local closed model. As $\alpha \rightarrow \infty$, the system becomes entirely open, and there is an essentially unlimited amount of carbon, as in the WKL model [53]. All parameters are assumed to be positive.

3.2.4 Parameters

The parameters originally present in the WKL model were set at the values given in Wang et al. 2008 [53], with the exception of \hat{d} which was adapted due to the separate loss terms in the equation for grazer carbon.

In order to select the ranges for the total carbon inside the system (T_C) and the fixed external carbon (β), the atmospheric carbon dioxide concentrations used in the experiments conducted by Urabe et al. (2003) [49] were converted to carbon concentrations with classical stoichiometry. The ambient level used was 360 ppm, which is equivalent to 360 mg/l, and one of the elevated values was 1500 ppm, or 1500 mg/l. These numbers were converted to 98.2 (mg C)/l and 409.4 (mg C)/l respectively using a relative atomic mass of carbon equal to 12.0107 g/mol and 15.9994 g/mol for oxygen, which gives a total mass of

carbon dioxide of 44.0095 g/mol [40].

Table 3.1: The parameter (P) values (V) used for simulations.

P	Description	V
r	Producer intrinsic growth rate	0.93 day ⁻¹
K	Producer light-dependent carrying capacity	0.25-2 (mg C)/l
c	Grazer maximal ingestion rate	0.75 day ⁻¹
\hat{c}	Producer maximal phosphorus uptake rate	0.2 (mg P)/(mg C)/day
a	Grazer carbon half-saturation constant	0.25 (mg C)/l
\hat{a}	Producer phosphorus half-saturation constant	0.008 (mg P)/l
\hat{e}	Grazer maximal conversion rate	0.74
d	Producer phosphorus loss rate	0.05 day ⁻¹
θ	Constant grazer P:C ratio	0.04 (mg P)/(mg C)
q	Producer minimal P:C ratio	0.004 (mg P)/(mg C)
T_P	Total system phosphorus	0.003-0.3 (mg P)/l
T_C	Total system carbon	98.2-409.4 (mg C)/l
\hat{d}	Grazer death rate	0.055 day ⁻¹
l_x	Respiration rate of producer	0.183 day ⁻¹
l_y	Respiration rate of grazer	0.165 day ⁻¹
γ	Scaling factor for C-dependent carrying capacity	0.0045-0.021
η	Asymptote for PCO function	0.901639
ζ	Difference between max and asymptote for PCO	0.670890
ξ	Exponent for PCO function	0.019552 1/(mg C)
α	Rate of C exchange between system and exterior	1e-6 - 1e6 day ⁻¹
β	Constant exterior C concentration	98.2-409.4 (mg C)/l

The carbon-dependent carrying capacity is given by $h(C) = \gamma C$. The range of the parameter γ was selected in order to allow for carbon limitation to occur before light limitation prevents growth at ambient carbon concentration. In particular, for $\gamma = 0.00767$, ambient carbon is limiting for $K > 0.75$, and for $\gamma = 0.01023$, ambient carbon is limiting for $K > 1.00$. This allows the addition of the carbon-dependent carrying capacity to have an impact given the range of K studied here.

The respiration parameters were selected by adapting those of Diehl (2007) [11] to the system parameters selected by Wang et al. (2008) [53]. Diehl modelled a *Daphnia*-algae system with explicit respiration of the grazer and algae, as well as a grazer death rate [11]. The values assigned were 0.1 day^{-1} for algal respiration, 0.09 day^{-1} for grazer respiration, and 0.03 day^{-1} for the grazer death rate [11]. Hence, the total loss rate for the grazer used by Diehl (2007) [11] is 0.12 day^{-1} , which is less than the value used for the WKL model [53], which is 0.22 day^{-1} . In order to match the rest of the parameters in the system, the values used by Diehl (2007) [11] were rescaled by the same factor (approximately 1.83) such that the total loss rate matched that in the WKL model [53].

The additional parameters for the local closed model with photorespiration are η , ζ , and ξ . The derivation of the values is described in more detail in Section 3.2.2. Essentially, a formula for net respiration in $\mu\text{molm}^{-2}\text{s}^{-1}$ was used to produce two points, which were then rescaled such that the value of $\rho(C)$ at ambient carbon dioxide is 1, and then used to find parameters for a function of the form $\rho(C) = \eta + \zeta e^{-\xi C}$.

For the parameter that quantifies the degree of openness of the system

in the open model, α , we know $\alpha = 0$ produces the local closed model, and that as $\alpha \rightarrow \infty$, the local open model tends towards the completely open WKL system with respiration. Thus, α was selected to range from 0.000001 to 1000000 to give a broad range in order to begin to consider the impact of α on the system.

3.3 Local Closed: Mathematical Analysis

3.3.1 Invariant set

Similar to the WKL model [53], we have a theorem that shows that solutions which start in a biologically meaningful region remain there for all forward time. As well as the biological constraints discussed in Section 2.3.1, there are two additional restrictions on this set. The first is that the producer population is also bounded by their maximal carbon-dependent carrying capacity ($h(T_C)$), similar to the light and phosphorus limitation conditions. The second is that the amount of carbon in the combined biomass pools should not exceed that in the whole system, similar to the original phosphorus condition. The proof of this theorem also very closely follows that of the dissipativity theorem for the WKL model [53].

Theorem 5. *Solutions of Equations (3.6)-(3.8) with initial conditions in the set Ω remain there for all forward times, where*

$$\Omega = \{(x, y, p) : 0 < x < \min\{K, T_P/q, h(T_C)\}, 0 < y, 0 < p, \\ p + \theta y < T_P, x + y < T_C\}.$$

Proof Let $X(t) \equiv (x(t), y(t), p(t))$ be a solution of Equations (3.6)-(3.8) with initial conditions in Ω . Then, $0 < x(0) < \min\{K, T_P/q, h(T_C)\}$, $0 < y(0)$, $0 < p(0)$, $p(0) + \theta y(0) < T_P$, and $x(0) + y(0) < T_C$. Assume for the sake of contradiction that there is time $t_1 > 0$ such that $X(t)$ touches or crosses the boundary of the closure of Ω ($\bar{\Omega}$) for the first time. Therefore, $(x(t), y(t), p(t)) \in \Omega$ for $0 \leq t < t_1$. We now consider cases for which part of the boundary of $\bar{\Omega}$ $X(t_1)$ lies on.

Case 1 $x(t_1) = 0$ but $p(t_1) \neq 0$. Since $(x(t), y(t), p(t)) \in \Omega$ for $0 \leq t < t_1$, then $0 < p(t)$ and $p(t) + \theta y(t) \leq T_P$ for $0 \leq t \leq t_1$. Also, all parameters are assumed to be positive. Therefore,

$$y(t) \leq T_P/\theta - p(t)/\theta < T_P/\theta$$

for $0 \leq t \leq t_1$. Let $p_1 = \min\{p(t) : t \in [0, t_1]\} > 0$, $x_1 = \max\{x(t) : t \in [0, t_1]\} > 0$, and $y_1 = \max\{y(t) : t \in [0, t_1]\} > 0$. Both x_1 and y_1 are guaranteed to exist since the initial conditions are in Ω and thus are positive. Then for $0 \leq t \leq t_1$, we have (using Equation (3.6))

$$\begin{aligned} \frac{dx}{dt} &= rx \left(1 - \frac{x}{\min\{K, p/q, h(T_C - x - y)\}} \right) - f(x)y - l_x x \\ &\geq rx \left(1 - \frac{\min\{K, T_P/q, h(T_C)\}}{\min\{K, p_1/q, h(T_C - x_1 - y_1)\}} \right) - f'(0)(T_P/\theta)x - l_x x \\ &= \left[r \left(1 - \frac{\min\{K, T_P/q, h(T_C)\}}{\min\{K, p_1/q, h(T_C - x_1 - y_1)\}} \right) - f'(0)(T_P/\theta) - l_x \right] x \equiv \mu x, \end{aligned}$$

where μ is a constant. Then, $x(t) \geq x(0)e^{\mu t}$ for $0 \leq t \leq t_1$, which implies $x(t_1) \geq x(0)e^{\mu t_1} > 0$, which is a contradiction.

The proof of this case relies on the following inequalities. First, for $t \in [0, t_1]$

$$p_1 \leq p(t) \Rightarrow p_1/q \leq p(t)/q.$$

Second, for $t \in [0, t_1]$

$$\begin{aligned} x(t) \leq x_1, y(t) \leq y_1 &\Rightarrow -x_1 \leq -x(t), -y_1 \leq -y(t) \\ &\Rightarrow T_C - x_1 - y_1 \leq T_C - x(t) - y(t) \\ &\Rightarrow h(T_C - x_1 - y_1) \leq h(T_C - x(t) - y(t)), \end{aligned}$$

since $h(C)$ is assumed to be non-decreasing.

Third, for $t \in [0, t_1]$

$$\begin{aligned} p_1/q \leq p(t)/q, h(T_C - x_1 - y_1) &\leq h(T_C - x(t) - y(t)) \\ \Rightarrow \min\{K, p_1/q, h(T_C - x_1 - y_1)\} &\leq \min\{K, p(t)/q, h(T_C - x(t) - y(t))\} \\ \Rightarrow \frac{x}{\min\{K, p(t)/q, h(T_C - x(t) - y(t))\}} &\leq \frac{x}{\min\{K, p_1/q, h(T_C - x_1 - y_1)\}} \\ \Rightarrow 1 - \frac{x}{\min\{K, p_1/q, h(T_C - x_1 - y_1)\}} &\leq 1 - \frac{x}{\min\{K, p(t)/q, h(T_C - x(t) - y(t))\}}. \end{aligned}$$

Fourth, since we assume that $f(0) = 0, f'(x) > 0, f''(x) \leq 0$ for $x \geq 0$, then $f(x) \leq f'(0)x$, where the right hand side is the linear approximation of $f(x)$ at 0.

Case 2 $x(t_1) = \min\{K, T_P/q, h(T_C)\}$. Since $(x(t), y(t), p(t)) \in \Omega$ for $0 \leq t <$

t_1 , we know $0 \leq y(t)$ and $p(t) + \theta y(t) \leq T_P$ for $0 \leq t \leq t_1$. Therefore,

$$p(t) \leq T_P - \theta y(t) \leq T_P$$

for $0 \leq t \leq t_1$. Clearly $T_C - x(t) - y(t) \leq T_C$ for $x(t), y(t) \geq 0$. Since $h(C)$ is non-decreasing, then $h(T_C - x(t) - y(t)) \leq h(T_C)$ for $x(t), y(t) \geq 0$. Hence, for $0 \leq t \leq t_1$, we have from Equation (3.6)

$$\begin{aligned} \frac{dx}{dt} &= rx \left(1 - \frac{x}{\min\{K, p/q, h(T_C - x - y)\}} \right) - f(x)y - l_x x \\ &\leq rx \left(1 - \frac{x}{\min\{K, T_P/q, h(T_C)\}} \right). \end{aligned}$$

Note that the right hand side is logistic growth in x with the carrying capacity given by $\min\{K, T_P/q, h(T_C)\}$. The standard comparison argument yields that $x(t) < \min\{K, T_P/q, h(T_C)\}$ for all $0 \leq t \leq t_1$, a contradiction.

The proof of this case requires on the following inequalities, for $0 \leq t < t_1$:

$$\begin{aligned} p(t) &\leq T_P, h(T_C - x(t) - y(t)) \leq h(T_C) \\ \Rightarrow \min\{K, p(t), h(T_C - x(t) - y(t))\} &\leq \min\{K, T_P, h(T_C)\} \\ \Rightarrow \frac{x}{\min\{K, T_P, h(T_C)\}} &\leq \frac{x}{\min\{K, p(t), h(T_C - x(t) - y(t))\}} \\ \Rightarrow -\frac{x}{\min\{K, p(t), h(T_C - x(t) - y(t))\}} &\leq -\frac{x}{\min\{K, T_P, h(T_C)\}} \\ \Rightarrow 1 - \frac{x}{\min\{K, p(t), h(T_C - x(t) - y(t))\}} &\leq 1 - \frac{x}{\min\{K, T_P, h(T_C)\}}. \end{aligned}$$

Case 3 $y(t_1) = 0$. For $0 \leq t \leq t_1$, we have from Equation (3.7)

$$\begin{aligned} \frac{dy}{dt} &= \hat{e} \min \left\{ 1, \frac{p/x}{\theta} \right\} f(x)y - \hat{d}y - l_y y \\ &= \left(\hat{e} \min \left\{ 1, \frac{p/x}{\theta} \right\} f(x) - \hat{d} - l_y \right) y \\ &\geq (-\hat{d} - l_y)y = -(\hat{d} + l_y)y, \end{aligned}$$

since all parameters are assumed to be positive; $f(0) = 0$, $f'(x) > 0$, $f''(x) \leq 0$ for $x \geq 0$; and $(x(t), y(t), p(t)) \in \Omega$ for $0 \leq t < t_1$. Hence, $y(t) \geq y(0)e^{-(\hat{d}+l_y)t} > 0$ for $0 \leq t \leq t_1$, a contradiction.

Case 4 $p(t_1) = 0$. Since $(x(t), y(t), p(t)) \in \Omega$ for $0 \leq t < t_1$, we know $p(t) + \theta y(t) \leq T_P$ for $0 \leq t \leq t_1$. Therefore, $T_P - p(t) - \theta y(t) \geq 0$ for $0 \leq t \leq t_1$, and since we assume that in general $g(0) = 0$ and $g'(P) > 0$ for $P \geq 0$, then

$$g(T_P - p(t) - \theta y(t)) \geq 0$$

for $0 \leq t \leq t_1$.

Also, since $0 \leq p(t)$ and $p(t) + \theta y(t) \leq T_P$ for $0 \leq t \leq t_1$, then

$$y(t) \leq T_P/\theta - p(t)/\theta \leq T_P/\theta$$

for $0 \leq t \leq t_1$, and therefore $-T_P/\theta \leq -y(t)$.

Thus, for $0 \leq t \leq t_1$, we have from Equation (3.8)

$$\begin{aligned} \frac{dp}{dt} &= g(T_P - p - \theta y)x - \frac{p}{x}f(x)y - dp \geq -\frac{p}{x}f(x)y - dp \\ &\geq [-f'(0)(T_P/\theta) - d]p \equiv \nu p, \end{aligned}$$

where ν is a constant. Thus, $p(t) \geq p(0)e^{\nu t} > 0$ for $0 \leq t \leq t_1$, a contradiction.

The proof of Case 4 also relies on the fact that since $f(0) = 0$, $f'(x) > 0$, $f''(x) \leq 0$ for $x \geq 0$, then $f(x) \leq f'(0)x$ and thus $-f'(0) \leq -f(x)/x$.

Case 5 $p(t_1) + \theta y(t_1) = T_P$. Let $z(t) = T_P - p(t) - \theta y(t)$. Since $p(t_1) + \theta y(t_1) = T_P$, then $z(t_1) = 0$. Also, since t_1 is assumed to be the first time that $X(t)$ touches or crosses the boundary of $\bar{\Omega}$, then $p(t) + \theta y(t) < T_P$ for $0 \leq t < t_1$ and thus $z(t) > 0$ for $0 \leq t < t_1$. Then for $0 \leq t \leq t_1$, we have

$$\begin{aligned}
\frac{dz}{dt} &= \frac{d}{dt}(T_P - p - \theta y) \\
&= \frac{d}{dt}T_P - \frac{dp}{dt} - \theta \frac{dy}{dt} \\
&= -\frac{dp}{dt} - \theta \frac{dy}{dt} \\
&= -\left(g(T_P - p - \theta y)x - \frac{p}{x}f(x)y - dp\right) \\
&\quad - \theta \left(\hat{e} \min\left\{1, \frac{p/x}{\theta}\right\} f(x)y - \hat{d}y - l_y y\right) \\
&= -g(T_P - p - \theta y)x + \frac{p}{x}f(x)y + dp - \theta \hat{e} \min\left\{1, \frac{p/x}{\theta}\right\} f(x)y \\
&\quad + \theta \hat{d}y + \theta l_y y \\
&\geq -g(T_P - p - \theta y)x + dp + \theta \hat{d}y + \theta l_y y \\
&\geq -g(z)x + dp + (\hat{d} + l_y)\theta y \\
&\geq -g'(0)z \min\{K, T_P/q, h(T_C)\} + \min\{d, \hat{d} + l_y\}(T_P - z) \\
&= \min\{d, \hat{d} + l_y\}T_P - [g'(0) \min\{K, T_P/q, h(T_C)\} + \min\{d, \hat{d} + l_y\}]z \\
&\equiv \tilde{\mu} - \tilde{\nu}z,
\end{aligned}$$

where $\tilde{u} > 0$ and $\tilde{\nu} > 0$ are constant. Thus $z(t) \geq e^{-\tilde{\nu}t}z(0) > 0$ for $0 \leq t \leq t_1$, a contradiction.

Case 6 $x(t_1) + y(t_1) = T_C$. Consider the limit of dx/dt as $t \rightarrow t_1$:

$$\begin{aligned}\lim_{t \rightarrow t_1} \frac{dx}{dt} &= \lim_{t \rightarrow t_1} \left[rx \left(1 - \frac{x}{\min\{K, p/q, h(T_C - x - y)\}} \right) - f(x)y - l_x x \right] \\ &= \lim_{t \rightarrow t_1} rx \left(1 - \frac{x}{\min\{K, p/q, h(T_C - x - y)\}} \right) - \lim_{t \rightarrow t_1} f(x)y - \lim_{t \rightarrow t_1} l_x x \\ &= rx(t_1) - \lim_{t \rightarrow t_1} \frac{rx^2}{\min\{K, p/q, h(T_C - x - y)\}} - f(x(t_1))y(t_1) - l_x x(t_1).\end{aligned}$$

Since $h(0) = 0$, then the limit as $t \rightarrow t_1$ of $\min\{K, p/q, h(T_C - x - y)\}$ is 0. However, $x(t_1) > 0$. Therefore, as $t \rightarrow t_1$, the limit of dx/dt is $-\infty$. Clearly this implies that $dy/dt \rightarrow -\infty$ as $t \rightarrow t_1$. But then as $t \rightarrow t_1$, $x(t) + y(t) \rightarrow -\infty$, a contradiction.

3.3.2 Equilibria

Consider the local closed model, Equations (3.6)-(3.8). Let $h(C) = \gamma C$. We consider two cases for f and g , dependent on if both f and g are Holling type I or Holling type II functional responses.

Holling type I

Substituting $f(x) = cx$, $g(P) = \hat{c}P$ and $h(C) = \gamma C$ into Equations (3.6) - (3.8), we get the following system:

$$\begin{aligned}\frac{dx}{dt} &= rx \left(1 - \frac{x}{\min\{K, p/q, \gamma(T_C - x - y)\}} \right) - cxy - l_x x, \\ \frac{dy}{dt} &= \hat{e} \min \left\{ 1, \frac{p/x}{\theta} \right\} cxy - \hat{d}y - l_y y, \\ \frac{dp}{dt} &= \hat{c}(T_P - p - \theta y)x - \frac{p}{x} cxy - dp.\end{aligned}$$

Equilibria satisfy

$$\begin{aligned}
0 &= \bar{x} \left(r \left(1 - \frac{\bar{x}}{\min\{K, \bar{p}/q, \gamma(T_C - \bar{x} - \bar{y})\}} \right) - c\bar{y} - l_x \right) \equiv \bar{x}F(\bar{x}, \bar{y}, \bar{p}), \\
0 &= \bar{y} \left(\hat{e} \min \left\{ 1, \frac{\bar{p}/\bar{x}}{\theta} \right\} c\bar{x} - \hat{d} - l_y \right) \equiv \bar{y}G(\bar{x}, \bar{y}, \bar{p}), \\
0 &= \hat{c}(T_P - \bar{p} - \theta\bar{y})\bar{x} - c\bar{p}\bar{y} - d\bar{p} \equiv H(\bar{x}, \bar{y}, \bar{p}).
\end{aligned}$$

Clearly the trivial extinction equilibrium $E_0 = (0, 0, 0)$ is a possible solution of the above. We can also explicitly find the form of the grazer extinction equilibrium. The grazer extinction equilibrium always takes the form $E_1 = (\bar{x}, 0, \bar{p})$, where \bar{x} and \bar{p} are decided by what is limiting the producer.

When the producer is phosphorus limited at equilibrium ($\bar{p}/q \leq K, \gamma(T_C - \bar{x} - \bar{y})$), the grazer extinction equilibrium is given by $(\bar{x}, 0, \bar{p})$ where

$$\begin{aligned}
\bar{x} &= \frac{\hat{c}T_P(r - l_x) - dqr}{\hat{c}qr}, \\
\bar{p} &= \frac{\hat{c}T_P(r - l_x) - dqr}{\hat{c}(r - l_x)}.
\end{aligned}$$

We assume all parameters are positive. For $\bar{x} \geq 0$, we need $\hat{c}T_P(r - l_x) - dqr \geq 0$. Then, for $\bar{p} \geq 0$, we need $r - l_x > 0$.

When the producer is light limited at equilibrium ($K \leq \bar{p}/q, \gamma(T_C - \bar{x} - \bar{y})$), we have $(\bar{x}, 0, \bar{p})$ where

$$\begin{aligned}
\bar{x} &= K \left(1 - \frac{l_x}{r} \right), \\
\bar{p} &= \frac{\hat{c}T_P K (r - l_x)}{dr + \hat{c}K(r - l_x)}.
\end{aligned}$$

Note that for this equilibrium to be biologically feasible (i.e., non-negative), we require $r - l_x \geq 0$, since

$$r - l_x \geq 0 \iff r \geq l_x \iff 1 \geq \frac{l_x}{r} \iff 1 - \frac{l_x}{r} \geq 0.$$

Lastly, when the producer is carbon limited at equilibrium ($\gamma(T_C - \bar{x} - \bar{y}) \leq K, \bar{p}/q$), we have $(\bar{x}, 0, \bar{p})$ where

$$\begin{aligned}\bar{x} &= \frac{\gamma T_C (r - l_x)}{r + \gamma r - \gamma l_x}, \\ \bar{p} &= \frac{\hat{c} \gamma T_C T_P (r - l_x)}{d(r + \gamma r - \gamma l_x) + \hat{c} \gamma T_C (r - l_x)}.\end{aligned}$$

For this equilibrium to be biologically feasible and not equal to E_0 , we require either $r - l_x > 0$ and $r + \gamma r - \gamma l_x > 0$, or $r - l_x < 0$ and $r + \gamma r - \gamma l_x < 0$.

There may also be coexistence equilibria, which would satisfy

$$\begin{aligned}0 &= r \left(1 - \frac{\bar{x}}{\min\{K, \bar{p}/q, \gamma(T_C - \bar{x} - \bar{y})\}} \right) - c\bar{y} - l_x = F(\bar{x}, \bar{y}, \bar{p}), \\ 0 &= \hat{e} \min \left\{ 1, \frac{\bar{p}/\bar{x}}{\theta} \right\} c\bar{x} - \hat{d} - l_y = G(\bar{x}, \bar{y}, \bar{p}), \\ 0 &= \hat{c}(T_P - \bar{p} - \theta\bar{y})\bar{x} - c\bar{p}\bar{y} - d\bar{p} = H(\bar{x}, \bar{y}, \bar{p}).\end{aligned}$$

The results of this section are summarized in the following theorem.

Theorem 6. *The local closed model (3.6) - (3.8) with Holling type I functional responses has the trivial extinction equilibrium $E_0 = (0, 0, 0)$ which always exists, up to one grazer extinction equilibrium E_1 , and may have coexistence equilibria, where the grazer extinction equilibrium satisfies the following:*

(i) If $\bar{p}/q \leq \min\{K, \gamma(T_C - \bar{x} - \bar{y})\}$, then

$$E_1 = \left(\frac{\hat{c}T_P(r - l_x) - dqr}{\hat{c}qr}, 0, \frac{\hat{c}T_P(r - l_x) - dqr}{\hat{c}(r - l_x)} \right);$$

(ii) If $K \leq \min\{\bar{p}/q, \gamma(T_C - \bar{x} - \bar{y})\}$, then

$$E_1 = \left(K \left(1 - \frac{l_x}{r} \right), 0, \frac{\hat{c}T_P K(r - l_x)}{dr + \hat{c}K(r - l_x)} \right);$$

(iii) If $\gamma(T_C - \bar{x} - \bar{y}) \leq \min\{K, \bar{p}/q\}$, then

$$E_1 = \left(\frac{\gamma T_C(r - l_x)}{r + \gamma r - \gamma l_x}, 0, \frac{\hat{c}\gamma T_C T_P(r - l_x)}{d(r + \gamma r - \gamma l_x) + \hat{c}\gamma T_C(r - l_x)} \right).$$

Holling type II

Using $f(x) = cx/(a + x)$, $g(P) = \hat{c}P/(\hat{a} + P)$, and $h(C) = \gamma C$,

$$\begin{aligned} \frac{dx}{dt} &= rx \left(1 - \frac{x}{\min\{K, p/q, \gamma(T_C - x - y)\}} \right) - \frac{cx}{a + x}y - l_x x, \\ \frac{dy}{dt} &= \hat{e} \min \left\{ 1, \frac{p/x}{\theta} \right\} \frac{cx}{a + x}y - \hat{d}y - l_y y, \\ \frac{dp}{dt} &= \frac{\hat{c}(T_P - p - \theta y)}{\hat{a} + T_P - p - \theta y}x - \frac{p}{x} \frac{cx}{a + x}y - dp. \end{aligned}$$

Equilibria satisfy

$$\begin{aligned} 0 &= \bar{x} \left(r \left(1 - \frac{\bar{x}}{\min\{K, \bar{p}/q, \gamma(T_C - \bar{x} - \bar{y})\}} \right) - \frac{c}{a + \bar{x}}\bar{y} - l_x \right) \equiv \bar{x}F(\bar{x}, \bar{y}, \bar{p}), \\ 0 &= \bar{y} \left(\hat{e} \min \left\{ 1, \frac{\bar{p}/\bar{x}}{\theta} \right\} \frac{c\bar{x}}{a + \bar{x}} - \hat{d} - l_y \right) \equiv \bar{y}G(\bar{x}, \bar{y}, \bar{p}), \\ 0 &= \frac{\hat{c}(T_P - \bar{p} - \theta\bar{y})}{\hat{a} + T_P - \bar{p} - \theta\bar{y}}\bar{x} - \frac{c\bar{p}}{a + \bar{x}}\bar{y} - d\bar{p} \equiv H(\bar{x}, \bar{y}, \bar{p}). \end{aligned}$$

Clearly the trivial extinction equilibrium $E_0 = (0, 0, 0)$ is a possible solution of this system. We can explicitly find the form of the grazer extinction equilibrium/a, dependent upon what is limiting the producer.

When the producer is phosphorus limited at equilibrium ($\bar{p}/q \leq K, \gamma(T_C - \bar{x} - \bar{y})$), the grazer extinction equilibrium is given by $(\bar{x}, \bar{y}, \bar{p})$ where

$$\begin{aligned}\bar{x} &= \frac{\bar{p}}{q} \left(1 - \frac{l_x}{r}\right) = \frac{dqr(\hat{a} + T_P)(r - l_x) - \hat{c}T_P(r - l_x)^2}{dq^2r^2 - \hat{c}qr(r - l_x)}, \\ \bar{y} &= 0, \\ \bar{p} &= \frac{dq(\hat{a} + T_P) - \hat{c}T_P \left(1 - \frac{l_x}{r}\right)}{dq - \hat{c} \left(1 - \frac{l_x}{r}\right)} = \frac{dqr(\hat{a} + T_P) - \hat{c}T_P(r - l_x)}{dqr - \hat{c}(r - l_x)}.\end{aligned}$$

Consider the equation for \bar{x} that includes \bar{p} . Since we require $\bar{x}, \bar{y}, \bar{p} \geq 0$ for the equilibrium to be biologically feasible, then we require $r - l_x \geq 0$, since otherwise \bar{x} is negative for positive \bar{p} . The equation for \bar{p} would also yield additional conditions for non-negativity, which are not included here.

When the producer is light limited at equilibrium ($K \leq \bar{p}/q, \gamma(T_C - \bar{x} - \bar{y})$), we have two possible grazer extinction equilibria, given by $(\bar{x}, \bar{y}, \bar{p})$ where

$$\begin{aligned}\bar{x} &= K \left(1 - \frac{l_x}{r}\right), \\ \bar{y} &= 0, \\ \bar{p} &= \frac{\hat{c}K(r - l_x) + dr(\hat{a} + T_P) \pm \sqrt{(\hat{c}K(r - l_x) + dr(\hat{a} + T_P))^2 - 4\hat{c}dKrT_P(r - l_x)}}{2dr}.\end{aligned}$$

For $\bar{x} \geq 0$ to be true, we need $r - l_x \geq 0$. Hence, for $r - l_x < 0$, this equilibrium is not biologically feasible. The equation for \bar{p} yields conditions for existence of the equilibrium that are not included here.

Lastly, when the producer is carbon limited at equilibrium ($\gamma(T_C - \bar{x} - \bar{y}) \leq K, \bar{p}/q$), we again have two possible grazer extinction equilibria, given by $(\bar{x}, \bar{y}, \bar{p})$ where

$$\begin{aligned}\bar{x} &= \frac{\gamma T_C(r - l_x)}{r + \gamma r - \gamma l_x}, \\ \bar{y} &= 0, \\ \bar{p} &= \frac{\hat{c}\gamma T_C(r - l_x) + d(\hat{a} + T_P)(r + \gamma r - \gamma l_x)}{2d(r + \gamma r - \gamma l_x)} \\ &\quad \pm \frac{\sqrt{(\hat{c}\gamma T_C(r - l_x) + d(\hat{a} + T_P)(r + \gamma r - \gamma l_x))^2 - 4\hat{c}d\gamma T_C T_P(r - l_x)(r + \gamma r - \gamma l_x)}}{2d(r + \gamma r - \gamma l_x)}.\end{aligned}$$

For $\bar{x} \geq 0$, we need either $r - l_x \geq 0$ and $r + \gamma r - \gamma l_x > 0$, or $r - l_x \leq 0$ and $r + \gamma r - \gamma l_x < 0$. Note that $r - l_x > 0$ and $r + \gamma r - \gamma l_x < 0$ is not possible for positive parameters. Thus, the equilibrium is not biologically feasible if $r - l_x < 0$ and $r + \gamma r - \gamma l_x > 0$. As in the light limited case, the equation for \bar{p} would also yield conditions for existence of the equilibria.

There may also be coexistence equilibria, which would satisfy

$$\begin{aligned}0 &= r \left(1 - \frac{\bar{x}}{\min\{K, \bar{p}/q, \gamma(T_C - \bar{x} - \bar{y})\}} \right) - \frac{c}{a + \bar{x}}\bar{y} - l_x = F(\bar{x}, \bar{y}, \bar{p}), \\ 0 &= \hat{e} \min \left\{ 1, \frac{\bar{p}/\bar{x}}{\theta} \right\} \frac{c\bar{x}}{a + \bar{x}} - \hat{d} - l_y = G(\bar{x}, \bar{y}, \bar{p}), \\ 0 &= \frac{\hat{c}(T_P - \bar{p} - \theta\bar{y})}{\hat{a} + T_P - \bar{p} - \theta\bar{y}}\bar{x} - \frac{c\bar{p}}{a + \bar{x}}\bar{y} - d\bar{p} = H(\bar{x}, \bar{y}, \bar{p}).\end{aligned}$$

The following theorem summarizes these results.

Theorem 7. *The local closed model (3.6) - (3.8) with Holling type II functional responses has the trivial extinction equilibrium $E_0 = (0, 0, 0)$ which always exists, up to two grazer extinction equilibria E_1 , and may have coexistence*

equilibria, where the grazer extinction equilibria satisfy the following:

(i) If $\bar{p}/q \leq \min\{K, \gamma(T_C - \bar{x} - \bar{y})\}$, then there is one grazer extinction equilibrium, given by

$$E_1 = \left(\frac{dqr(\hat{a} + T_P)(r - l_x) - \hat{c}T_P(r - l_x)^2}{dq^2r^2 - \hat{c}qr(r - l_x)}, 0, \frac{dqr(\hat{a} + T_P) - \hat{c}T_P(r - l_x)}{dqr - \hat{c}(r - l_x)} \right);$$

(ii) If $K \leq \min\{\bar{p}/q, \gamma(T_C - \bar{x} - \bar{y})\}$, then there are two grazer extinction equilibria, given by $E_1 = (\bar{x}, 0, \bar{p})$ where

$$\bar{x} = K \left(1 - \frac{l_x}{r} \right),$$

$$\bar{p} = \frac{\hat{c}K(r - l_x) + dr(\hat{a} + T_P) \pm \sqrt{(\hat{c}K(r - l_x) + dr(\hat{a} + T_P))^2 - 4\hat{c}dKrT_P(r - l_x)}}{2dr};$$

(iii) If $\gamma(T_C - \bar{x} - \bar{y}) \leq \min\{K, \bar{p}/q\}$, then there are two grazer extinction equilibria, given by $E_1 = (\bar{x}, 0, \bar{p})$ where

$$\bar{x} = \frac{\gamma T_C(r - l_x)}{r + \gamma r - \gamma l_x},$$

$$\bar{p} = \frac{\hat{c}\gamma T_C(r - l_x) + d(\hat{a} + T_P)(r + \gamma r - \gamma l_x)}{2d(r + \gamma r - \gamma l_x)} \pm \frac{\sqrt{(\hat{c}\gamma T_C(r - l_x) + d(\hat{a} + T_P)(r + \gamma r - \gamma l_x))^2 - 4\hat{c}d\gamma T_C T_P(r - l_x)(r + \gamma r - \gamma l_x)}}{2d(r + \gamma r - \gamma l_x)}.$$

3.3.3 Stability

For the trivial extinction steady state, we have a theorem with a sufficient condition for stability in the local closed model. This is very similar to a theorem proven for the WKL model [53], and the proof follows similarly. Note that this theorem holds for the general forms of f , g , and h .

Theorem 8. *If $d > mg(T_P)$, where $m = \min\{x(0)/p(0), [1 + (d - l_x)/r]/q\}$, then the trivial steady state $E_0 = (0, 0, 0)$ for (3.6) - (3.8) is globally asymptotically stable.*

Proof: Let $u = x/p$, then

$$\begin{aligned}
\frac{du}{dt} &= \frac{d}{dt} \frac{x}{p} = \frac{(dx/dt)p - x(dp/dt)}{p^2} = \frac{dx/dt}{p} - x \frac{dp/dt}{p^2} \\
&= \frac{rx}{p} \left(1 - \frac{x}{\min\{K, p/q, h(T_C - x - y)\}} \right) - \frac{f(x)y}{p} - \frac{l_x x}{p} \\
&\quad - \frac{x^2}{p^2} g(T_P - p - \theta y) + \frac{f(x)y}{p} + d \frac{x}{p} \\
&= \frac{rx}{p} \left(1 - \frac{x}{\min\{K, p/q, h(T_C - x - y)\}} \right) - \frac{l_x x}{p} - \frac{x^2}{p^2} g(T_P - p - \theta y) + d \frac{x}{p} \\
&= ru \left(1 - \frac{x}{\min\{K, p/q, h(T_C - x - y)\}} \right) - l_x u - u^2 g(T_P - p - \theta y) + du.
\end{aligned}$$

Since $g(0) = 0$ and $g'(P) > 0$ for $P \geq 0$, then $-u^2 g(T_P - p - \theta y) \leq 0$. Note that $\min\{K, p/q, h(T_C - x - y)\} \leq p/q$ if and only if

$$-\frac{1}{\min\{K, p/q, h(T_C - x - y)\}} \leq -\frac{1}{p/q}.$$

Thus

$$\begin{aligned}
\frac{du}{dt} &\leq ru \left(1 - \frac{x}{p/q} \right) - l_x u + du \\
&= ru(1 - qu) - l_x u + du = ru(1 - qu) + (d - l_x)u \\
&\leq ru(1 - qu) + ru \frac{d - l_x}{r} = ru \left(1 - qu + \frac{d - l_x}{r} \right).
\end{aligned}$$

Hence, $u \leq \min\{x(0)/p(0), [1 + (d - l_x)/r]/q\} \equiv m$. Consider the equation for (dp/dt) :

$$\begin{aligned}\frac{dp}{dt} &= g(T_P - p - \theta y)x - \frac{p}{x}f(x)y - dp \leq g(T_P)x - dp \\ &\leq g(T_P)mp - dp = (g(T_P)m - d)p.\end{aligned}$$

Since $d > mg(T_P)$ implies $g(T_P)m - d < 0$, then $dp/dt < 0$ and thus $p \rightarrow 0$ as $t \rightarrow \infty$.

Now, consider the equation for (dx/dt) :

$$\begin{aligned}\frac{dx}{dt} &= rx \left(1 - \frac{x}{\min\{K, p/q, h(T_C - x - y)\}} \right) - f(x)y - l_x x \\ &\leq rx(1 - (qx/p)).\end{aligned}$$

Hence $\limsup_{t \rightarrow \infty} x(t) \leq p/q$ and $x \rightarrow 0$ as $t \rightarrow \infty$. Given the dependence of y on x , this implies that $y \rightarrow 0$ as $t \rightarrow \infty$. Therefore, the extinction steady state $E_0 = (0, 0, 0)$ is globally asymptotically stable if $d > mg(T_P)$, where $m = \min\{x(0)/p(0), [1 + (d - l_x)/r]/q\}$.

It remains to investigate the stability of the other boundary equilibria. We have

$$\begin{aligned}\frac{dx}{dt} &= xF(x, y, p), \\ \frac{dy}{dt} &= yG(x, y, p), \\ \frac{dp}{dt} &= H(x, y, p).\end{aligned}$$

The Jacobian matrix is

$$A = \begin{bmatrix} F + xF_x & xF_y & xF_p \\ yG_x & G + yG_y & yG_p \\ H_x & H_y & H_p \end{bmatrix}.$$

Let A_{kk} be the determinant of the matrix produced by removing row k and column k from matrix A . By Routh-Hurwitz criterion, all eigenvalues of A have strictly negative real parts if the following conditions hold [53]: $\text{tr}A < 0$; $\det A < 0$; and $\det A - (\text{tr}A)(\sum_{k=1}^3 A_{kk}) > 0$.

Once again, we consider Equations (3.6)-(3.8) where f and g are both Holling type I functional responses, then when both are Holling type II functional responses. Throughout, we assume $h(C) = \gamma C$.

Regardless of what form f and g take, we will have to consider six cases:

1. $\bar{p}/q \leq \min\{K, \gamma(T_C - \bar{x} - \bar{y})\}$ and $\bar{p} < \theta\bar{x}$: producer is nutrient limited and grazer is limited by food quality;
2. $\bar{p}/q \leq \min\{K, \gamma(T_C - \bar{x} - \bar{y})\}$ and $\bar{p} > \theta\bar{x}$: producer is nutrient limited and grazer is limited by food quantity;
3. $K \leq \min\{\bar{p}/q, \gamma(T_C - \bar{x} - \bar{y})\}$ and $\bar{p} < \theta\bar{x}$: producer is light limited and grazer is limited by food quality;
4. $K \leq \min\{\bar{p}/q, \gamma(T_C - \bar{x} - \bar{y})\}$ and $\bar{p} > \theta\bar{x}$: producer is light limited and grazer is limited by food quantity;
5. $\gamma(T_C - \bar{x} - \bar{y}) \leq \min\{K, \bar{p}/q\}$ and $\bar{p} < \theta\bar{x}$: producer is carbon limited and grazer is limited by food quality;

6. $\gamma(T_C - \bar{x} - \bar{y}) \leq \min\{K, \bar{p}/q\}$ and $\bar{p} > \theta\bar{x}$: producer is carbon limited and grazer is limited by food quantity.

Holling type I

For $f(x) = cx$, $g(P) = \hat{c}P$, and $h(C) = \gamma C$,

$$\begin{aligned} \frac{\partial F}{\partial x} &= \begin{cases} -\frac{r}{\min\{K, p/q\}}, & \gamma(T_C - x - y) \geq K \text{ or } p/q, \\ -\frac{r(T_C - y)}{\gamma(T_C - x - y)^2}, & \gamma(T_C - x - y) < K \text{ and } p/q, \end{cases} \\ \frac{\partial F}{\partial y} &= \begin{cases} -c, & \gamma(T_C - x - y) \geq K \text{ or } p/q, \\ -\frac{rx}{\gamma(T_C - x - y)^2} - c, & \gamma(T_C - x - y) < K \text{ and } p/q, \end{cases} \\ \frac{\partial F}{\partial p} &= \begin{cases} 0, & p/q \geq K \text{ or } \gamma(T_C - x - y), \\ \frac{rxq}{p^2}, & p/q < K \text{ and } \gamma(T_C - x - y), \end{cases} \\ \frac{\partial G}{\partial x} &= \begin{cases} \hat{c}c, & 1 < p/x/\theta, \\ 0, & 1 \geq p/x/\theta, \end{cases} \\ \frac{\partial G}{\partial y} &= 0, \\ \frac{\partial G}{\partial p} &= \begin{cases} 0, & 1 < p/x/\theta, \\ \frac{\hat{c}c}{\theta}, & 1 \geq p/x/\theta, \end{cases} \\ \frac{\partial H}{\partial x} &= \hat{c}(T_P - p - \theta y), \\ \frac{\partial H}{\partial y} &= -\hat{c}\theta x - cp, \\ \frac{\partial H}{\partial p} &= -\hat{c}x - cy - d. \end{aligned}$$

We compute the products/sums we need for the Jacobian:

$$\begin{aligned}
xF_x &= \begin{cases} -\frac{rx}{\min\{K, p/q\}}, & \gamma(T_C - x - y) \geq K \text{ or } p/q, \\ -\frac{rx(T_C - y)}{\gamma(T_C - x - y)^2}, & \gamma(T_C - x - y) < K \text{ and } p/q, \end{cases} \\
F + xF_x &= \begin{cases} r - \frac{2rx}{\min\{K, p/q\}} - cy - l_x, & \gamma(T_C - x - y) \geq K \text{ or } p/q, \\ r - \frac{rx(2T_C - x - 2y)}{\gamma(T_C - x - y)^2} - cy - l_x, & \gamma(T_C - x - y) < K \text{ and } p/q, \end{cases} \\
xF_y &= \begin{cases} -cx, & \gamma(T_C - x - y) \geq K \text{ or } p/q, \\ -\frac{rx^2}{\gamma(T_C - x - y)^2} - cx, & \gamma(T_C - x - y) < K \text{ and } p/q, \end{cases} \\
xF_p &= \begin{cases} 0, & p/q \geq K \text{ or } \gamma(T_C - x - y), \\ \frac{rx^2q}{p^2}, & p/q < K \text{ and } \gamma(T_C - x - y), \end{cases} \\
yG_x &= \begin{cases} \hat{e}cy, & 1 < p/x/\theta, \\ 0, & 1 \geq p/x/\theta, \end{cases} \\
yG_y &= 0, \\
G + yG_y &= G = \hat{e} \min \left\{ 1, \frac{p/x}{\theta} \right\} cx - \hat{d} - l_y, \\
yG_p &= \begin{cases} 0, & 1 < p/x/\theta, \\ \frac{\hat{e}cy}{\theta}, & 1 \geq p/x/\theta. \end{cases}
\end{aligned}$$

There are different Jacobian matrices dependent upon the limiting factors. We determine the entries based on what is limiting for the producer (nutrient, light, or carbon) and grazer (quality or quantity), then substitute the equilibria found in Section 3.3.2.

CASE 1: Nutrient and quality

The corresponding Jacobian matrix is

$$A_1 = \begin{bmatrix} a_{11} & a_{12} & a_{13} \\ a_{21} & a_{22} & a_{23} \\ a_{31} & a_{32} & a_{33} \end{bmatrix},$$

where

$$a_{11} = l_x - r,$$

$$a_{12} = \frac{-c\hat{c}T_P(r - l_x) + cdqr}{\hat{c}qr},$$

$$a_{13} = \frac{(r - l_x)^2}{qr},$$

$$a_{21} = 0,$$

$$a_{22} = \frac{c\hat{c}\hat{e}T_P(r - l_x) - cd\hat{e}qr}{\hat{c}\theta(r - l_x)} - \hat{d} - l_y,$$

$$a_{23} = 0,$$

$$a_{31} = \frac{dqr}{r - l_x},$$

$$a_{32} = -\frac{\hat{c}T_P\theta(r - l_x) - dqr\theta}{qr} - \frac{c\hat{c}T_P(r - l_x) - cdqr}{\hat{c}(r - l_x)},$$

$$a_{33} = -\frac{\hat{c}T_P(r - l_x)}{qr}.$$

Determining the eigenvalues here is not particularly illuminating, as in the nutrient limiting cases in Chapter 2. The eigenvalues, trace, and determinant of this matrix are in Appendix A. From the explicit form of the eigenvalues, we do observe that stability does not depend upon K , T_C , or γ . Given that these factors pertain to light or carbon limitation, and thus do not appear in the

equations in this case due to the minimum term, this result is not unexpected.

CASE 2: Nutrient and quantity

The corresponding Jacobian matrix is

$$A_2 = \begin{bmatrix} a_{11} & a_{12} & a_{13} \\ a_{21} & a_{22} & a_{23} \\ a_{31} & a_{32} & a_{33} \end{bmatrix},$$

where

$$a_{11} = l_x - r,$$

$$a_{12} = \frac{-c\hat{c}T_P(r - l_x) + cdqr}{\hat{c}qr},$$

$$a_{13} = \frac{(r - l_x)^2}{qr},$$

$$a_{21} = 0,$$

$$a_{22} = \frac{c\hat{c}\hat{e}T_P(r - l_x) - cd\hat{e}qr}{\hat{c}qr} - \hat{d} - l_y,$$

$$a_{23} = 0,$$

$$a_{31} = \frac{dqr}{r - l_x},$$

$$a_{32} = -\frac{\hat{c}T_P\theta(r - l_x) - dqr\theta}{qr} - \frac{c\hat{c}T_P(r - l_x) - cdqr}{\hat{c}(r - l_x)},$$

$$a_{33} = -\frac{\hat{c}T_P(r - l_x)}{qr}.$$

Once again, the eigenvalues do not readily provide stability conditions, as in the nutrient limiting cases in Chapter 2. The eigenvalues, trace, and determinant of this matrix are in Appendix A. From the form of the eigenvalues, we observe that stability does not depend upon K , T_C , γ , or θ , because these

parameters do not appear in the equations for the case where nutrient and quantity are limiting due to the minimum functions.

CASE 3: Light and quality

Here, the Jacobian is

$$A_3 = \begin{bmatrix} a_{11} & a_{12} & a_{13} \\ a_{21} & a_{22} & a_{23} \\ a_{31} & a_{32} & a_{33} \end{bmatrix},$$

where

$$a_{11} = l_x - r,$$

$$a_{12} = -cK \left(1 - \frac{l_x}{r} \right),$$

$$a_{13} = 0,$$

$$a_{21} = 0,$$

$$a_{22} = \frac{c\hat{c}\hat{e}KT_P(r - l_x)}{\hat{c}K\theta(r - l_x) + dr\theta} - \hat{d} - l_y,$$

$$a_{23} = 0,$$

$$a_{31} = \frac{\hat{c}drT_P}{\hat{c}K(r - l_x) + dr},$$

$$a_{32} = -\hat{c}\theta K \left(1 - \frac{l_x}{r} \right) - \frac{c\hat{c}KT_P(r - l_x)}{\hat{c}K(r - l_x) + dr},$$

$$a_{33} = -\hat{c}K \left(1 - \frac{l_x}{r} \right) - d.$$

For this matrix, a cofactor expansion along the third column of $(A_3 - \lambda I)$ yields the product of $a_{33} - \lambda$ and the determinant of a 2 x 2 upper triangular matrix. Thus, the eigenvalues of A_3 are along the main diagonal.

The eigenvalues of A_3 are

$$\begin{aligned}\lambda_1 &= l_x - r, \\ \lambda_2 &= \frac{c\hat{c}\hat{e}KT_P(r - l_x)}{\hat{c}K\theta(r - l_x) + dr\theta} - \hat{d} - l_y, \\ \lambda_3 &= -\hat{c}K\left(1 - \frac{l_x}{r}\right) - d.\end{aligned}$$

Stability requires all of these to have a negative real part. For the first eigenvalue, we need $l_x - r < 0$, or $r - l_x > 0$. Note that when this is true,

$$l_x - r < 0 \iff r - l_x > 0 \iff 1 - \frac{l_x}{r} > 0,$$

since r is positive.

Thus if λ_1 is negative, then $\lambda_3 < 0$. Then we just need λ_2 to be negative:

$$\frac{c\hat{c}\hat{e}KT_P(r - l_x)}{\hat{c}K\theta(r - l_x) + dr\theta} - \hat{d} - l_y < 0 \iff \frac{c\hat{c}\hat{e}KT_P(r - l_x)}{\hat{c}K\theta(r - l_x) + dr\theta} < \hat{d} + l_y.$$

Hence, when $r - l_x > 0$ and

$$\frac{c\hat{c}\hat{e}KT_P(r - l_x)}{\hat{c}K\theta(r - l_x) + dr\theta} < \hat{d} + l_y,$$

the grazer extinction equilibrium is a stable node.

Conversely, when $r - l_x > 0$ and

$$\frac{c\hat{c}\hat{e}KT_P(r - l_x)}{\hat{c}K\theta(r - l_x) + dr\theta} > \hat{d} + l_y,$$

the grazer extinction equilibrium is a saddle with a two-dimensional stable

manifold and a one-dimensional unstable manifold.

Now, when $r - l_x < 0$ (i.e., $\lambda_1 > 0$), the sign of neither λ_2 nor λ_3 is guaranteed. Thus, when $r - l_x < 0$ and both of the two following conditions hold, the grazer extinction equilibrium is a saddle with a two-dimensional stable manifold and a one-dimensional unstable manifold:

$$\begin{aligned} \frac{c\hat{c}\hat{K}T_P(r - l_x)}{\hat{c}K\theta(r - l_x) + dr\theta} &< \hat{d} + l_y, \\ -\hat{c}K \left(1 - \frac{l_x}{r}\right) &< d. \end{aligned}$$

If one of these two conditions fails, the equilibrium is a saddle with a one-dimensional stable manifold and a two-dimensional unstable manifold; if both fail, the equilibrium is an unstable node. However, when $r - l_x < 0$, the equilibrium is not biologically feasible.

CASE 4: Light and quantity

Here

$$A_4 = \begin{bmatrix} a_{11} & a_{12} & a_{13} \\ a_{21} & a_{22} & a_{23} \\ a_{31} & a_{32} & a_{33} \end{bmatrix},$$

where

$$a_{11} = l_x - r,$$

$$a_{12} = -cK \left(1 - \frac{l_x}{r}\right),$$

$$a_{13} = 0,$$

$$\begin{aligned}
a_{21} &= 0, \\
a_{22} &= \hat{e}cK \left(1 - \frac{l_x}{r}\right) - \hat{d} - l_y, \\
a_{23} &= 0, \\
a_{31} &= \frac{\hat{c}drT_P}{\hat{c}K(r - l_x) + dr}, \\
a_{32} &= -\hat{c}\theta K \left(1 - \frac{l_x}{r}\right) - \frac{c\hat{c}KT_P(r - l_x)}{\hat{c}K(r - l_x) + dr}, \\
a_{33} &= -\hat{c}K \left(1 - \frac{l_x}{r}\right) - d.
\end{aligned}$$

As in Case 3, the eigenvalues are the values along the main diagonal. That is,

$$\begin{aligned}
\lambda_1 &= l_x - r, \\
\lambda_2 &= \hat{e}cK \left(1 - \frac{l_x}{r}\right) - \hat{d} - l_y, \\
\lambda_3 &= -\hat{c}K \left(1 - \frac{l_x}{r}\right) - d.
\end{aligned}$$

As with the light and quantity case, $r - l_x > 0$ means both λ_1 and λ_3 are negative. Therefore the only other condition we require for stability is that

$$\hat{e}cK \left(1 - \frac{l_x}{r}\right) - \hat{d} - l_y < 0 \iff \hat{e}cK \left(1 - \frac{l_x}{r}\right) < \hat{d} + l_y.$$

Hence, the grazer extinction equilibrium is a stable node when $r - l_x > 0$ and

$$\hat{e}cK \left(1 - \frac{l_x}{r}\right) < \hat{d} + l_y.$$

It is a saddle with a two-dimensional stable manifold and a one-dimensional unstable manifold for $r - l_x > 0$ and

$$\hat{e}cK \left(1 - \frac{l_x}{r} \right) > \hat{d} + l_y,$$

since these conditions mean that $\lambda_1, \lambda_3 < 0$ and $\lambda_2 > 0$.

Now, when $r - l_x < 0$, then $\lambda_1 > 0$. Moreover, since $r - l_x < 0$ implies that $1 - l_x/r < 0$, then $\lambda_2 < 0$. However, the sign of λ_3 is not guaranteed from $r - l_x < 0$. Thus, when $r - l_x < 0$ and the following condition holds, the grazer extinction equilibrium is a saddle with a two-dimensional stable manifold and a one-dimensional unstable manifold:

$$-\hat{c}K \left(1 - \frac{l_x}{r} \right) < d.$$

If this condition fails (i.e., $\lambda_3 > 0$), then the equilibrium is a saddle with a one-dimensional stable manifold and a two-dimensional unstable manifold. However, when $r - l_x < 0$, the equilibrium is not biologically feasible.

CASE 5: Carbon and quality

The Jacobian takes the form

$$A_5 = \begin{bmatrix} a_{11} & a_{12} & a_{13} \\ a_{21} & a_{22} & a_{23} \\ a_{31} & a_{32} & a_{33} \end{bmatrix},$$

where

$$\begin{aligned}
a_{11} &= -\frac{(r-l_x)(r+\gamma r-\gamma l_x)}{r}, \\
a_{12} &= -\frac{\gamma(r-l_x)^2}{r} - \frac{c\gamma T_C(r-l_x)}{r+\gamma r-\gamma l_x}, \\
a_{13} &= 0, \\
a_{21} &= 0, \\
a_{22} &= \frac{c\hat{c}\hat{e}\gamma T_C T_P(r-l_x)}{d\theta(r+\gamma r-\gamma l_x) + \hat{c}\gamma\theta T_C(r-l_x)} - \hat{d} - l_y, \\
a_{23} &= 0, \\
a_{31} &= \frac{\hat{c}dT_P(r+\gamma r-\gamma l_x)}{d(r+\gamma r-\gamma l_x) + \hat{c}\gamma T_C(r-l_x)}, \\
a_{32} &= -\frac{\hat{c}\theta\gamma T_C(r-l_x)}{r+\gamma r-\gamma l_x} - \frac{c\hat{c}\gamma T_C T_P(r-l_x)}{d(r+\gamma r-\gamma l_x) + \hat{c}\gamma T_C(r-l_x)}, \\
a_{33} &= -\frac{\hat{c}\gamma T_C(r-l_x)}{r+\gamma r-\gamma l_x} - d.
\end{aligned}$$

A 3 x 3 matrix with zeros in these specific entries has its eigenvalues along the main diagonal, as in Cases 3 and 4. Thus, in this case

$$\begin{aligned}
\lambda_1 &= -\frac{(r-l_x)(r+\gamma r-\gamma l_x)}{r}, \\
\lambda_2 &= \frac{c\hat{c}\hat{e}\gamma T_C T_P(r-l_x)}{d\theta(r+\gamma r-\gamma l_x) + \hat{c}\gamma\theta T_C(r-l_x)} - \hat{d} - l_y, \\
\lambda_3 &= -\frac{\hat{c}\gamma T_C(r-l_x)}{r+\gamma r-\gamma l_x} - d.
\end{aligned}$$

Consider $r + \gamma r - \gamma l_x$ and $r - l_x$. We see that for $r, \gamma, l_x > 0$,

$$r + \gamma r - \gamma l_x < 0 \Rightarrow r + \gamma(r - l_x) < 0 \Rightarrow r - l_x < -\frac{r}{\gamma} \Rightarrow r - l_x < 0.$$

Also, since all parameters are assumed to be positive,

$$r - l_x > 0 \Rightarrow \gamma(r - l_x) > 0 \Rightarrow r + \gamma(r - l_x) > 0 \Rightarrow r + \gamma r - \gamma l_x > 0.$$

For stability of the grazer extinction equilibrium, we need $\lambda_2 < 0$, which requires

$$\frac{c\hat{c}\hat{\epsilon}\gamma T_C T_P(r - l_x)}{d\theta(r + \gamma r - \gamma l_x) + \hat{c}\gamma\theta T_C(r - l_x)} < \hat{d} + l_y$$

and either $r + \gamma r - \gamma l_x < 0$ (in which case $r - l_x < 0$) or $r - l_x > 0$ (in which case $r + \gamma r - \gamma l_x > 0$). Then, the grazer extinction equilibrium is a stable node since $\lambda_1, \lambda_3 < 0$ when $r + \gamma r - \gamma l_x$ and $r - l_x$ have the same sign.

For either $r + \gamma r - \gamma l_x < 0$ or $r - l_x > 0$, and

$$\frac{c\hat{c}\hat{\epsilon}\gamma T_C T_P(r - l_x)}{d\theta(r + \gamma r - \gamma l_x) + \hat{c}\gamma\theta T_C(r - l_x)} > \hat{d} + l_y,$$

the grazer extinction equilibrium is a saddle with a two-dimensional stable manifold and a one-dimensional unstable manifold.

Now, for $r - l_x < 0$ and $r + \gamma r - \gamma l_x > 0$ we have a few cases. λ_1 is guaranteed to be positive, but the signs of λ_2 and λ_3 depend on additional conditions.

For $\lambda_2 < 0$, we need either $d(r + \gamma r - \gamma l_x) + \hat{c}\gamma T_C(r - l_x) > 0$ or $d(r + \gamma r - \gamma l_x) + \hat{c}\gamma T_C(r - l_x) < 0$ and

$$\frac{c\hat{c}\hat{\epsilon}\gamma T_C T_P(r - l_x)}{d\theta(r + \gamma r - \gamma l_x) + \hat{c}\gamma\theta T_C(r - l_x)} < \hat{d} + l_y.$$

For $\lambda_3 < 0$, we need

$$-\frac{\hat{c}\gamma T_C(r - l_x)}{r + \gamma r - \gamma l_x} < d.$$

Hence, for $r - l_x < 0$ and $r + \gamma r - \gamma l_x > 0$, we can have either a saddle with a one- or two-dimensional unstable manifold, or an unstable node. However, when $r - l_x < 0$ and $r + \gamma r - \gamma l_x > 0$, the equilibrium is not biologically feasible.

CASE 6: Carbon and quantity

The Jacobian is as follows:

$$A_6 = \begin{bmatrix} a_{11} & a_{12} & a_{13} \\ a_{21} & a_{22} & a_{23} \\ a_{31} & a_{32} & a_{33} \end{bmatrix},$$

where

$$\begin{aligned} a_{11} &= -\frac{(r - l_x)(r + \gamma r - \gamma l_x)}{r}, \\ a_{12} &= -\frac{\gamma(r - l_x)^2}{r} - \frac{c\gamma T_C(r - l_x)}{r + \gamma r - \gamma l_x}, \\ a_{13} &= 0, \\ a_{21} &= 0, \\ a_{22} &= \frac{\hat{c}\gamma T_C(r - l_x)}{r + \gamma r - \gamma l_x} - \hat{d} - l_y, \\ a_{23} &= 0, \\ a_{31} &= \frac{\hat{c}dT_P(r + \gamma r - \gamma l_x)}{d(r + \gamma r - \gamma l_x) + \hat{c}\gamma T_C(r - l_x)}, \end{aligned}$$

$$a_{32} = -\frac{\hat{c}\theta\gamma T_C(r-l_x)}{r+\gamma r-\gamma l_x} - \frac{c\hat{c}\gamma T_C T_P(r-l_x)}{d(r+\gamma r-\gamma l_x) + \hat{c}\gamma T_C(r-l_x)},$$

$$a_{33} = -\frac{\hat{c}\gamma T_C(r-l_x)}{r+\gamma r-\gamma l_x} - d.$$

As in the previous case, this matrix has its eigenvalues along the main diagonal. Thus, we have

$$\lambda_1 = -\frac{(r-l_x)(r+\gamma r-\gamma l_x)}{r},$$

$$\lambda_2 = \frac{\hat{c}\gamma T_C(r-l_x)}{r+\gamma r-\gamma l_x} - \hat{d} - l_y,$$

$$\lambda_3 = -\frac{\hat{c}\gamma T_C(r-l_x)}{r+\gamma r-\gamma l_x} - d.$$

If $r+\gamma r-\gamma l_x < 0$, then we know $r-l_x < 0$. Therefore, if $r+\gamma r-\gamma l_x < 0$, then $\lambda_1, \lambda_3 < 0$ and we also need

$$\frac{\hat{c}\gamma T_C(r-l_x)}{r+\gamma r-\gamma l_x} < \hat{d} + l_y.$$

If $r-l_x > 0$, then we know $r+\gamma r-\gamma l_x > 0$ and therefore $\lambda_1, \lambda_3 < 0$. For λ_2 to be less than 0 and therefore for stability we also require

$$\frac{\hat{c}\gamma T_C(r-l_x)}{r+\gamma r-\gamma l_x} < \hat{d} + l_y.$$

Hence, the grazer extinction equilibrium is a stable node for

$$\frac{\hat{c}\gamma T_C(r-l_x)}{r+\gamma r-\gamma l_x} < \hat{d} + l_y$$

and either $r + \gamma r - \gamma l_x < 0$ or $r - l_x > 0$.

For either $r + \gamma r - \gamma l_x < 0$ or $r - l_x > 0$, and

$$\frac{\hat{c}\gamma T_C(r - l_x)}{r + \gamma r - \gamma l_x} > \hat{d} + l_y,$$

the grazer extinction equilibrium is a saddle with a two-dimensional stable manifold and a one-dimensional unstable manifold.

For $r - l_x < 0$ and $r + \gamma r - \gamma l_x > 0$, we have $\lambda_1 > 0$ and $\lambda_2 < 0$. Therefore, we have a saddle. If $\lambda_3 < 0$, the saddle has a two-dimensional stable manifold and a one-dimensional unstable manifold; if $\lambda_3 > 0$, it has a one-dimensional stable manifold and a two-dimensional unstable manifold. Note that for $r - l_x < 0$ and $r + \gamma r - \gamma l_x > 0$, the equilibrium is not biologically feasible.

The stability results for Cases 3 to 6 are summarized in the following theorem.

Theorem 9. *For the local closed model (3.6) - (3.8) with Holling type I functional responses, the following stability results hold for the grazer extinction equilibrium $E_1 = (\bar{x}, \bar{y}, \bar{p})$.*

(i) *If $K \leq \min\{\bar{p}/q, \gamma(T_C - \bar{x} - \bar{y})\}$ and $\bar{p} < \theta\bar{x}$, then the equilibrium is a stable node for $r - l_x > 0$ and*

$$\frac{c\hat{c}\hat{e}KT_P(r - l_x)}{\hat{c}K\theta(r - l_x) + dr\theta} < \hat{d} + l_y,$$

and otherwise it is either a saddle with a one- or two-dimensional unstable manifold, or an unstable node.

(ii) *If $K \leq \min\{\bar{p}/q, \gamma(T_C - \bar{x} - \bar{y})\}$ and $\bar{p} > \theta\bar{x}$, then the equilibrium is a*

stable node for $r - l_x > 0$ and

$$\hat{e}cK \left(1 - \frac{l_x}{r}\right) < \hat{d} + l_y,$$

and otherwise it is a saddle with either a one- or two-dimensional unstable manifold.

(iii) If $\gamma(T_C - \bar{x} - \bar{y}) \leq \min\{K, \bar{p}/q\}$ and $\bar{p} < \theta\bar{x}$, then the equilibrium is a stable node for either $r + \gamma r - \gamma l_x < 0$ or $r - l_x > 0$, and

$$\frac{\hat{c}\hat{e}\gamma T_C T_P(r - l_x)}{d\theta(r + \gamma r - \gamma l_x) + \hat{c}\gamma\theta T_C(r - l_x)} < \hat{d} + l_y,$$

and otherwise it is either a saddle with a one- or two-dimensional unstable manifold, or an unstable node.

(iv) If $\gamma(T_C - \bar{x} - \bar{y}) \leq \min\{K, \bar{p}/q\}$ and $\bar{p} > \theta\bar{x}$, then the equilibrium is a stable node for either $r + \gamma r - \gamma l_x < 0$ or $r - l_x > 0$, and

$$\frac{\hat{e}c\gamma T_C(r - l_x)}{r + \gamma r - \gamma l_x} < \hat{d} + l_y,$$

and otherwise it is a saddle with a one- or two-dimensional unstable manifold.

Note that for Cases 3 and 4, the equilibrium is biologically feasible only for $r - l_x \geq 0$; for Cases 5 and 6, we require either $r - l_x > 0$ and $r + \gamma r - \gamma l_x > 0$, or $r - l_x < 0$ and $r + \gamma r - \gamma l_x < 0$. Hence, the only biologically feasible classifications for the equilibrium in these cases are either a stable node or a saddle with a two-dimensional stable manifold and a one-dimensional unstable manifold.

Holling type II

For $f(x) = cx/(a+x)$, $g(P) = \hat{c}P/(\hat{a}+P)$, and $h(C) = \gamma C$,

$$\begin{aligned} \frac{\partial F}{\partial x} &= \begin{cases} -\frac{r}{\min\{K, p/q\}} + \frac{cy}{(a+x)^2}, & \gamma(T_C - x - y) \geq K \text{ or } p/q, \\ -\frac{r(T_C - y)}{\gamma(T_C - x - y)^2} + \frac{cy}{(a+x)^2}, & \gamma(T_C - x - y) < K \text{ and } p/q, \end{cases} \\ \frac{\partial F}{\partial y} &= \begin{cases} -\frac{c}{a+x}, & \gamma(T_C - x - y) \geq K \text{ or } p/q, \\ -\frac{rx}{\gamma(T_C - x - y)^2} - \frac{c}{a+x}, & \gamma(T_C - x - y) < K \text{ and } p/q, \end{cases} \\ \frac{\partial F}{\partial p} &= \begin{cases} 0, & p/q \geq K \text{ or } \gamma(T_C - x - y), \\ \frac{rxq}{p^2}, & p/q < K \text{ and } \gamma(T_C - x - y), \end{cases} \\ \frac{\partial G}{\partial x} &= \begin{cases} \frac{ac\hat{e}}{(a+x)^2}, & 1 < p/x/\theta, \\ -\frac{c\hat{e}p}{\theta(a+x)^2}, & 1 > p/x/\theta, \end{cases} \\ \frac{\partial G}{\partial y} &= 0, \\ \frac{\partial G}{\partial p} &= \begin{cases} 0, & 1 < p/x/\theta, \\ \frac{c\hat{e}}{\theta(a+x)}, & 1 > p/x/\theta, \end{cases} \\ \frac{\partial H}{\partial x} &= \frac{\hat{c}(T_P - p - \theta y)}{\hat{a} + T_P - p - \theta y} + \frac{cpy}{(a+x)^2}, \\ \frac{\partial H}{\partial y} &= -\frac{\hat{a}\hat{c}\theta x}{(\hat{a} + T_P - p - \theta y)^2} - \frac{cp}{a+x}, \\ \frac{\partial H}{\partial p} &= -\frac{\hat{a}\hat{c}x}{(\hat{a} + T_P - p - \theta y)^2} - \frac{cy}{a+x} - d. \end{aligned}$$

Note that since the producer phosphorus equation has no minimum term, the partial derivatives of $H(x, y, p)$ do not depend on what is limiting the producer or grazer, and thus are the same in all cases.

The necessary products and sums for the Jacobian are

$$\begin{aligned}
xF_x &= \begin{cases} -\frac{rx}{\min\{K, p/q\}} + \frac{cxy}{(a+x)^2}, & \gamma(T_C - x - y) \geq K \text{ or } p/q, \\ -\frac{rx(T_C - y)}{\gamma(T_C - x - y)^2} + \frac{cxy}{(a+x)^2}, & \gamma(T_C - x - y) < K \text{ and } p/q, \end{cases} \\
F + xF_x &= \begin{cases} r - \frac{2rx}{\min\{K, p/q\}} - \frac{acy}{(a+x)^2} - l_x, & \gamma(T_C - x - y) \geq K \text{ or } p/q, \\ r - \frac{rx(2T_C - x - 2y)}{\gamma(T_C - x - y)^2} - \frac{acy}{(a+x)^2} - l_x, & \gamma(T_C - x - y) < K \text{ and } p/q, \end{cases} \\
xF_y &= \begin{cases} -\frac{cx}{a+x}, & \gamma(T_C - x - y) \geq K \text{ or } p/q, \\ -\frac{rx^2}{\gamma(T_C - x - y)^2} - \frac{cx}{a+x}, & \gamma(T_C - x - y) < K \text{ and } p/q, \end{cases} \\
xF_p &= \begin{cases} 0, & p/q \geq K \text{ or } \gamma(T_C - x - y), \\ \frac{rx^2q}{p^2}, & p/q < K \text{ and } \gamma(T_C - x - y), \end{cases} \\
yG_x &= \begin{cases} \frac{ac\hat{e}y}{(a+x)^2}, & 1 < p/x/\theta, \\ -\frac{c\hat{e}py}{\theta(a+x)^2}, & 1 > p/x/\theta, \end{cases} \\
yG_y &= 0, \\
G + yG_y &= \hat{e} \min \left\{ 1, \frac{p/x}{\theta} \right\} \frac{cx}{a+x} - \hat{d} - l_y, \\
yG_p &= \begin{cases} 0, & 1 < p/x/\theta, \\ \frac{c\hat{e}y}{\theta(a+x)}, & 1 > p/x/\theta. \end{cases}
\end{aligned}$$

There are different Jacobian matrices dependent upon the limiting factors. We determine the entries based on what is limiting for the producer (nutrient, light, or carbon) and grazer (quality or quantity), then substitute the equilibria found in 3.3.2.

CASE 1: Nutrient and quality

The corresponding Jacobian matrix is

$$B_1 = \begin{bmatrix} l_x - r & -\frac{c\bar{p}(r - l_x)}{aqr + \bar{p}(r - l_x)} & \frac{(r - l_x)^2}{qr} \\ 0 & \frac{c\hat{e}\bar{p}}{\theta(a + \bar{x})} - \hat{d} - l_y & 0 \\ \frac{dqr}{r - l_x} & -\frac{\hat{a}\hat{c}\theta\bar{x}}{(\hat{a} + T_P - \bar{p})^2} - \frac{c\bar{p}}{a + \bar{x}} & -\frac{\hat{a}\hat{c}\bar{x}}{(\hat{a} + T_P - \bar{p})^2} - d \end{bmatrix}.$$

As with the corresponding Holling type I case, the eigenvalues (see Appendix A) are not particularly illuminating. Also similar to the Holling type I case, stability does not depend on K , T_C , or γ . Given the producer is nutrient limited at this equilibrium, it is reasonable that the light-dependent and carbon-dependent carrying capacities have no impact on its stability.

CASE 2: Nutrient and quantity

The corresponding Jacobian is

$$B_2 = \begin{bmatrix} l_x - r & -\frac{c\bar{p}(r - l_x)}{aqr + \bar{p}(r - l_x)} & \frac{(r - l_x)^2}{qr} \\ 0 & \frac{c\hat{e}\bar{p}(r - l_x)}{aqr + \bar{p}(r - l_x)} - \hat{d} - l_y & 0 \\ \frac{dqr}{r - l_x} & -\frac{\hat{a}\hat{c}\theta\bar{x}}{(\hat{a} + T_P - \bar{p})^2} - \frac{c\bar{p}}{a + \bar{x}} & -\frac{\hat{a}\hat{c}\bar{x}}{(\hat{a} + T_P - \bar{p})^2} - d \end{bmatrix}.$$

The eigenvalues (see Appendix A) do not provide any stability conclusions in this case. As in Case 2 for Holling type I functional responses, stability does not depend on K , T_C , γ , or θ . The producer is nutrient limited at equilibrium, so K , T_C and γ should not impact stability of the equilibrium. Note that since the grazer is quantity limited at equilibrium, we would also expect the stability of the equilibrium to not depend on the grazer's P:C ratio, θ .

CASE 3: Light and quality

Here

$$B_3 = \begin{bmatrix} l_x - r & -\frac{cK(r - l_x)}{ar + K(r - l_x)} & 0 \\ 0 & \frac{c\hat{c}r\bar{p}}{\theta(ar + K(r - l_x))} - \hat{d} - l_y & 0 \\ \frac{\hat{c}(T_P - \bar{p})}{\hat{a} + T_P - \bar{p}} & -\frac{\hat{a}\hat{c}K\theta(r - l_x)}{r(\hat{a} + T_P - \bar{p})^2} - \frac{cr\bar{p}}{ar + K(r - l_x)} & -\frac{\hat{a}\hat{c}K(r - l_x)}{r(\hat{a} + T_P - \bar{p})^2} - d \end{bmatrix}.$$

Note that for ease of reading, \bar{p} has not been substituted in. As in the previous sections, we know that a matrix of this form (i.e., with zeros in these entries) has its eigenvalues along the main diagonal:

$$\begin{aligned} \lambda_1 &= l_x - r, \\ \lambda_2 &= \frac{c\hat{c}r\bar{p}}{\theta(ar + K(r - l_x))} - \hat{d} - l_y, \\ \lambda_3 &= -\frac{\hat{a}\hat{c}K(r - l_x)}{r(\hat{a} + T_P - \bar{p})^2} - d. \end{aligned}$$

Stability requires $r - l_x > 0$. Then, $\lambda_1 < 0$ and $\lambda_3 < 0$. In order for the second eigenvalue to be negative, we require

$$\frac{c\hat{c}r\bar{p}}{\theta(ar + K(r - l_x))} < \hat{d} + l_y.$$

Therefore, the equilibrium is a stable node when $r - l_x > 0$ and the above condition is satisfied.

If the condition for $\lambda_2 < 0$ is not satisfied but $r - l_x > 0$, then the equilibrium is a saddle with a two-dimensional stable manifold and a one-dimensional unstable manifold. If $r - l_x < 0$, then $\lambda_1 > 0$, and the equilibrium is either a

saddle with a one- or two-dimensional unstable manifold or an unstable node, depending on the signs of λ_2 and λ_3 . However, $r - l_x \geq 0$ is required for the equilibrium to be biologically feasible.

CASE 4: Light and quantity

Here, the Jacobian matrix is

$$B_4 = \begin{bmatrix} l_x - r & -\frac{cK(r - l_x)}{ar + K(r - l_x)} & 0 \\ 0 & \frac{c\hat{c}K(r - l_x)}{ar + K(r - l_x)} - \hat{d} - l_y & 0 \\ \frac{\hat{c}(T_P - \bar{p})}{\hat{a} + T_P - \bar{p}} & -\frac{\hat{a}\hat{c}K(r - l_x)}{r(\hat{a} + T_P - \bar{p})^2} - \frac{cr\bar{p}}{ar + K(r - l_x)} & -\frac{\hat{a}\hat{c}K(r - l_x)}{r(\hat{a} + T_P - \bar{p})^2} - d \end{bmatrix}.$$

The eigenvalues are along the main diagonal. Hence

$$\begin{aligned} \lambda_1 &= l_x - r, \\ \lambda_2 &= \frac{c\hat{c}K(r - l_x)}{ar + K(r - l_x)} - \hat{d} - l_y, \\ \lambda_3 &= -\frac{\hat{a}\hat{c}K(r - l_x)}{r(\hat{a} + T_P - \bar{p})^2} - d. \end{aligned}$$

For λ_1 to be less than 0, we require $r - l_x > 0$. Then, $\lambda_3 < 0$ for positive parameter values. In order to ensure $\lambda_2 < 0$, and thus to make this equilibrium a stable node, we would also require

$$\frac{c\hat{c}K(r - l_x)}{ar + K(r - l_x)} < \hat{d} + l_y,$$

in addition to $r - l_x > 0$.

If the parameters satisfy $r - l_x > 0$ but $\lambda_2 > 0$, then the equilibrium is a saddle with a two-dimensional stable manifold and a one-dimensional unstable

manifold. If $r - l_x < 0$, then $\lambda_1 > 0$, and the classification of the equilibrium depends on the signs of λ_2 and λ_3 . If both are negative, then the equilibrium is a saddle with a one-dimensional unstable manifold; if they have opposite signs, it is a saddle with a two-dimensional unstable manifold; and if both are positive, then it is an unstable node. However, $r - l_x \geq 0$ is required for the equilibrium to be biologically feasible.

CASE 5: Carbon and quality

Here

$$B_5 = \begin{bmatrix} b_{11} & b_{12} & b_{13} \\ b_{21} & b_{22} & b_{23} \\ b_{31} & b_{32} & b_{33} \end{bmatrix},$$

where

$$\begin{aligned} b_{11} &= -\frac{(r - l_x)(r + \gamma r - \gamma l_x)}{r}, \\ b_{12} &= -\frac{\gamma(r - l_x)^2}{r} - \frac{c\gamma T_C(r - l_x)}{a(r + \gamma r - \gamma l_x) + \gamma T_C(r - l_x)}, \\ b_{13} &= 0, \\ b_{21} &= 0, \\ b_{22} &= \frac{c\hat{e}(r + \gamma r - \gamma l_x)\bar{p}}{a\theta(r + \gamma r - \gamma l_x) + \gamma\theta T_C(r - l_x)} - \hat{d} - l_y, \\ b_{23} &= 0, \\ b_{31} &= \frac{\hat{c}(T_P - \bar{p})}{\hat{a} + T_P - \bar{p}}, \\ b_{32} &= -\frac{\hat{a}\hat{c}\gamma\theta T_C(r - l_x)}{(r + \gamma r - \gamma l_x)(\hat{a} + T_P - \bar{p})^2} - \frac{c(r + \gamma r - \gamma l_x)\bar{p}}{a(r + \gamma r - \gamma l_x) + \gamma T_C(r - l_x)}, \\ b_{33} &= -\frac{\hat{a}\hat{c}\gamma T_C(r - l_x)}{(r + \gamma r - \gamma l_x)(\hat{a} + T_P - \bar{p})^2} - d. \end{aligned}$$

The corresponding eigenvalues are along the main diagonal:

$$\begin{aligned}\lambda_1 &= -\frac{(r-l_x)(r+\gamma r-\gamma l_x)}{r}, \\ \lambda_2 &= \frac{c\hat{e}(r+\gamma r-\gamma l_x)\bar{p}}{a\theta(r+\gamma r-\gamma l_x)+\gamma\theta T_C(r-l_x)} - \hat{d} - l_y, \\ \lambda_3 &= -\frac{\hat{a}\hat{c}\gamma T_C(r-l_x)}{(r+\gamma r-\gamma l_x)(\hat{a}+T_P-\bar{p})^2} - d.\end{aligned}$$

For these eigenvalues, we consider stability cases using $r-l_x$ and $r+\gamma r-\gamma l_x$. As in the Holling type I corresponding case, we recognize that $r+\gamma r-\gamma l_x < 0$ implies $r-l_x < 0$, and $r-l_x > 0$ implies $r+\gamma r-\gamma l_x > 0$, when all parameters are assumed to be positive. Therefore we consider three cases.

If $r+\gamma r-\gamma l_x < 0$ (and therefore $r-l_x < 0$), then $\lambda_1 < 0$ and $\lambda_3 < 0$. The sign of λ_2 depends on the sign of \bar{p} . Looking at the forms of the equilibria in Section 3.3.2, we observe that for $r+\gamma r-\gamma l_x < 0$ and $r-l_x < 0$, both equilibria have a positive \bar{p} . Hence, the equilibrium is a stable node for $r+\gamma r-\gamma l_x < 0$ and

$$\frac{c\hat{e}(r+\gamma r-\gamma l_x)\bar{p}}{a\theta(r+\gamma r-\gamma l_x)+\gamma\theta T_C(r-l_x)} < \hat{d} + l_y.$$

If $r+\gamma r-\gamma l_x < 0$ but the additional condition is not satisfied, then the equilibrium is a saddle with a two-dimensional stable manifold and a one-dimensional unstable manifold.

If $r-l_x > 0$ (and therefore $r+\gamma r-\gamma l_x > 0$), then $\lambda_1 < 0$ and $\lambda_3 < 0$. Since $\bar{p} > 0$ for $r-l_x > 0$ and both forms of \bar{p} , then the equilibrium is a stable node for $r-l_x > 0$ and

$$\frac{c\hat{e}(r+\gamma r-\gamma l_x)\bar{p}}{a\theta(r+\gamma r-\gamma l_x)+\gamma\theta T_C(r-l_x)} < \hat{d} + l_y.$$

If $r - l_x > 0$ but $\lambda_2 > 0$ because the above condition is not satisfied, then the equilibrium is a saddle with a two-dimensional stable manifold and a one-dimensional unstable manifold.

Lastly, if $r - l_x < 0$ and $r + \gamma r - \gamma l_x > 0$, then $\lambda_1 > 0$. The signs of λ_2 and λ_3 depend on additional conditions. For the equilibrium to be a saddle with a two-dimensional stable manifold and a one-dimensional unstable manifold when $r - l_x < 0$ and $r + \gamma r - \gamma l_x > 0$, we require

$$\begin{aligned} \frac{c\hat{e}(r + \gamma r - \gamma l_x)\bar{p}}{a\theta(r + \gamma r - \gamma l_x) + \gamma\theta T_C(r - l_x)} &< \hat{d} + l_y, \\ -\frac{\hat{a}\hat{c}\gamma T_C(r - l_x)}{(r + \gamma r - \gamma l_x)(\hat{a} + T_P - \bar{p})^2} &< d. \end{aligned}$$

Note that here the sign of \bar{p} is not determined by the signs of $r - l_x$ and $r + \gamma r - \gamma l_x$ alone. If either one of these additional conditions is not satisfied (i.e., $\lambda_2 > 0$ or $\lambda_3 > 0$) and the other is satisfied, then the equilibrium is a saddle with a one-dimensional stable manifold and a two-dimensional unstable manifold. If both of these additional conditions are not satisfied, then the equilibrium is an unstable node. However, in this case, the equilibrium is only biologically feasible when the signs of $r - l_x$ and $r + \gamma r - \gamma l_x$ are the same.

CASE 6: Carbon and quantity

The Jacobian takes the form

$$B_6 = \begin{bmatrix} b_{11} & b_{12} & b_{13} \\ b_{21} & b_{22} & b_{23} \\ b_{31} & b_{32} & b_{33} \end{bmatrix},$$

where

$$\begin{aligned}
b_{11} &= -\frac{(r-l_x)(r+\gamma r-\gamma l_x)}{r}, \\
b_{12} &= -\frac{\gamma(r-l_x)^2}{r} - \frac{c\gamma T_C(r-l_x)}{a(r+\gamma r-\gamma l_x)+\gamma T_C(r-l_x)}, \\
b_{13} &= 0, \\
b_{21} &= 0, \\
b_{22} &= \frac{c\hat{c}\gamma T_C(r-l_x)}{a(r+\gamma r-\gamma l_x)+\gamma T_C(r-l_x)} - \hat{d} - l_y, \\
b_{23} &= 0, \\
b_{31} &= \frac{\hat{c}(T_P - \bar{p})}{\hat{a} + T_P - \bar{p}}, \\
b_{32} &= -\frac{\hat{a}\hat{c}\gamma\theta T_C(r-l_x)}{(r+\gamma r-\gamma l_x)(\hat{a}+T_P-\bar{p})^2} - \frac{c(r+\gamma r-\gamma l_x)\bar{p}}{a(r+\gamma r-\gamma l_x)+\gamma T_C(r-l_x)}, \\
b_{33} &= -\frac{\hat{a}\hat{c}\gamma T_C(r-l_x)}{(r+\gamma r-\gamma l_x)(\hat{a}+T_P-\bar{p})^2} - d.
\end{aligned}$$

Once again, the eigenvalues are along the main diagonal:

$$\begin{aligned}
\lambda_1 &= -\frac{(r-l_x)(r+\gamma r-\gamma l_x)}{r}, \\
\lambda_2 &= \frac{c\hat{c}\gamma T_C(r-l_x)}{a(r+\gamma r-\gamma l_x)+\gamma T_C(r-l_x)} - \hat{d} - l_y, \\
\lambda_3 &= -\frac{\hat{a}\hat{c}\gamma T_C(r-l_x)}{(r+\gamma r-\gamma l_x)(\hat{a}+T_P-\bar{p})^2} - d.
\end{aligned}$$

We consider cases based on $r-l_x$ and $r+\gamma r-\gamma l_x$. Note that we cannot have $r-l_x > 0$ and $r+\gamma r-\gamma l_x < 0$ for positive r, γ and l_x .

If $r-l_x < 0$ and $r+\gamma r-\gamma l_x < 0$, then $\lambda_1 < 0$ and $\lambda_3 < 0$. Therefore, the

equilibrium is a stable node if $r + \gamma r - \gamma l_x < 0$ and

$$\frac{c\hat{e}\gamma T_C(r - l_x)}{a(r + \gamma r - \gamma l_x) + \gamma T_C(r - l_x)} < \hat{d} + l_y.$$

If this additional condition is not satisfied (i.e., $\lambda_2 > 0$), then the equilibrium is a saddle with a two-dimensional stable manifold and a one-dimensional unstable manifold.

Similarly, if $r - l_x > 0$ and $r + \gamma r - \gamma l_x > 0$, then $\lambda_1 < 0$ and $\lambda_3 < 0$. Hence, the equilibrium is a stable node if $r - l_x > 0$ and

$$\frac{c\hat{e}\gamma T_C(r - l_x)}{a(r + \gamma r - \gamma l_x) + \gamma T_C(r - l_x)} < \hat{d} + l_y.$$

If the above condition is not satisfied, then the equilibrium is a saddle with a two-dimensional stable manifold and a one-dimensional unstable manifold.

If $r - l_x < 0$ and $r + \gamma r - \gamma l_x > 0$, then $\lambda_1 > 0$. The equilibrium is a saddle with a two-dimensional stable manifold and a one-dimensional unstable manifold if

$$\begin{aligned} \frac{c\hat{e}\gamma T_C(r - l_x)}{a(r + \gamma r - \gamma l_x) + \gamma T_C(r - l_x)} &< \hat{d} + l_y, \\ -\frac{\hat{a}\hat{c}\gamma T_C(r - l_x)}{(r + \gamma r - \gamma l_x)(\hat{a} + T_P - \bar{p})^2} &< d. \end{aligned}$$

If either of these conditions is not met, the equilibrium is a saddle with a one-dimensional stable manifold and a two-dimensional unstable manifold; if both conditions are not met, the equilibrium is an unstable node. Note that if $r - l_x < 0$ and $r + \gamma r - \gamma l_x > 0$, then the equilibrium is not biologically

feasible.

The stability results for Cases 3 and 4 are summarized in the following theorem.

Theorem 10. *For the local closed model (3.6) - (3.8) with Holling type II functional responses, the following stability results hold for a grazer extinction equilibrium $E_1 = (\bar{x}, \bar{y}, \bar{p})$.*

(i) *If $K \leq \min\{\bar{p}/q, \gamma(T_C - \bar{x} - \bar{y})\}$ and $\bar{p} < \theta\bar{x}$, then the equilibrium is a stable node for $r - l_x > 0$ and*

$$\frac{c\hat{e}r\bar{p}}{\theta(ar + K(r - l_x))} < \hat{d} + l_y,$$

and otherwise it is either a saddle with a one- or two-dimensional unstable manifold, or an unstable node.

(ii) *If $K \leq \min\{\bar{p}/q, \gamma(T_C - \bar{x} - \bar{y})\}$ and $\bar{p} > \theta\bar{x}$, then the equilibrium is a stable node for $r - l_x > 0$ and*

$$\frac{c\hat{e}K(r - l_x)}{ar + K(r - l_x)} < \hat{d} + l_y,$$

and otherwise it is either a saddle with a one- or two-dimensional unstable manifold, or an unstable node.

As in the Holling type I cases, for the equilibrium to be biologically feasible in Cases 3 and 4, we require $r - l_x \geq 0$. Thus, in applications, we expect to see either a stable node or a saddle with a one-dimensional unstable manifold.

The stability results for Cases 5 and 6 are summarized in the following theorem. Case 5 is summarized in parts (i)-(iii), and Case 6 in parts (iv)-(vi).

Theorem 11. *For the local closed model (3.6) - (3.8) with Holling type II functional responses, the following stability results hold for a grazer extinction equilibrium $E_1 = (\bar{x}, \bar{y}, \bar{p})$.*

(i) *If $\gamma(T_C - \bar{x} - \bar{y}) \leq \min\{K, \bar{p}/q\}$, $\bar{p} < \theta\bar{x}$, $r - l_x < 0$, and $r + \gamma r - \gamma l_x < 0$, then the equilibrium is a stable node if*

$$\frac{c\hat{e}(r + \gamma r - \gamma l_x)\bar{p}}{a\theta(r + \gamma r - \gamma l_x) + \gamma\theta T_C(r - l_x)} < \hat{d} + l_y,$$

and otherwise it is a saddle with a two-dimensional stable manifold and a one-dimensional unstable manifold.

(ii) *If $\gamma(T_C - \bar{x} - \bar{y}) \leq \min\{K, \bar{p}/q\}$, $\bar{p} < \theta\bar{x}$, $r - l_x > 0$, and $r + \gamma r - \gamma l_x > 0$, then the equilibrium is a stable node if*

$$\frac{c\hat{e}(r + \gamma r - \gamma l_x)\bar{p}}{a\theta(r + \gamma r - \gamma l_x) + \gamma\theta T_C(r - l_x)} < \hat{d} + l_y,$$

and otherwise it is a saddle with a two-dimensional stable manifold and a one-dimensional unstable manifold.

(iii) *If $\gamma(T_C - \bar{x} - \bar{y}) \leq \min\{K, \bar{p}/q\}$, $\bar{p} < \theta\bar{x}$, $r - l_x < 0$, and $r + \gamma r - \gamma l_x > 0$, then the equilibrium is a saddle with a two-dimensional stable manifold and a one-dimensional unstable manifold if both of the following hold:*

$$\begin{aligned} \frac{c\hat{e}(r + \gamma r - \gamma l_x)\bar{p}}{a\theta(r + \gamma r - \gamma l_x) + \gamma\theta T_C(r - l_x)} &< \hat{d} + l_y, \\ -\frac{\hat{a}\hat{c}\gamma T_C(r - l_x)}{(r + \gamma r - \gamma l_x)(\hat{a} + T_P - \bar{p})^2} &< d. \end{aligned}$$

Otherwise it is either a saddle with a one-dimensional stable manifold and a

two-dimensional unstable manifold or an unstable node.

(iv) If $\gamma(T_C - \bar{x} - \bar{y}) \leq \min\{K, \bar{p}/q\}$, $\bar{p} > \theta\bar{x}$, $r - l_x < 0$, and $r + \gamma r - \gamma l_x < 0$, then the equilibrium is a stable node if

$$\frac{c\hat{e}\gamma T_C(r - l_x)}{a(r + \gamma r - \gamma l_x) + \gamma T_C(r - l_x)} < \hat{d} + l_y,$$

and otherwise it is a saddle with a two-dimensional stable manifold and a one-dimensional unstable manifold.

(v) If $\gamma(T_C - \bar{x} - \bar{y}) \leq \min\{K, \bar{p}/q\}$, $\bar{p} > \theta\bar{x}$, $r - l_x > 0$, and $r + \gamma r - \gamma l_x > 0$, then the equilibrium is a stable node if

$$\frac{c\hat{e}\gamma T_C(r - l_x)}{a(r + \gamma r - \gamma l_x) + \gamma T_C(r - l_x)} < \hat{d} + l_y,$$

and otherwise it is a saddle with a two-dimensional stable manifold and a one-dimensional unstable manifold.

(vi) If $\gamma(T_C - \bar{x} - \bar{y}) \leq \min\{K, \bar{p}/q\}$, $\bar{p} > \theta\bar{x}$, $r - l_x < 0$, and $r + \gamma r - \gamma l_x > 0$, then the equilibrium is a saddle with a two-dimensional stable manifold and a one-dimensional unstable manifold if both of the following hold:

$$\begin{aligned} \frac{c\hat{e}\gamma T_C(r - l_x)}{a(r + \gamma r - \gamma l_x) + \gamma T_C(r - l_x)} &< \hat{d} + l_y, \\ -\frac{\hat{a}\hat{c}\gamma T_C(r - l_x)}{(r + \gamma r - \gamma l_x)(\hat{a} + T_P - \bar{p})^2} &< d. \end{aligned}$$

Otherwise it is either a saddle with a one-dimensional stable manifold and a two-dimensional unstable manifold or an unstable node.

Note that both (iii) and (vi) are not biologically feasible.

3.4 Numerical Dynamics

3.4.1 Numerical simulations comparing models

For all numerical simulations, we used Holling type II functional responses for f and g ; that is, $f(x) = cx/(a + x)$, $g(P) = \hat{c}P/(\hat{a} + P)$, and $h(C) = \gamma C$. In order to compare the dynamics between models, simulations were run using `ode23s`, with a time span of $[0, 200]$. For all cases, we assumed $\gamma = 0.01023$, and we used the same initial conditions for all models, although initial conditions differed between parameter combinations dependent upon the value of T_P . Eight simulations in total were ran for each combination of $T_C \in \{98.2, 409.4\}$, $T_P \in \{0.003, 0.030, 0.300\}$, and $K \in \{0.25, 0.75, 1.00, 2.00\}$. For the local open model, we used $C(0) = \beta - x(0) - y(0)$ for $\beta = T_C$. The simulations included one each for the local closed model, the local closed model with PCO, and the WKL model with explicit respiration, and five for the local open model, varying $\alpha \in \{1e - 6, 1e - 3, 1e0, 1e3, 1e6\}$, for a total of 8 simulations for each combination of T_C , T_P and K . The resulting dynamics were plotted and compared. We also individually graphed what was limiting the growth of the producer and grazer, as well as the resulting producer P:C. All other parameters were held constant at the values given in Table 3.1.

Here the WKL model with explicit respiration follows the form of the model in Section 2.2, but with the term $-l_x x$ added to the producer equation (Equation (2.1)). Grazer respiration is already modelled in the basic WKL model with the term $\hat{d}y$. For the WKL model, we used $\hat{d} = 0.22$, where \hat{d} is the total loss rate of the grazer, including both respiration and death; for the new models presented here, we used $l_y = 0.165$ for respiration loss

and $\hat{d} = 0.055$ for loss due to death, for a total loss rate of 0.22. Therefore, addition of producer respiration is sufficient to eliminate cellular respiration as the differing factor between the models, allowing us to focus on the differences in the level of openness and the mechanisms considered.

Overall, the models did not differ much within the parameter regimes considered here. We tended to see grazer extinction when one of the potentially limiting parameters is very low. As the limiting parameter increased, the system switched to coexistence at an equilibrium, then coexistence in oscillations. We know that the local closed model can also demonstrate a switch back to coexistence and then grazer extinction at high parameter values (see Section 3.4.2). We would have to look at additional parameter values if we wanted to verify if the other models also exhibit this behaviour, since the behaviour was observed outside the regimes investigated here. Qualitatively, the dynamics seem to be very similar between the models, with the exceptions of the cases where the WKL model with respiration is drastically different from our three models due to carbon limitation (i.e., $T_C = 98.2, T_P = 0.030, K = 2.00$, and $T_C = 98.2, T_P = 0.300, K = 2.00$ – see Figure 3.1). Quantitatively, it appears that the local closed model with PCO is the most different from the rest. In particular, this model differs the most at higher total carbon levels, where it demonstrated different periods of oscillations, as well as different maximum or minimum values.

When considering the limiting factor for producer growth, we notice that the models often agreed, and the results seem to be fairly logical (e.g., light limited at $K = 0.25$; phosphorus limited at $T_P = 0.003$ so long as $K \geq 0.75$). We determined the limiting factor by computing $\min\{K, p(t)/q, h(C(t))$ for

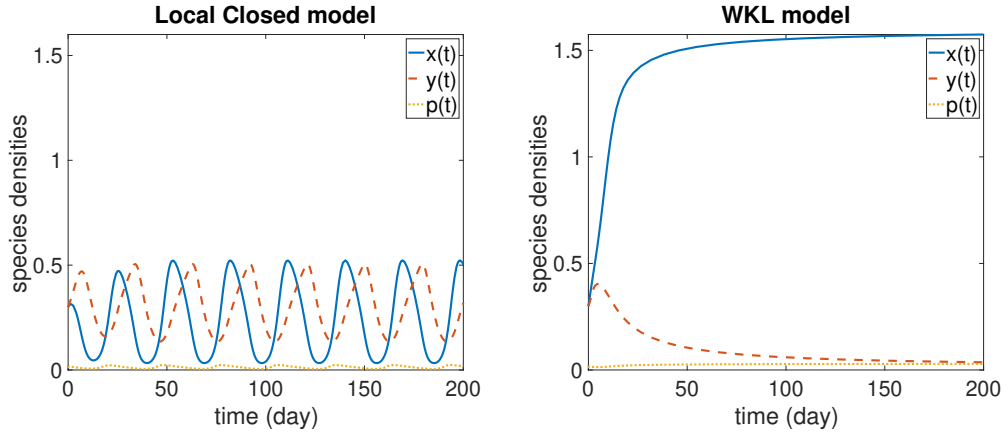


Figure 3.1: Comparison of the local closed model and WKL model for $K = 2$, $T_C = 98.2$, $T_P = 0.03$, $\gamma = 0.01023$. The local closed model exhibits coexistence oscillations, while the WKL model is approaching the grazer extinction equilibrium.

each time in the array produced by ode23s. Phosphorus limitation is rare in the intermediate or high phosphorus regimes – it mostly occurs at the starts of troughs in oscillations. Phosphorus limitation in producer oscillation troughs is likely due to the high concentration of phosphorus in the grazer pool causing the available phosphorus to considerable decline. There are some cases where there is alternation between limiting factors, which will be discussed later in this section. The degree to which this switching happened varied with α – as α increased, we observed less carbon limitation. It is interesting that in the cases where there are different limitations between models, we still see the same dynamics, likely due to the very small difference between K and $h(T_C)$ in these regimes. Carbon limitation never occurs for high carbon with the parameters considered here. With both phosphorus and light limitation of producer growth included, the WKL model with explicit respiration would be essentially equivalent to the new models for high system carbon.

At very low concentrations of available phosphorus, the grazers are always

quality limited (i.e., $p/x/\theta < 1$) and tend towards extinction. For intermediate system phosphorus and low light-dependent carrying capacity of the producer, the grazers are always quantity limited (i.e., $p/x/\theta > 1$) except at the initial condition we used. For high phosphorus, the grazers are quantity limited after the initial condition. We observed switching between quantity and quality limitation for $K = 1.00$ or 2.00 , $T_C = 98.2$, $T_P = 0.3$; and for $K = 1.00$, $T_C = 409.4$, $T_P = 0.03$. The grazers are quality limited in an interval between their oscillation's trough and the crest (i.e., while the population is increasing). Unlike with the producer limiting factors, which differed dependent on α , we rarely saw any difference between the models in what was limiting the grazer, except when the WKL dynamics were completely different than the rest (i.e., intermediate/high phosphorus, ambient carbon, and very high light).

We observed that the producer's P:C oscillates whenever the system variables are oscillating. When the systems tend towards grazer extinction, producer P:C settles quickly to a plateau. The grazers over-grazing immediately before their subsequent decline appears to coincide with sharp dips in producer P:C. Other than the cases where the WKL dynamics were completely different than the rest, we did not notice differences between models for P:C for ambient carbon. This also holds for the high carbon but very low phosphorus cases. At high carbon and intermediate phosphorus levels, we started to see differences in P:C between the model considering photorespiration and the other models. The local closed model with PCO exhibits the following differences from the other models:

- Lower plateau: $T_P = 0.003, \forall K$; $T_P = 0.03, K = 0.25$ and 2 ; $T_P = 0.3, K = 0.25$.

- Lower trough, higher crest for oscillations: $T_P = 0.03$ and 0.3 , $K = 0.75$.
- Lower trough, lower crest for oscillations: $T_P = 0.03$ and 0.3 , $K = 1.00$;
 $T_P = 0.3$, $K = 2.00$.

The oscillations produced may also have a different period in the case where $T_P = 0.3$ and $K = 1.00$, although any difference is minimal and hard to distinguish visually.

For the open models, we did also examine the changes in free carbon with time (i.e., $C(t)$) for different parameter values. In particular, when we used for our initial condition $C(0) = \beta$ instead of $C(0) = \beta - x(0) - y(0)$, we observed that as α increases, the changes in C are more rapid, and the range of values of C decreases severely. When the other system variables are oscillating, C also oscillates, with the amplitude of the oscillations decreasing with increasing α . The oscillations also get much sharper for higher α , especially for higher K . In general for $C(0) = \beta - x(0) - y(0)$, the system starts out with slightly less free carbon than the external environment, and thus must immediately compensate to equilibrate with the environment. This change is more immediate for higher α since the system can compensate very quickly. The oscillations are much harder to distinguish in this case because they are very small relative to the initial carbon gradient across the boundary, especially for higher α .

Overall, we observed a lot of similarities in the dynamics between models. We saw more quality limitation of grazers in the high carbon case only for $K = 2.00$, $T_P = 0.03$, where the new models matched the WKL model rather than oscillating. This change was due to the lessening of carbon limitation of the producer growth for elevated carbon dioxide.

As mentioned previously, there were a few parameter regimes where we

observed alternation of limiting factors for the growth of the species. One such parameter regime shows all three types of producer limitation, and both types of grazer limitation: $K = 1.00, T_C = 98.2, T_P = 0.034, \gamma = 0.01023$. This parameter regime corresponds to high light, ambient total system carbon, and intermediate system phosphorus.

In Figure 3.2 (a), we see that for this parameter combination, the system is oscillating. The producer alternates between carbon limitation at its crests, phosphorus limitation in the troughs, and then light limitation until it switches back to carbon limitation, as shown in Figure 3.2 (b). From Figure 3.2 (c), we observe that the grazer is primarily quantity limited, but is briefly quality limited between the trough and the crest. Superimposing Figures 3.2 (b) and (c) allow us to see how the limiting factors and carbon densities of the two populations align, as shown in Figure 3.3. We notice that the producer becomes carbon limited near or immediately after the grazer population begins to recover from its minimum. Conversely, the producer becoming light, then phosphorus, then light limited in short succession aligns with just after the grazer population begins to decline from its maximum. The grazer being phosphorus (i.e., quality) limited tends to align with where the producer is at its crest and shortly after, when the producer P:C has declined to accommodate the additional carbon uptake despite no additional available phosphorus.

We observe that carbon limitation can be reduced or even completely removed by increasing the openness of the system, as shown in Figure 3.4. We see that as the parameter α increases, there is more light limitation and less carbon limitation. By $\alpha = 1$, the only remaining carbon limitation is at the initial condition. This is as expected, since carbon limitation requires $K > h(C)$,

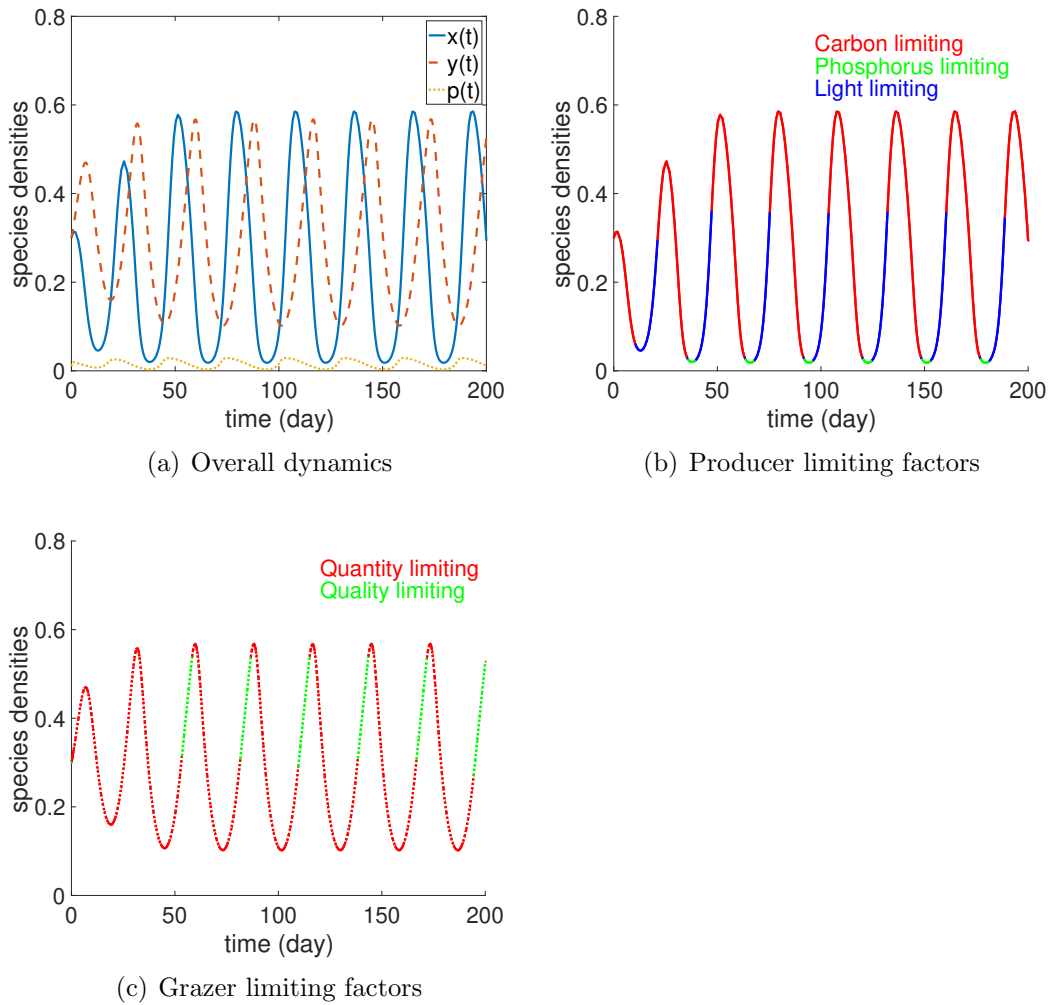


Figure 3.2: Local closed model special case: $K = 1.00$, $T_C = 98.2$, $T_P = 0.034$, $\gamma = 0.01023$. In (a) we see that the system is undergoing coexistence oscillations, while (b) and (c) show the limiting factors at a given time for the producer and grazer respectively.

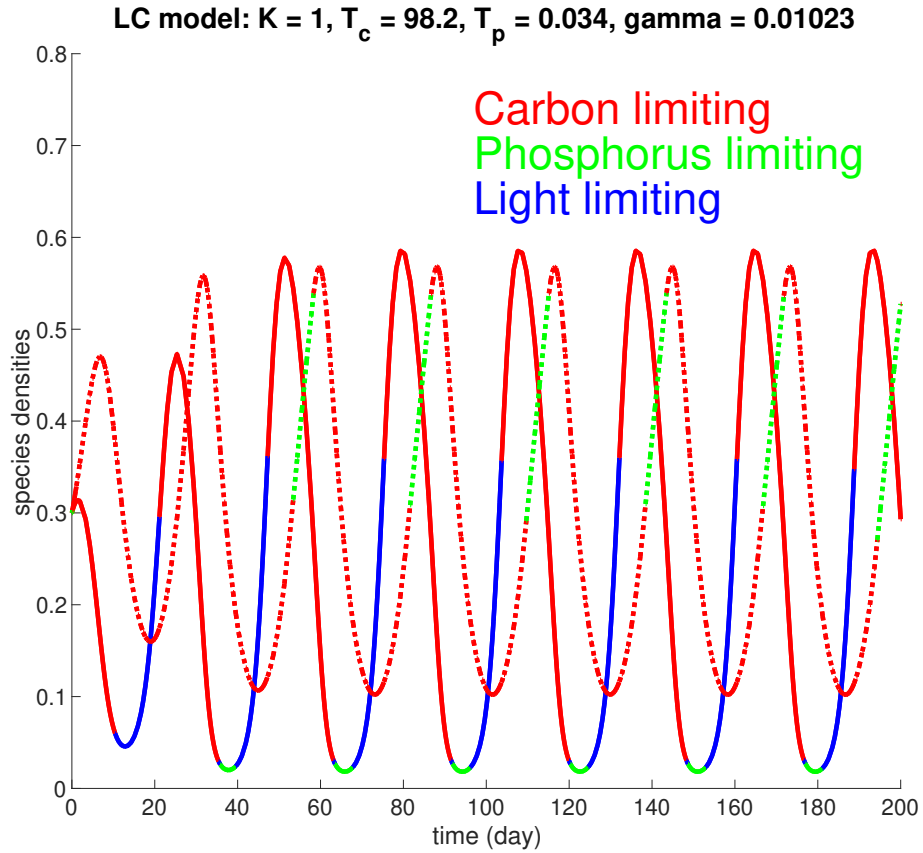


Figure 3.3: Local closed species limiting factors in the special case: $K = 1.00$, $T_C = 98.2$, $T_P = 0.034$, $\gamma = 0.01023$. The dotted line represents the grazer, and the solid the producer. From this we can see how the limiting factors of the two different species align with each other and with the carbon densities of the populations.

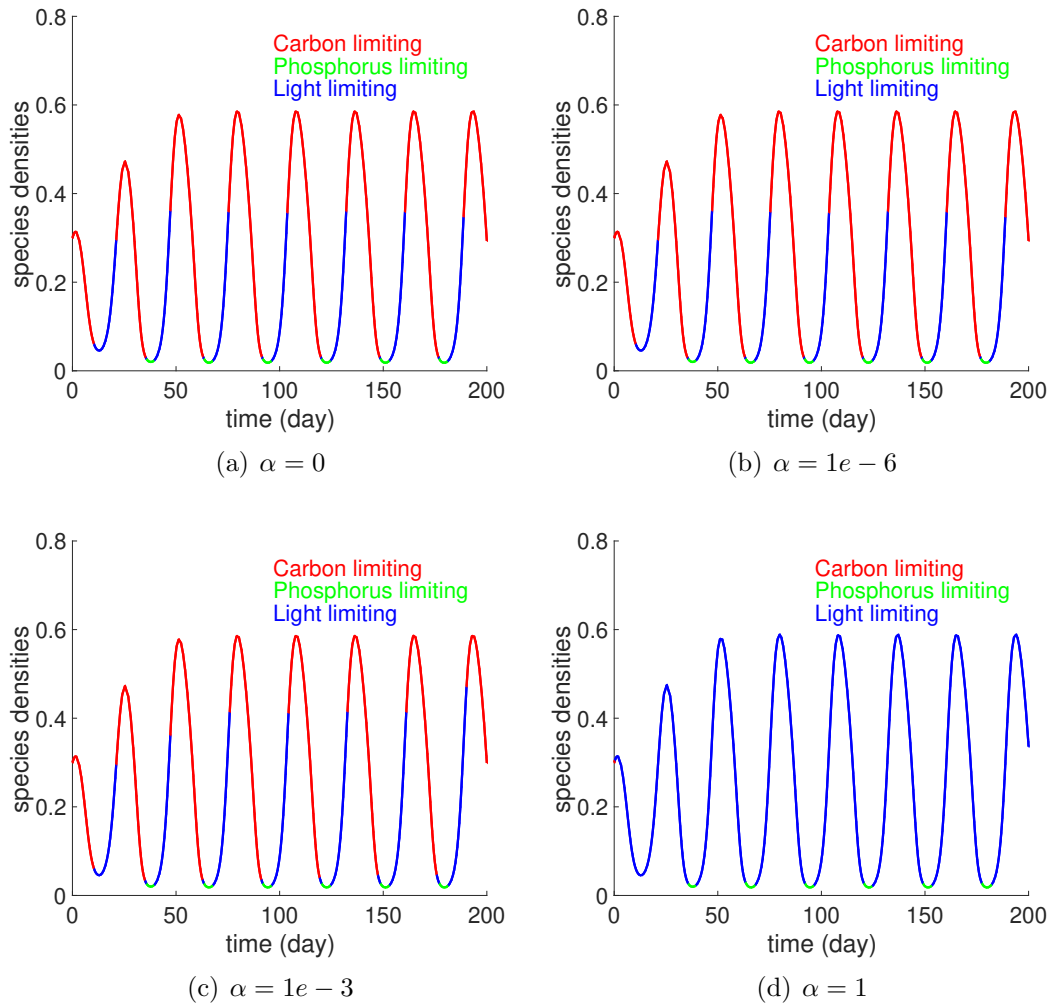


Figure 3.4: Local open model special case: $K = 1.00, T_C = \beta = 98.2, T_P = 0.034, \gamma = 0.01023$. The parameter α increases from (a) to (d), corresponding to an increased “openness” of the system. As the system becomes more open, carbon limitation is lessened.

and if C is fixed at or near ambient levels, then for this value of K , the condition will not be satisfied, as demonstrated by Figure 3.4.

As mentioned previously, one possible reason for the similarity in dynamics despite varying limiting factors based on α is because alternation of carbon and light limitation requires K and $h(T_C)$ (or $h(\beta)$ for the open system) to be very close to each other. This results in the numerical difference between having a denominator of K and $h(C)$ in the producer equation being insufficient to change the dynamics drastically.

3.4.2 One parameter bifurcation analysis

In order to compare and contrast the impacts on dynamics of the parameters that determine limitation of the producer, MatCont was used to perform bifurcation analysis for K , T_C and T_P for the local closed model only [10]. Multiple diagrams were generated for each parameter, varying the other two parameters as well as γ to get as broad an idea of the impact of each parameter as reasonably possible. In general, the regimes for the non-bifurcating parameters included combinations of $K \in \{0.25, 0.75, 1.00, 2.00\}$, $T_C \in \{98.2, 409.4\}$, $T_P \in \{0.003, 0.030, 0.300\}$, and $\gamma \in \{0.0045, 0.00767, 0.01023, 0.021\}$.

For all one parameter diagrams, a solid blue curve represents a stable equilibrium point; a magenta dashed curve is an unstable equilibrium point; and a cyan dotted curve represents the minimum/maximum of a stable limit cycle.

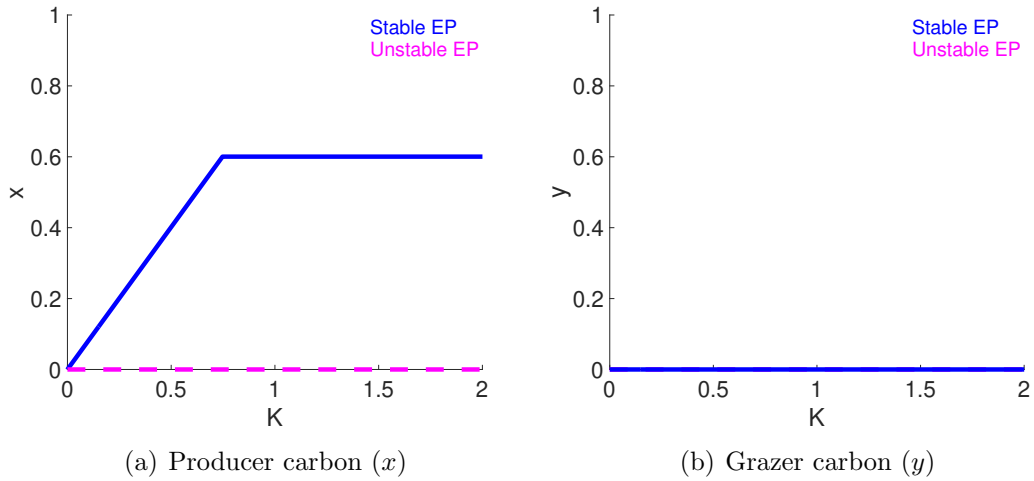


Figure 3.5: K bifurcation diagrams: $T_P = 0.003$, $T_C = 98.2$, $\gamma = 0.01023$. x is on the left and y is on the right. There are no bifurcations. The grazer extinction equilibrium is stable for all values of K shown.

Light-dependent carrying capacity: K

For low phosphorus ($T_P = 0.003$), both ambient ($T_C = 98.2$) and high ($T_C = 409.4$) carbon produced the grazer extinction equilibrium for K up to at least 2, as shown in Figure 3.5. At equilibrium for the parameter combination shown, the producers are light limited for low K , then phosphorus limited for higher K , with the change occurring around $K = 0.75$. The grazers are initially quantity limited for $K < 0.09$, and then quality limited.

For intermediate phosphorus ($T_P = 0.030$), the results vary more. For ambient carbon ($T_C = 98.2$), the system tends towards the grazer extinction equilibrium for $K \in (0, 0.20440)$. Then there is a transcritical bifurcation, at which point the coexistence equilibrium becomes biologically feasible and stable. For $\gamma = 0.0045$, there are no more bifurcations for K up to at least 2, as shown in Figure 3.6. In this case, the producers are light limited for low K

until around $K = 0.44$, after which they are carbon limited; the grazers are quantity limited throughout at equilibrium.

For $\gamma \in \{0.00767, 0.01023, 0.021\}$, the coexistence equilibrium remains stable until $K = 0.72004$. At this point, there is a Hopf bifurcation at which a stable limit cycle emerges. The limit cycle remains stable for K up to at least 2 for $\gamma \in \{0.00767, 0.01023\}$, as shown in Figure 3.7. For both the grazer and coexistence equilibrium, the producer is light limited and the grazer is quantity limited for the parameter combination shown. For $\gamma = 0.021$, there is a saddle-node bifurcation at $K = 1.41757$ and there are new stable and unstable coexistence equilibria. As shown in Figure 3.8, the stable branch remains stable for K up to at least 4. Note that although the curves appear to overlap, the x value for this second stable coexistence equilibrium is slightly smaller than the grazer extinction equilibrium value (difference is approximately 0.0056); conversely, the y value is slightly larger for coexistence than grazer extinction (difference is approximately 0.0065). At equilibrium for $\gamma = 0.021$, the producers are light limited before the limit cycle ($K < 0.72$), and after the limit cycle until around $K = 2.028$, after which they are carbon limited; the grazers are quantity limited before the limit cycle ($K < 0.72$), and quality limited after the limit cycle ($K > 1.42$).

For high carbon ($T_C = 409.4$), the system tends towards the grazer extinction equilibrium for $K \in (0, 0.20440)$, then there is a transcritical bifurcation, causing the coexistence equilibrium to become stable. This lasts until $K = 0.72004$, at which point a stable limit cycle emerges. The limit cycle is stable until the saddle-node bifurcation at $K = 1.41757$, where a stable and an unstable coexistence equilibrium appear. The stable coexistence equilibrium

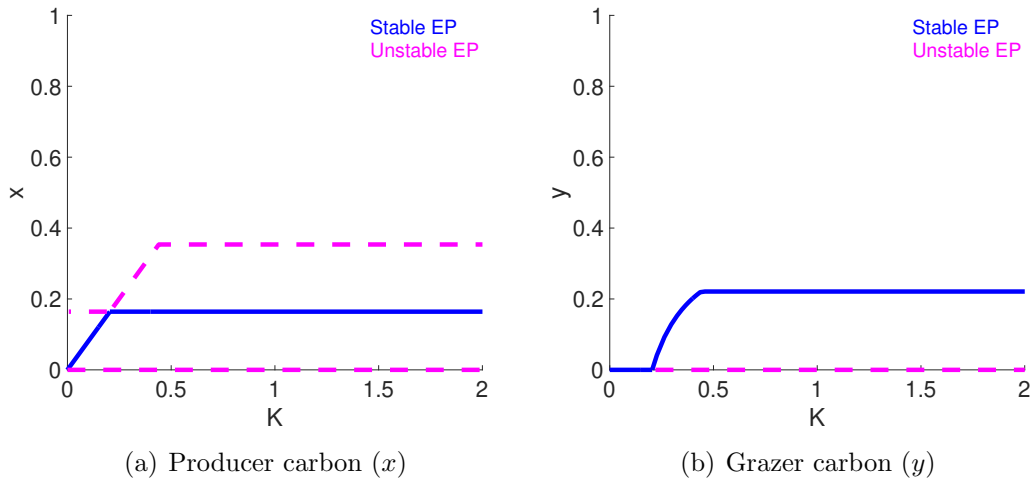


Figure 3.6: K bifurcation diagrams: $T_P = 0.030$, $T_C = 98.2$, $\gamma = 0.0045$. x is on the left and y is on the right. There is a transcritical bifurcation around $K = 0.20$. For $K < 0.20$, the grazer extinction equilibrium is stable; for $K > 0.20$, the coexistence equilibrium is biologically feasible and stable.

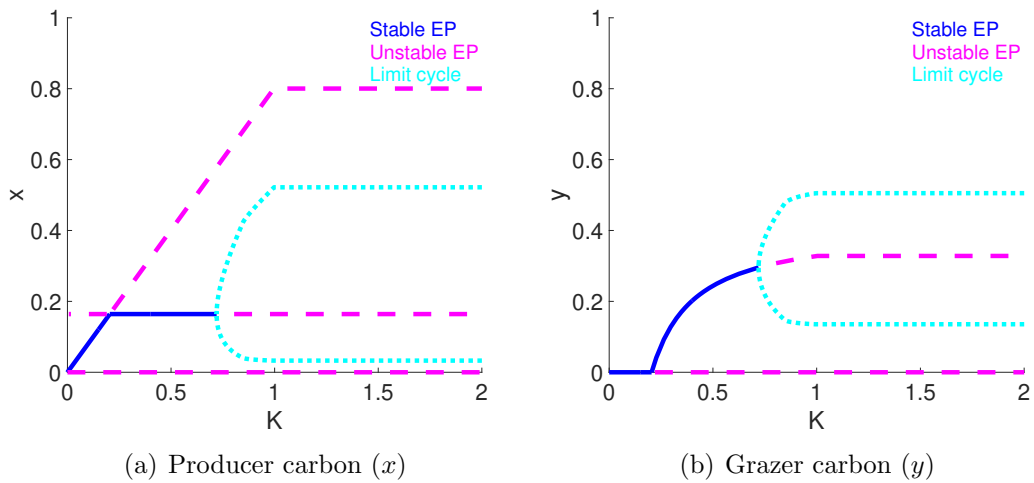


Figure 3.7: K bifurcation diagrams: $T_P = 0.030$, $T_C = 98.2$, $\gamma = 0.01023$. x is on the left and y is on the right. There is a transcritical bifurcation around $K = 0.20$ and a Hopf bifurcation around $K = 0.72$. The stable behaviour is as follows: for $K < 0.20$, grazer extinction equilibrium; for $0.20 < K < 0.72$, coexistence equilibrium; and for $K > 0.75$, coexistence oscillations.

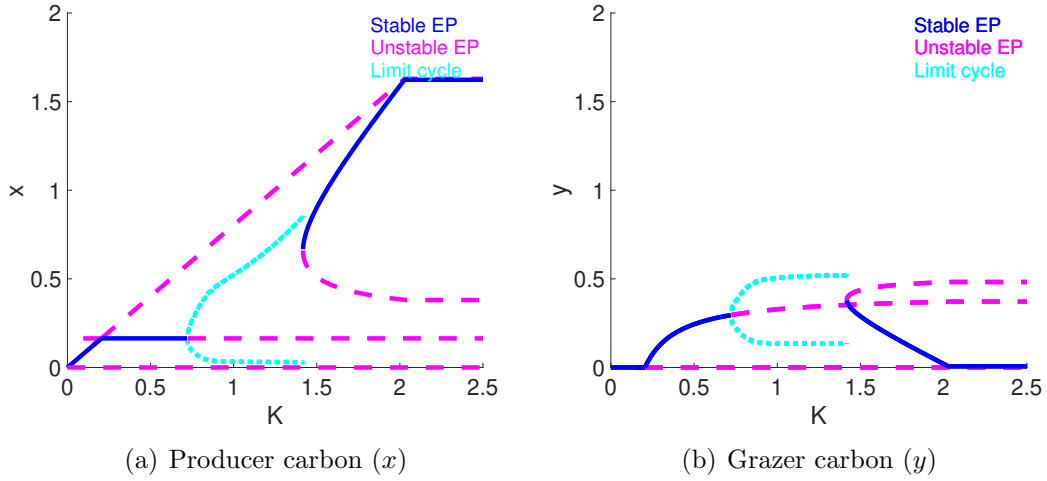


Figure 3.8: K bifurcation diagrams: $T_P = 0.030$, $T_C = 98.2$, $\gamma = 0.021$. x is on the left and y is on the right. There is a transcritical bifurcation around $K = 0.20$, a Hopf bifurcation around $K = 0.72$, and a saddle-node bifurcation around $K = 1.42$. The stable behaviour is as follows: for $K < 0.20$, grazer extinction equilibrium; for $0.20 < K < 0.72$, coexistence equilibrium; for $0.72 < K < 1.42$, coexistence oscillations; and for $K > 1.42$, a second coexistence equilibrium.

remains stable until $K = 2.04143$ when there is another transcritical bifurcation, at which point the system returns to the grazer extinction equilibrium. The multiple bifurcations are shown in Figure 3.9. Bifurcation analysis of the grazer extinction equilibrium for values of K higher than 2 revealed that this additional transcritical bifurcation occurs for $T_C > 201.19309$. At equilibrium, the producer is light limited for $K < 4.1540$; the grazer is quantity limited before the limit cycle ($K < 0.72$), and quality limited after the limit cycle ($K > 1.42$).

For high phosphorus ($T_P = 0.300$) and ambient carbon, we observe the same bifurcations as intermediate phosphorus for $\gamma \in \{0.0045, 0.00767, 0.01023\}$. However, for $\gamma = 0.021$, we do not see the saddle-node bifurcation, and instead it follows the same pattern as $T_P = 0.030$ (intermediate phosphorus),

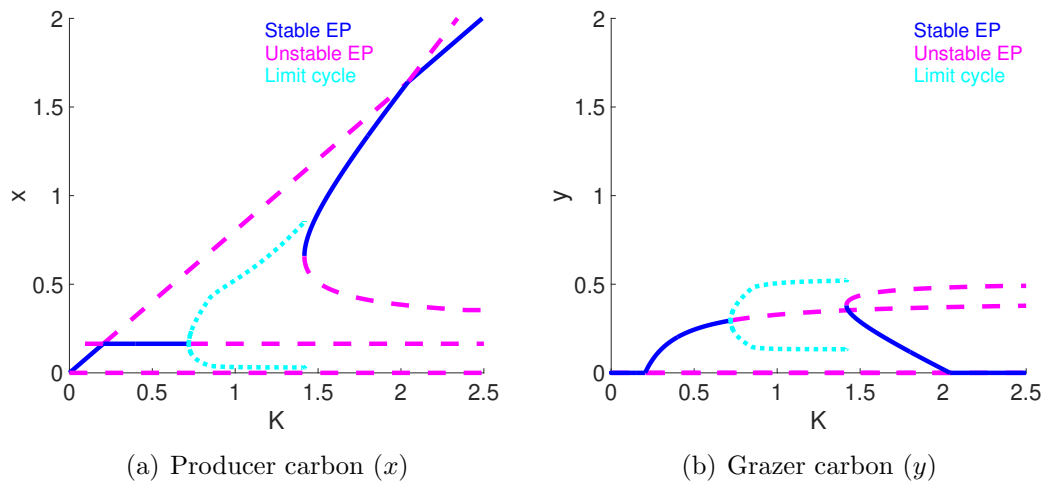


Figure 3.9: K bifurcation diagrams: $T_P = 0.030$, $T_C = 409.4$, $\gamma = 0.01023$. x is on the left and y is on the right. There is a transcritical bifurcation around $K = 0.20$, a Hopf bifurcation around $K = 0.72$, a saddle-node bifurcation around $K = 1.42$, and another transcritical bifurcation around $K = 2.04$. The stable behaviour is as follows: for $K < 0.20$, grazer extinction equilibrium; for $0.20 < K < 0.72$, coexistence equilibrium; for $0.72 < K < 1.42$, coexistence oscillations; for $1.42 < K < 2.04$, a second coexistence equilibrium; and for $K > 2.04$, grazer extinction equilibrium.

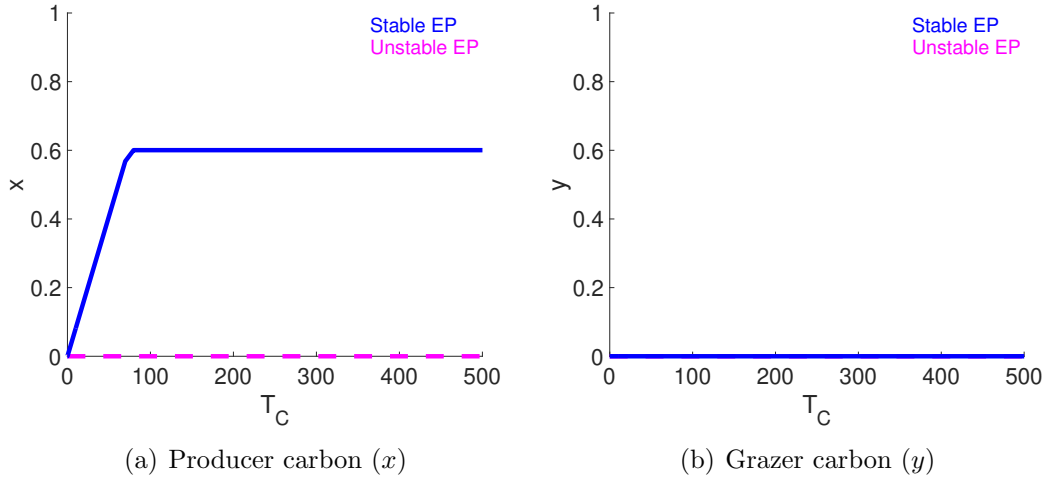


Figure 3.10: T_C bifurcation diagrams: $K = 1.00$, $T_P = 0.003$, $\gamma = 0.01023$. x is on the left and y is on the right. There are no bifurcations. The grazer extinction equilibrium is stable for all values of T_C shown.

$T_C = 98.2$ (ambient carbon), and $\gamma = 0.01023$ (shown in Figure 3.7). For high carbon, we observe the same bifurcations as $T_P = 0.030$ (intermediate phosphorus), $T_C = 98.2$ (ambient carbon), and $\gamma = 0.01023$, regardless of γ .

Total system carbon: T_C

In all cases, for sufficiently low T_C , the system tends towards a grazer extinction equilibrium. For low phosphorus ($T_P = 0.003$), this equilibrium remains stable until T_C at least 1000 (Figure 3.10). For intermediate/high phosphorus, this equilibrium becomes unstable at a transcritical bifurcation, at which point the coexistence equilibrium becomes stable. The bifurcation value does not depend on T_P or K , but it does occur at a lower value for higher γ , likely since an increase in γ would increase $h(C)$ and cause carbon limitation to end at a lower value.

Regardless of if T_P is intermediate or high, the range of T_C for which the

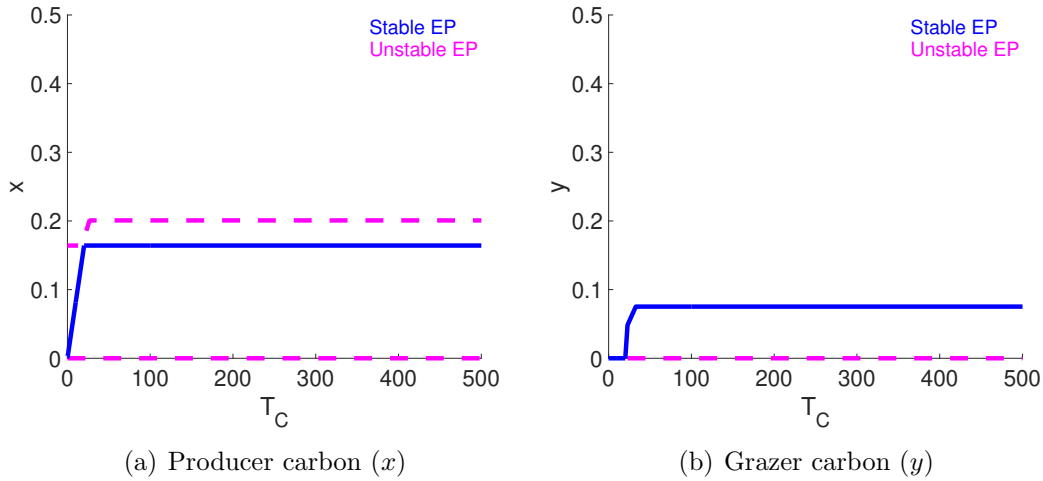


Figure 3.11: T_C bifurcation diagrams: $K = 0.25$, $T_P = 0.030$, $\gamma = 0.01023$. x is on the left and y is on the right. There is a transcritical bifurcation around $T_C = 20.14$. For $T_C < 20.14$, the grazer extinction equilibrium is stable; for $T_C > 20.14$, the coexistence equilibrium is feasible and stable.

system trends towards the coexistence equilibrium remains the same. For $K = 0.25$, the coexistence equilibrium remains stable for T_C up to at least 1000, as shown in Figure 3.11. For $K \in \{0.75, 1.00, 2.00\}$, the coexistence equilibrium remains stable until a Hopf bifurcation point, where a stable limit cycle appears. As with the transcritical bifurcation, the Hopf bifurcation value is lower for higher γ .

For intermediate phosphorus ($T_P = 0.030$), with $K \in \{0.75, 1.00\}$, the limit cycle remains stable for T_C up to at least 1000, as shown in Figure 3.12. This also holds for high phosphorus ($T_P = 0.300$) and for $K \in \{0.75, 1.00, 2.00\}$. However, for intermediate phosphorus ($T_P = 0.030$) and very high light ($K = 2.00$), the limit cycle becomes unstable or disappears entirely at a saddle-node bifurcation, the value of which decreases with increasing γ , as shown in Figure 3.13. After this bifurcation, the coexistence equilibrium is stable once more,

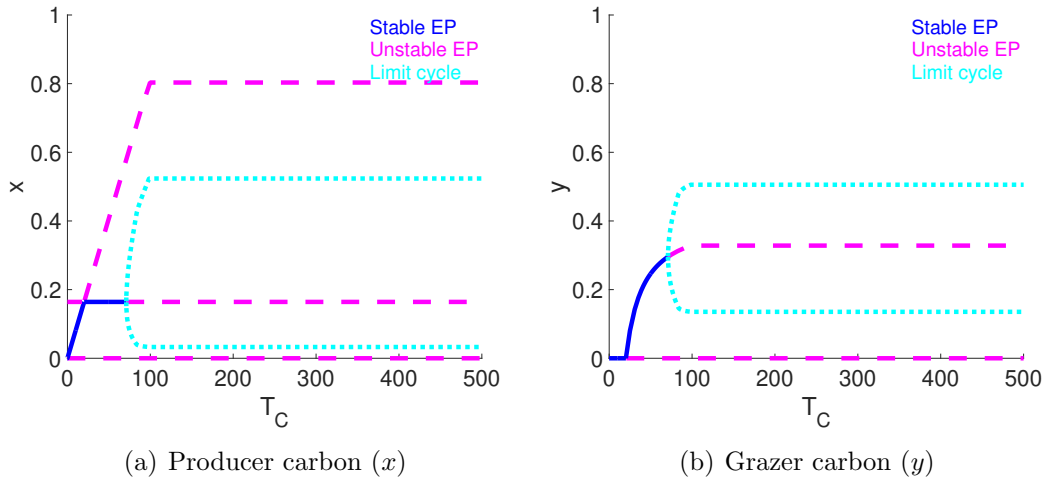


Figure 3.12: T_C bifurcation diagrams: $K = 1.00$, $T_P = 0.030$, $\gamma = 0.01023$. x is on the left and y is on the right. There is a transcritical bifurcation around $T_C = 20.14$ and a Hopf bifurcation at $T_C = 70.96$. For $T_C < 20.14$, the grazer extinction equilibrium is stable; for $20.14 < T_C < 70.96$, the coexistence equilibrium is stable; and for $T_C > 70.96$, the limit cycle is stable.

for up to at least $T_C = 1000$.

Note that for the low phosphorus case shown in Figure 3.10, the producers are carbon limited at equilibrium until around $T_C = 73$, after which point they are phosphorus limited; the grazers are quantity limited until around $T_C = 8.9$, after which they are quality limited. For the low light case shown in Figure 3.11, the producers are carbon limited at equilibrium until around $T_C = 24$, after which they are light limited; the grazers are quantity limited throughout. For the intermediate light and phosphorus case shown in Figure 3.12, the producers are carbon limited at equilibrium throughout and the grazers are quantity limited before the limit cycle at equilibrium ($T_C < 70.96$). For the high light case shown in Figure 3.13, the producers are carbon limited at equilibrium before the limit cycle ($T_C < 70.96$), as well as after the limit

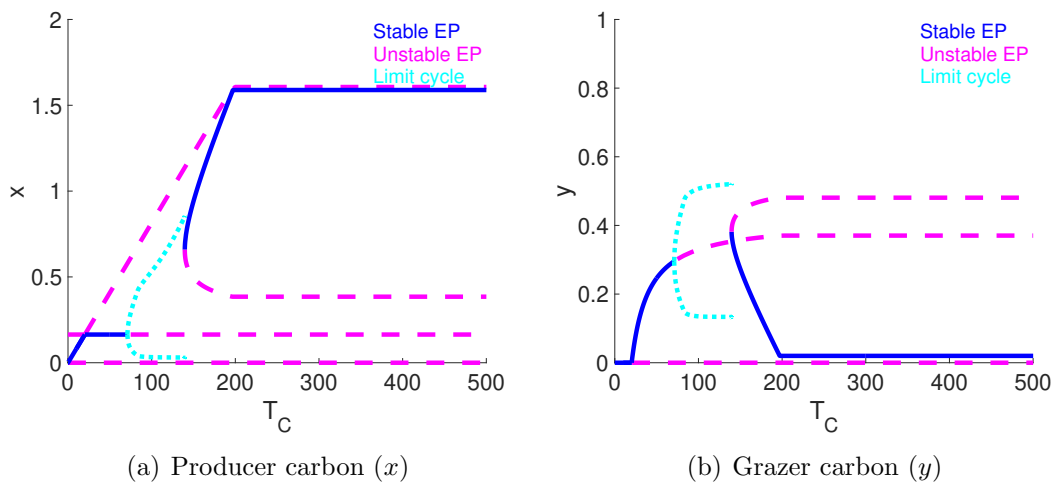


Figure 3.13: T_C bifurcation diagrams: $K = 2.00$, $T_P = 0.030$, $\gamma = 0.01023$. x is on the left and y is on the right. There is a transcritical bifurcation around $T_C = 20.14$, a Hopf bifurcation at $T_C = 70.96$, and a saddle-node bifurcation around $T_C = 139.61$. For $T_C < 20.14$, the grazer extinction equilibrium is stable; for $20.14 < T_C < 70.96$, the coexistence equilibrium is stable; for $70.96 < T_C < 139.61$, the limit cycle is stable; for $T_C > 139.61$, the second coexistence equilibrium is stable. Note the different axes scales between (a) and (b).

cycle until around $T_C = 196$, after which they are light limited. The grazers are quantity limited before the limit cycle ($T_C < 70.96$), and quality limited after the limit cycle ($T_C > 139.61$).

Total system phosphorus: T_P

All bifurcation diagrams for T_P begin with the stable grazer extinction equilibrium, until it becomes unstable and the coexistence equilibrium becomes stable at a transcritical bifurcation. The bifurcation value depends on K and γ . In general, as K increases, the bifurcation value of T_P increases, until a point. For $\gamma = 0.0045$, the maximum T_P bifurcation value appears to be 0.00963; for $\gamma = 0.00767$, it is $T_P = 0.01354$; for $\gamma = 0.01023$, it is $T_P = 0.01670$; and for $\gamma = 0.021$, it is at least $T_P = 0.02947$ (achieved for $K = 2.00$). The bifurcation values for high carbon ($T_C = 409.4$) match those for ambient carbon ($T_C = 98.2$) and the maximum γ value ($\gamma = 0.021$), with the exception of $K = 2.00$, $\gamma = 0.0045$ and $T_C = 409.4$, which has a slightly lower bifurcation value.

The transcritical bifurcation yields stability for the coexistence equilibrium. For a sufficiently low light-dependent carrying capacity, $K = 0.25$, the coexistence equilibrium remains stable for T_P up to at least 3 regardless of γ or T_C , as shown in Figure 3.14. This also holds for all K when $\gamma = 0.0045$ at ambient carbon ($T_C = 98.2$). For all other parameter combinations investigated, the coexistence equilibrium remains stable until a saddle-node bifurcation. The relative saddle-node bifurcation values follow a similar pattern to the transcritical bifurcation values. For any regimes that underwent the saddle-node bifurcation, the limit cycle remains stable for T_P up to at least 3, as shown in

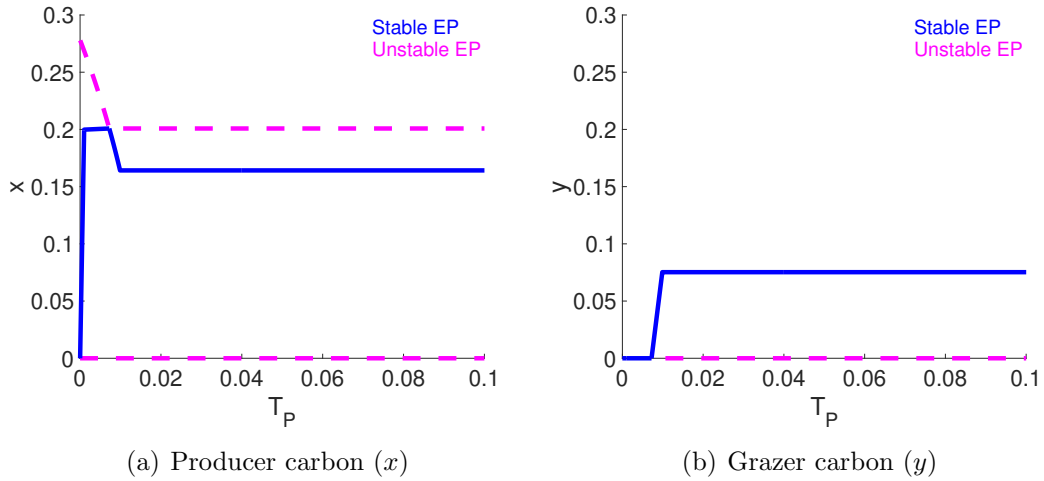


Figure 3.14: T_P bifurcation diagrams: $K = 0.25$, $T_C = 98.2$, $\gamma = 0.0045$. x is on the left and y is on the right. There is a transcritical bifurcation around $T_P = 0.0072$. For $T_P < 0.0072$, the grazer extinction equilibrium is stable; and for $T_P > 0.0072$, the coexistence equilibrium is feasible and stable.

Figure 3.15. Given the dynamics, there should likely be another saddle-node bifurcation along the unstable coexistence equilibrium, followed by a Hopf bifurcation, but these could not be located using MatCont. Note that as the limit cycle approaches the visible saddle-node bifurcation from the right, the period increases drastically. A similar behaviour was observed for ambient carbon for $K = 1.00$ with $\gamma = 0.01023$ or 0.021 , and for $K = 2.00$ with $\gamma = 0.01023$; as well as for high carbon for $K = 1.00$ with $\gamma = 0.0045$. In all of these cases except the one shown in Figure 3.15, MatCont detected a limit point bifurcation of cycles.

We can consider what factors are limiting at equilibrium for these diagrams. For Figure 3.14, the producers are limited by phosphorus until around $T_P = 0.0010$, after which they are light limited; the grazers are quality (phosphorus) limited until around $T_P = 0.0099$, after which they are quantity lim-

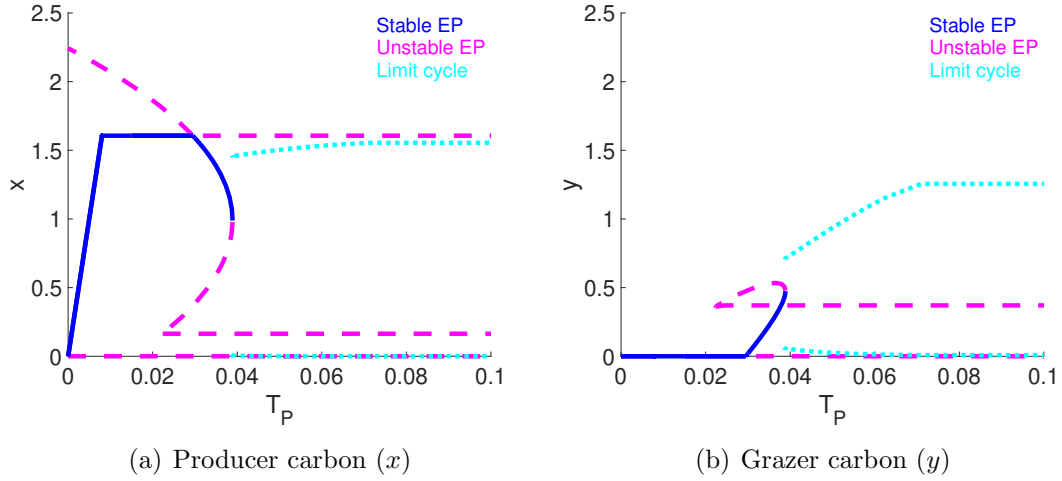


Figure 3.15: T_P bifurcation diagrams: $K = 2.00$, $T_C = 98.2$, $\gamma = 0.021$. x is on the left and y is on the right. There is a transcritical bifurcation around $T_P = 0.029$ and a saddle-node bifurcation at $T_P = 0.039$. An additional saddle-node bifurcation and Hopf bifurcation may also occur. For $T_P < 0.029$, the grazer extinction equilibrium is stable; for $0.029 < T_P < 0.039$, the coexistence equilibrium is stable; and for $T_P > 0.039$, the limit cycle is stable.

ited. For Figure 3.15, the producers are limited by phosphorus until around $T_P = 0.0080$, after which they are light limited; the grazers are quality (phosphorus) limited throughout. We observe that there is a pattern here: the producers are limited by phosphorus until $T_P = Kq$.

There were some cases where bistability was observed. At ambient carbon ($T_C = 98.2$), bistability occurred for $K = 0.75$, $\gamma \in \{0.00767, 0.01023, 0.021\}$; $K = 1.00$, $\gamma \in \{0.00767, 0.01023, 0.021\}$; and $K = 2.00$, $\gamma \in \{0.00767, 0.01023\}$. Of the high carbon ($T_C = 409.4$) bifurcation diagrams produced, bistability was observed for $K = 0.75$, $\gamma = 0.021$. The bifurcation diagrams look similar to Figure 3.16, which demonstrates the high carbon bistability observed. The limitations at equilibrium in this figure follow the same pattern as Figure 3.15, with the change around $T_P = 0.0030$.

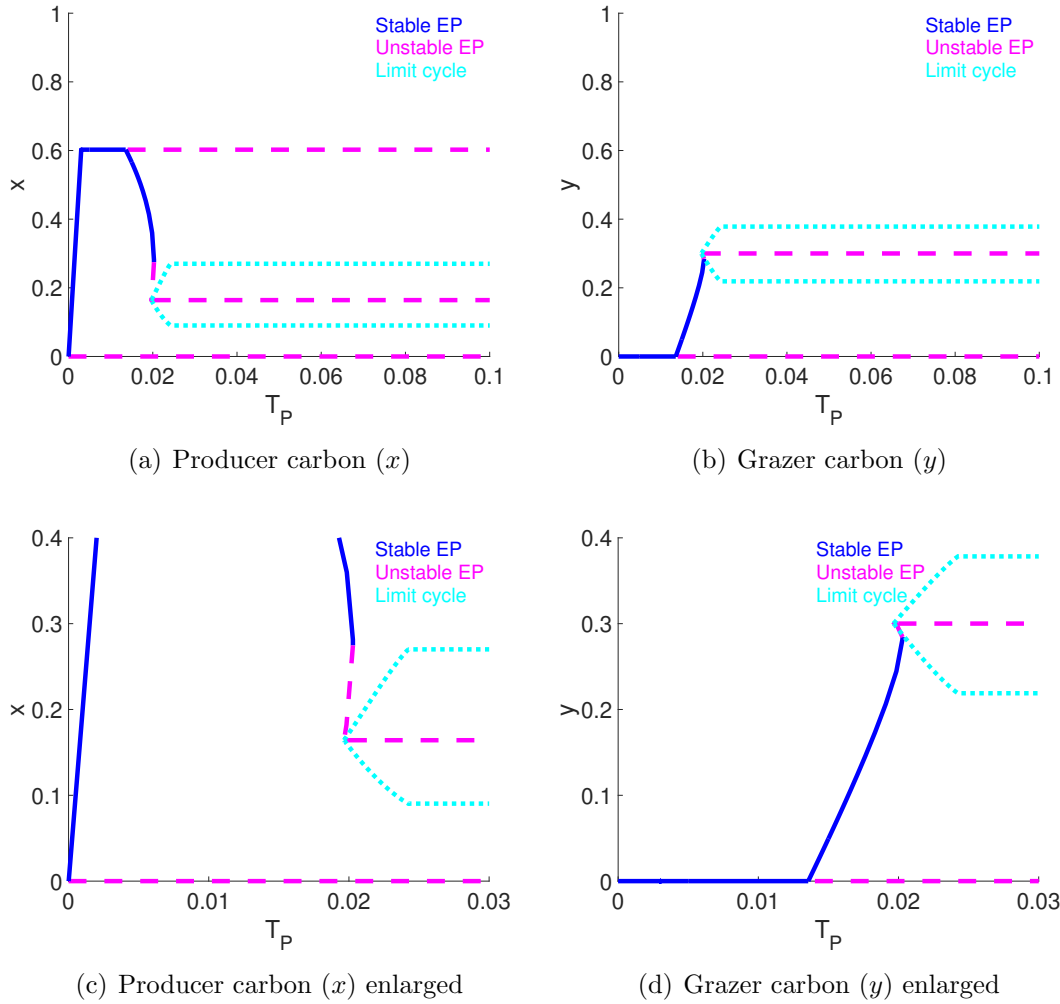


Figure 3.16: T_P bifurcation diagrams: $K = 0.75$, $T_C = 409.4$, $\gamma = 0.021$. x is on the left and y is on the right. There is a transcritical bifurcation around $T_P = 0.014$, a saddle-node bifurcation at $T_P = 0.0196$, a Hopf bifurcation at $T_P = 0.0197$ and a second saddle-node bifurcation at $T_P = 0.0203$. For $T_P < 0.014$, the grazer extinction equilibrium is stable; for $0.014 < T_P < 0.0203$, the coexistence equilibrium is stable; and for $T_P > 0.0197$, the limit cycle is stable.

More specifically, a stable equilibrium point and a stable limit cycle were both observed for the same parameter values but different initial conditions, as shown in Figure 3.17. Note that $T_P = 0.02$ lies in the bistable region, since this is between the Hopf bifurcation and the second saddle-node bifurcation in Figure 3.16. The brief interval of stability of the second coexistence equilibrium branch between the first saddle-node bifurcation and the Hopf bifurcation is too small to distinguish in the diagram. There is also an unstable equilibrium around $(x, y, p) = (0.1642, 0.3001, 0.0069)$, with eigenvalues given by $\lambda_1 = -3.7428$; $\lambda_2 = 0.0059 + 0.2686i$; and $\lambda_3 = 0.0059 - 0.2686i$. Given how close the real part of λ_2 and λ_3 is to 0, tristability may also be possible. However, the correct parameter regime to produce tristability has not yet been determined. Given the relative bifurcation values of the first saddle-node bifurcation and the Hopf bifurcation, we would guess tristability would occur for some $T_P \in (0.0196, 0.0197)$.

3.4.3 Two parameter bifurcation analysis

Two parameter bifurcation diagrams were also generated using MatCont [10] for the local closed model. Note that for low phosphorus, there are no bifurcations – the grazer extinction equilibrium is stable for all parameter combinations considered with $T_P = 0.003$. Bifurcation diagrams were made for each pair of light-dependent carrying capacity, total system phosphorus, and total system carbon. In addition to the two parameters being considered, the other two of K , T_P , T_C , and γ are also varied within the sets described in the previous section.

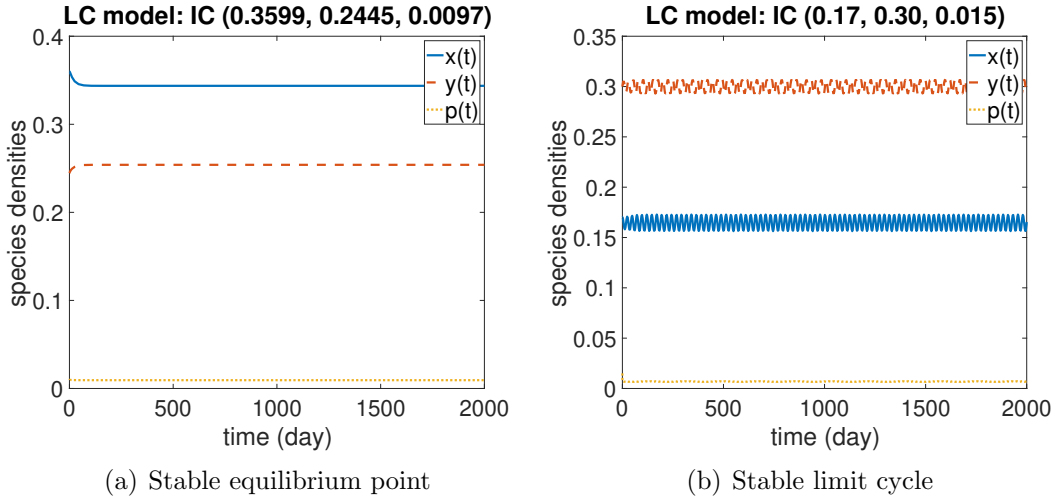


Figure 3.17: Bistable states for the local closed model, with $K = 0.75$, $T_C = 409.4$, $T_P = 0.020$, $\gamma = 0.021$, and two distinct initial conditions. For $(x(0), y(0), p(0)) = (0.3599, 0.2445, 0.0097)$, the coexistence equilibrium point is stable; for $(x(0), y(0), p(0)) = (0.17, 0.30, 0.015)$, coexistence oscillations are stable.

Light-dependent carrying capacity (K) and total system carbon (T_C)

Recall that for low phosphorus, there are no bifurcations and thus the two parameter bifurcation diagrams would have no curves. The intermediate and high phosphorus diagrams have more bifurcations and regions.

For intermediate phosphorus ($T_P = 0.030$), the resulting diagrams are similar to Figure 3.18 (a). Note that changing γ has no impact on the K bifurcation values, while the T_C bifurcation points occur at a lower value for higher γ . We see that for the lowest values of K and T_C , there is extinction of the grazer; then as either or both parameters increase, there is a transcritical bifurcation and the coexistence equilibrium becomes stable; then there is a Hopf bifurcation and there is a stable limit cycle; then after a saddle-node bifurcation, another coexistence equilibrium becomes stable; and then after a transcritical bifurcation, the grazer extinction equilibrium becomes stable

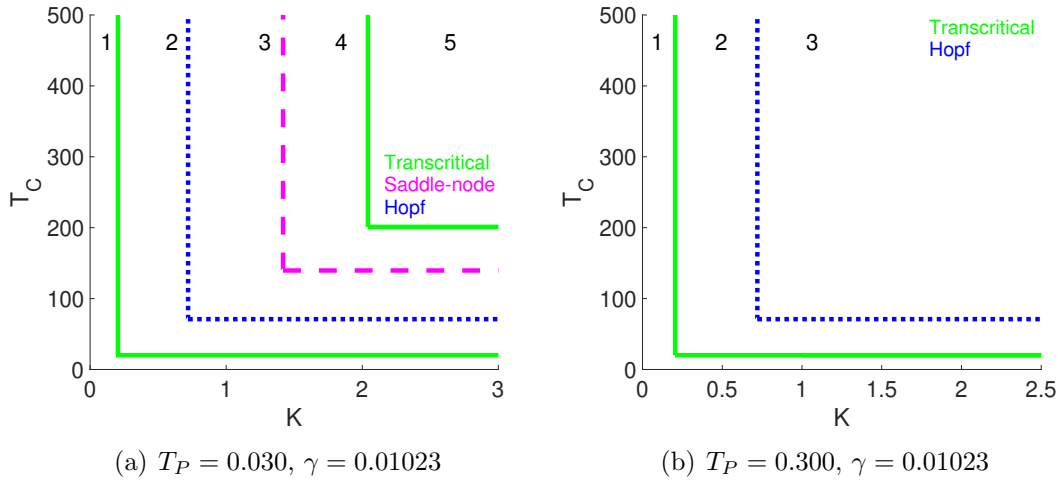


Figure 3.18: Two parameter bifurcation diagram for light-dependent carrying capacity (K) and total system carbon (T_C). The stable behaviours in the regions are: (1) extinction of the grazer; (2) coexistence equilibrium; (3) coexistence limit cycle; (4) coexistence equilibrium; and (5) extinction of the grazer. There is a Generalized Hopf point where the Hopf curves intersect.

once more. There is a Generalized Hopf point where the vertical and horizontal Hopf curves intersect. For Figure 3.18 (a), this occurs at $K = 0.721274$ and $T_C = 70.962739$.

For high phosphorus ($T_P = 0.300$), the diagrams are similar to Figure 3.18 (b). Unlike the intermediate phosphorus case, there are only three regions. As the parameters increase, the system's stable behaviour shifts from the grazer extinction equilibrium, to the coexistence equilibrium, to a limit cycle. There is no switch to another coexistence equilibrium and then back to the grazer extinction equilibrium in this case. Similar to the intermediate phosphorus case, there is a Generalized Hopf point where the Hopf curves intersect. For Figure 3.18 (b), this occurs at $K = 0.721273$ and $T_C = 70.962739$.

Light-dependent carrying capacity (K) and total system phosphorus (T_P)

For ambient carbon ($T_C = 98.2$), two categories of diagrams were observed. The first occurred for $\gamma = 0.0045$, and is shown in Figure 3.19 (a); the second is shown in Figure 3.19 (b) and occurs for $\gamma \in \{0.00767, 0.01023, 0.021\}$. For the lowest value of γ , there are only two sections: extinction of the grazer closest to the axes, then coexistence after the transcritical bifurcation. For higher values of γ , we see more regions. The general pattern is similar to what has been observed thus far: as either or both parameter values increase, the stable behaviour is the grazer extinction equilibrium before the transcritical bifurcation, then the coexistence equilibrium before the Hopf or saddle-node bifurcation, and then the stable limit cycle.

For ambient carbon and higher γ , there is an interesting transition across the saddle-node bifurcation curve (see Figure 3.19 (b)). For K larger than the Hopf bifurcation value, the saddle-node bifurcation value approximates where the stable behaviour switches from the coexistence equilibrium to the coexistence limit cycle. However, for the brief portion of the saddle-node bifurcation occurring at K less than the Hopf bifurcation value, a coexistence equilibrium is stable both before and after this bifurcation. Consider, for example, $K = 0.65$. The bifurcation is now a change in which coexistence equilibria is stable: for T_P less than the saddle-node bifurcation value, the equilibrium value requires the producers to be light limited and the grazers to be quality limited; for T_P greater than the saddle-node bifurcation value, the equilibrium value requires the producers to be light limited and the grazers to be quantity

limited. Comparatively, for $K = 0.25$, the producer is light limited and the grazer is quantity limited for T_P greater than the transcritical bifurcation; for $K = 1$, the producer is carbon limited and the grazer is quality limited. This suggests that the saddle-node curve should intersect the transcritical curve at some point with $0.25 < K < 0.5$; however, this point could not be found using MatCont.

For high carbon ($T_C = 409.4$), varying γ does not appear to have a large effect – only causing a very small difference in bifurcation values for T_P . Otherwise the shape and layout of the regions in the high carbon case match the high γ dynamics for $T_C = 98.2$, as shown in Figure 3.19 (c). However, the slopes of the slanted transcritical and saddle-node bifurcation curves are steeper, allowing for the case with four bifurcations seen in Figure 3.9 since a horizontal line at $T_P = 0.030$ can intersect all four curves, as shown in Figure 3.19 (d).

As in the T_P one parameter bifurcation diagrams, there are regions of potential bistability. For Figure 3.19 (b), there is a very small region between the horizontal saddle-node and Hopf bifurcation curves where bistability was observed in the one parameter diagrams for T_P . Figure 3.19 (c) is more complicated. For the T_P bifurcation diagrams, parts of regions 4 and 5 seemed to possibly allow bistability between an equilibrium and a limit cycle. However, for the K bifurcation diagrams made, region 4 had only a stable grazer extinction equilibrium, and region 5 had only a stable coexistence equilibrium. In these cases, any definitive conclusions on the potential for bistability would require further study.

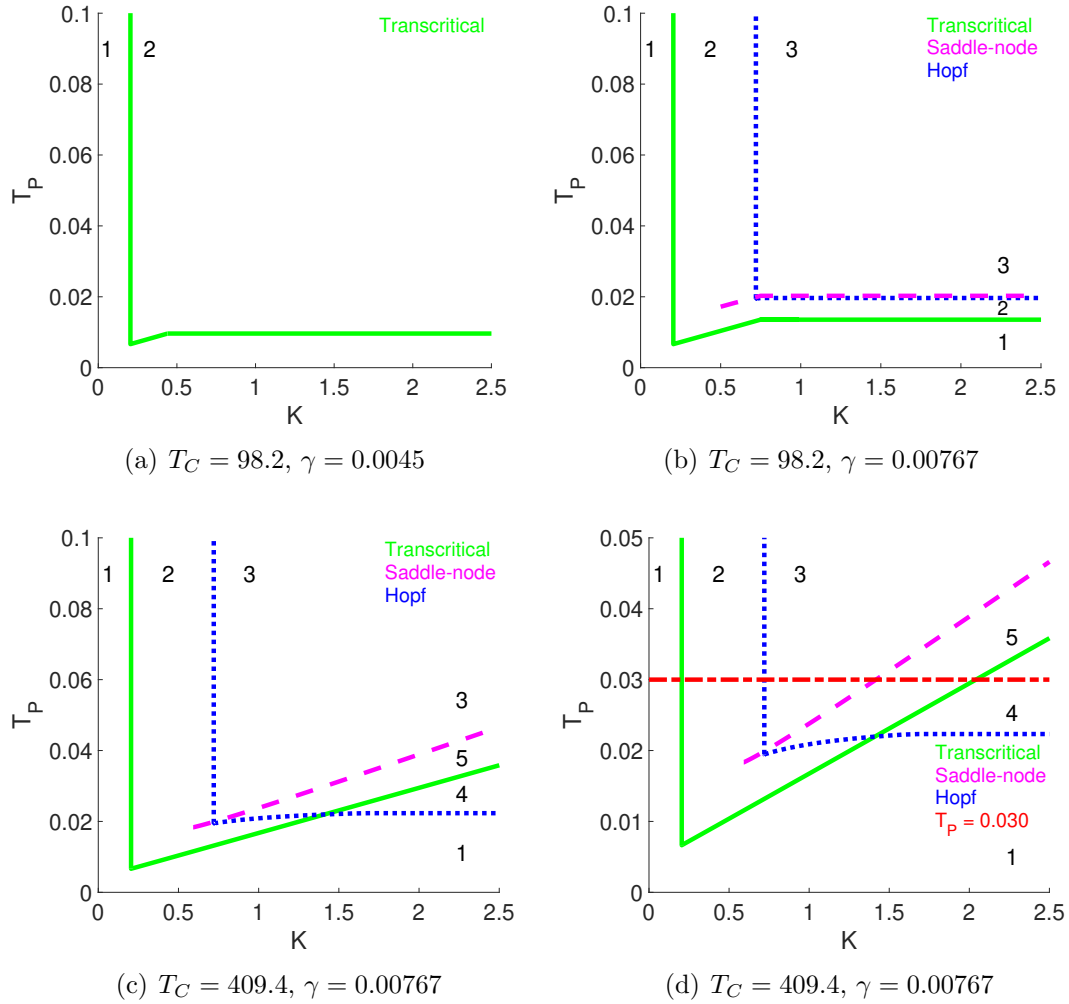


Figure 3.19: Two parameter bifurcation diagram for light-dependent carrying capacity (K) and total system phosphorus (T_P). The stable behaviours in the regions are: (1) extinction of the grazer; (2) coexistence equilibrium; (3) coexistence limit cycle; (4) bistability or grazer extinction equilibrium; and (5) bistability or coexistence equilibrium. Note that (d) explains the behaviour observed in Figure 3.9.

Total system carbon (T_C) and total system phosphorus (T_P)

The two parameter bifurcation diagrams for T_C and T_P appear to produce three general patterns. The first occurs for $K = 0.25$, and all γ investigated. In this case we see again the pattern of a stable grazer extinction equilibrium, then a transcritical bifurcation, and then a stable coexistence equilibrium as parameters increase. This is shown in Figure 3.20 (a).

The second pattern occurs for $\gamma = 0.0045$ for $K \in \{0.75, 1.00, 2.00\}$. Here we see that for the lowest parameter values, there is extinction of the grazer. Then there is a transcritical bifurcation, which yields a coexistence equilibrium. There is a vertical Hopf bifurcation curve, and a primarily horizontal saddle-node curve. As parameters increase beyond this, there is a stable limit cycle, as shown in Figure 3.20 (b). There is also a cusp point along the saddle-node curve. For Figure 3.20 (b), this point occurs at $T_C = 107.82902$ and $T_P = 0.01694185$.

Similar to some of the light and total system phosphorus diagrams, in this pattern we see an extension of the saddle-node curve into the coexistence equilibrium region. For $T_C = 99.9629$ and $T_P = 0.015$, the producer is carbon limited at equilibrium, while the grazer is quality limited; for $T_C = 99.9629$ and $T_P = 0.020$, the producer is carbon limited and the grazer is quantity limited. Therefore, the extension of the saddle-node curve into Region 2 is indicative of a switch between quality and quantity limitation of the grazer. Although both are coexistence equilibria, they likely have different forms.

The third general two parameter bifurcation diagram was observed for $K \in \{0.75, 1.00, 2.00\}$ and $\gamma \in \{0.00767, 0.01023, 0.021\}$. This diagram closely

resembles Figure 3.19 (b), and follows the similar pattern we have observed several times: as either or both parameter values increase, the stable behaviour is the grazer extinction equilibrium before the transcritical bifurcation, then the coexistence equilibrium before the Hopf or saddle-node bifurcation, and then the stable limit cycle. At the intersection of the Hopf curves, there is a Generalized Hopf point. For Figure 3.20 (c), this codimension 2 bifurcation occurs at $T_C = 94.455184$ and $T_P = 0.0195455$.

For both Figure 3.20 (b) and (c), there is a region of potential bistability between the horizontal Hopf curve and the horizontal saddle-node curve. While this region was observed in the one parameter T_P bifurcation diagrams, the appropriate T_C bifurcation diagrams have yet to be completed. Further investigation would be required to validate the bistable region indicated by the horizontal Hopf curve.

3.5 Discussion

There are many ecological stoichiometry models which have been developed to explicitly track the impacts of multiple elements on ecological interactions. However, these models usually assume that the system is completely open to carbon. This limits their usefulness in studying the potential impacts of increased atmospheric carbon dioxide concentration on food webs, since the availability of carbon for photosynthesis is not modelled. It has been proven that an increase in atmospheric carbon dioxide can cause an increase in the rate of photosynthesis, and a corresponding increase in growth and production of autotrophs. When producer-grazer systems are closed to nutrients such as

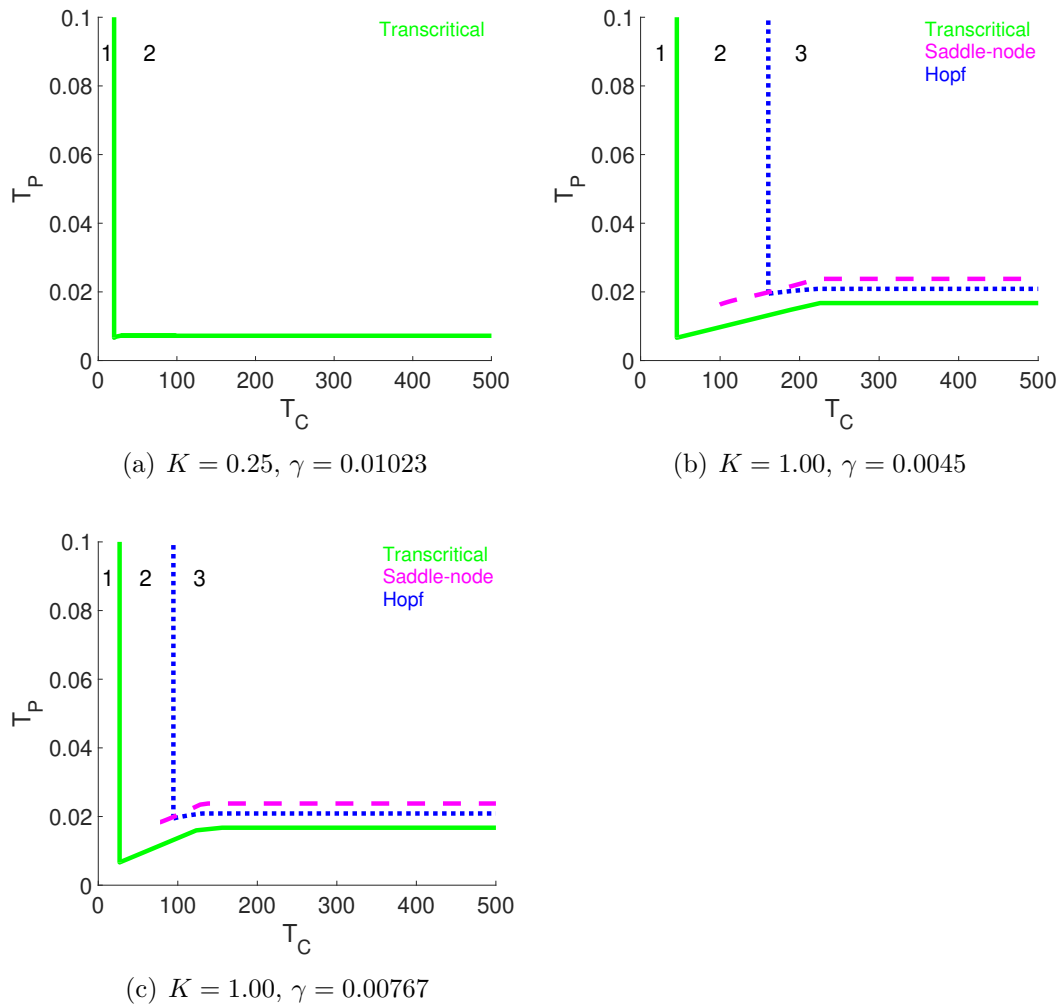


Figure 3.20: Two parameter bifurcation diagram for total system carbon (T_C) and total system phosphorus (T_P). The stable behaviours in the regions are: (1) extinction of the grazer; (2) coexistence equilibrium; and (3) coexistence limit cycle. In (b) there is a cusp point at $T_C = 107.8, T_P = 0.01694$; in (c), there is a Generalized Hopf point where the Hopf curves intersect.

phosphorus or nitrogen, the resulting decrease in nutrient levels in the producer can impact the growth of the grazers, which tend to have higher, more rigid nutrient requirements [44, 49].

In order to study the potential impacts of the current global increase in atmospheric carbon dioxide on producer-grazer systems, several models were developed to allow for explicit consideration of carbon availability. All three models were based on the WKL model [53], which was itself based on the LKE model [29]. The first model developed here has an additional carbon-dependent carrying capacity ($h(C)$) for producer growth in the minimum term, as well as explicit consideration of respiration. This “local closed model” is closed to carbon. The second model builds on the local closed model by including the reduction in photorespiration rate observed due to elevated CO_2 by using a function of free system carbon that reduces the producer respiration rate with more free carbon in the system, and is here called the “local closed model with PCO”. The third, and final model, extends the local closed model by allowing for some degree of openness in the system for carbon, and is therefore called the “local open model”.

Most of the analysis completed here was for the local closed model. For this model, there is a biologically meaningful region which is positively invariant. There is also a sufficient condition for global asymptotic stability of the total extinction equilibrium, which depends on several parameters, including the total phosphorus in the system. If we assume Holling type I functional responses for f and g , there are between 1 and 2 boundary equilibria, and there may also be coexistence equilibria. When f and g take the form of Holling type II functional responses, there are between 1 and 3 boundary equilibria,

and potentially coexistence equilibria. There are many complicated conditions for stability of these equilibria, dependent upon which factors are limiting for producer and grazer growth at the equilibria.

Bifurcation analysis of the local closed model generally demonstrated sequential limitation by the different growth factors for the producer, with the general pattern being stability of a grazer extinction equilibrium, then a coexistence equilibrium, and then a limit cycle. Occasionally the system also transitions to a second stable coexistence equilibrium via a saddle-node bifurcation, and very rarely, the system then returns to the grazer extinction equilibrium.

The three parameters examined in the bifurcation analysis were K , T_C , and T_P . These parameters contribute to determining the limiting factors for growth of the producer and grazer. We note the similarities between the diagrams for K and T_C in particular. For example, for low phosphorus and $\gamma = 0.01023$, we have Figure 3.5 and 3.10. In both diagrams, the grazer extinction equilibrium was stable throughout, and for a sufficiently high value of the bifurcating parameter, we have the same phosphorus limited grazer extinction equilibrium. We can similarly match the rest of the K and T_C diagrams, with the exception of the last K diagram. The figures match up as follows: 3.6 and 3.11; 3.7 and 3.12; and 3.8 and 3.13. The corresponding T_C diagram for Figure 3.9 is not shown here, but we found that there is also a second transcritical bifurcation in T_C for values of K higher than 2.04 around $T_C = 201.19309$. Although they follow a similar pattern, the T_P bifurcation diagrams are not nearly as similar to K and T_C as they are to each other.

The similarity between the qualitative impacts of K and T_C explains the

matching vertical and horizontal lines intersecting at almost right angles observed in the two parameter bifurcation diagrams for these parameters, shown in Figure 3.18. We also note the similarities between Figures 3.19 and 3.20, particularly between the low γ and light cases (a), and the intermediate γ and light cases (b). Here changing γ is an analogue for changing T_C , since $T_C \gg x, y$, and thus changing either γ or T_C has a similar impact on $h(C) = \gamma(T_C - x - y)$. Altogether, these similarities suggest that the light-dependent producer carrying capacity should not be included as well as the carbon-dependent producer carrying capacity in these new models.

Simulations were used to compare the three models, along with the WKL model with respiration, for a variety of parameter combinations. In general, the combinations examined either produced a grazer extinction equilibrium, a coexistence equilibrium, or coexistence oscillations. In certain cases, bistability between a coexistence equilibrium and a limit cycle was observed. Overall, the dynamics seemed to be very similar between the models, with the exception of the cases where the WKL model with respiration is drastically different from our three models. Even though the differences were minimal, the most distinct model at high carbon was the one incorporating consideration of reduction of photorespiration with increased availability of carbon. Taken together, the models suggest that increased carbon sequestration and decreased stoichiometric quality of producers would require sufficient light and nutrients, as expected given the application of Liebig's Law of the Minimum.

There are limitations for both these models and their analyses. All three models rely on an assumption of independent colimitation of producer growth by light, carbon, and phosphorus. The assumption of independent colimitation

by light and phosphorus is a common assumption in ecological stoichiometry models [29, 53]. Also, there is evidence for independent colimitation by carbon and phosphorus [43]. However, there is no strong support for the assumption of independent colimitation of producer growth by light and carbon. This simplifying assumption is not only a limitation on applicability of the results, but it also may unrealistically limit the growth of the producer. There is empirical evidence that elevated carbon dioxide is correlated to increased growth of plants growing in shade [24, 31, 57]. This is likely because elevated carbon dioxide increases light use efficiency, partially since the increase in carbon fixation due to reduction of photorespiration requires no additional light [12], as well as because elevated CO₂ can decrease the light compensation point of a leaf [30]. This evidence supports the theory that colimitation of light and carbon may not be independent.

Additional impacts of increased carbon dioxide on producers that were not incorporated into this model include changes in carbon allocation, changes in light or nutrient efficiencies, changes in dark respiration (mitochondrial/cellular respiration), and changes in decomposition rates. There is contradictory evidence for changes in carbon allocation. Some evidence seems to support an increase in plant root:shoot ratio and leaf area [15]; some supports no stimulation in foliage [12]; and some suggests an increase in fine root allocation at the expense of wood and leaves, or increase in wood allocation at the expense of leaves [9, 41]. Similarly, the evidence for changes in respiration is inconsistent, with plants grown in elevated carbon dioxide exhibiting an increase, decrease, or no significant change in dark respiration rates [25]. Lastly, incorporation of changes in the rates of decomposition in this model, such as those discussed

in [8], would require relaxation of the assumption that carbon and phosphorus released by the producer and grazer is immediately available for use.

There are many opportunities for future work for both this specific research question and these models. The vast majority of analysis completed is for the local closed model, and thus the more complicated models remain to be analyzed. In particular, it would be interesting to consider the impact of the “openness” (α) for the local open model. For the model with PCO, a more evidence-based method of selecting $\rho(C)$, as well as modification to see at what point dynamics shift, may allow us to better understand the impacts of increased global atmospheric carbon dioxide concentration on producer-grazer systems. Also, the bifurcation analysis completed is local. Even with the variety of parameter regimes considered, there are likely other behaviours that would be observed in natural systems that are not explored here.

Modelling wise, incorporation of more factors such as those described above may be interesting. In addition, a model considering nitrogen instead of phosphorus as a limiting nutrient could be illuminating. Nitrogen is a commonly limiting nutrient in terrestrial systems [44], and it may be more closely related to photosynthesis since up to 25% of leaf nitrogen is used in Rubisco, the carbon fixation enzyme, and increased efficiency of Rubisco due to increased atmospheric carbon dioxide concentration causes a reduction in allocation of nitrogen to Rubisco [12].

Additional research questions that could be addressed using these models include investigation of dynamic shifts due to elevated carbon dioxide specifically for terrestrial versus aquatic systems, similar to Chapter 2; and investigation of the impact of elevated atmospheric carbon dioxide concentration on

competition between grazers with different nutrient requirements.

Lastly, all of these models would likely benefit from data fitting and validation. As it stands, many of the parameter regions examined are primarily theoretical. It would be valuable to apply data from free-air carbon enrichment experiments, as well as experiments such as those conducted by Urabe et al. (2003) [49] to understand which parameter regions require further study.

Chapter 4

Discussion

4.1 Conclusions

Many stoichiometric models have been developed from the LKE model, which was itself developed to address the paradox in which abundant producers did not increase abundance of the grazers which consumed them [29]. The WKL model relaxed the assumption that there was no free phosphorus in the medium [53]. Prior to this thesis, analyses of the WKL model in particular include stability analysis assuming Holling type I functional responses, and local bifurcation analysis for the light-dependent carrying capacity, K . Although analyses focussing on K provide information about the potential for this paradox occurring, they do not address other questions, such as how the different producer turnover rates between terrestrial and aquatic ecosystems impact dynamics. Also, since this model, as well as most other stoichiometric models, requires the system to be open to carbon, it is difficult to answer questions about the impacts of elevated atmospheric carbon dioxide concentrations on ecosystems

using the WKL model.

From chapter 2, we observe that the WKL model suggests that aquatic ecosystems are more prone to exhibiting coexistence than terrestrial ecosystems when we assume that the producer's intrinsic growth rate (r) and the grazer's ingestion rate (c) are the only two parameters that differ between these ecosystems. Local sensitivity analysis implies c has more influence than r on the asymptotic system state, and changing K influences the impact of r more than c . However, other parameters seem to be more influential. At extreme values of K , the grazer loss rate is relatively influential, and if \hat{d} is too high relative to c , extinction of the grazer is guaranteed. Intermediate light levels in some terrestrial ecosystems may explain persistence of grazer populations observed naturally, while a lower grazer loss rate may explain terrestrial grazer persistence in low light conditions.

In chapter 3, we developed a few different models to study the impacts of elevated atmospheric carbon dioxide concentration on producer-grazer systems. For the local closed model, the focus of this chapter, we have a biologically meaningful forward invariant set, a sufficient condition for global asymptotic stability of the total extinction equilibrium, and the forms and some stability results for the grazer extinction equilibria using either Holling type I or II functional responses. We observed sequential limitation by the producer growth factors, where the limiting parameter increasing forces the system to follow a pattern of a stable grazer extinction equilibrium, then a stable coexistence equilibrium, and then a stable limit cycle. Ultimately, the three models produced very similar results for the parameter regimes examined.

4.2 Future Work

Future work to address differences between terrestrial and aquatic ecosystems could include examination of larger parameter ranges. In particular, parameter ranges or combinations determined via data fitting could be particularly illuminating. Also, explicit consideration of the grazer's loss rate in addition to the parameters that determine the producer turnover time may allow us to understand how terrestrial grazer populations persist naturally. This may require relaxation of the assumption of strict homeostasis for the grazer, which may require a different model [54, 55]. Global stability, bifurcation, and sensitivity analyses could also be useful, as those completed here are all local.

For the impact of elevated carbon dioxide on producer-grazer systems, future work could include consideration of other effects assumed to be negligible here, such as changes in carbon allocation, dark respiration rates, and decomposition rates. Analyses for the local closed model with PCO and the local open model also have yet to be done. Similarly, global analyses for the local closed model could also be completed. Due to its close ties to photosynthesis, modelling nitrogen instead of phosphorus as the limiting nutrient may be illuminating, although considerably more complicated due to systems rarely being closed to nitrogen. One might also have to consider if colimitation between nitrogen and the photosynthetic factors is independent. However, before any of this is completed, it would be beneficial to use data to validate these models, and decide what parameter regimes are realistic.

Bibliography

- [1] Elizabeth A Ainsworth and Alistair Rogers. The response of photosynthesis and stomatal conductance to rising $[\text{CO}_2]$: mechanisms and environmental interactions. *Plant, Cell and Environment*, 30(3):258–270, 2007.
- [2] Lale Asik, Jackson Kulik, Kevin Long, and Angela Peace. Dynamics of a stoichiometric producer–grazer system with seasonal effects on light level. *Mathematical Biosciences and Engineering*, 16(1):501–515, 2018.
- [3] Lale Asik and Angela Peace. Dynamics of a producer–grazer model incorporating the effects of phosphorus loading on grazer’s growth. *Bulletin of Mathematical Biology*, 81(5):1352–1368, 2019.
- [4] Steffen Burkhardt and Ulf Riebesell. CO_2 availability affects elemental composition (C: N: P) of the marine diatom *Skeletonema costatum*. *Marine Ecology Progress Series*, 155:67–76, 1997.
- [5] Just Cebrian. Patterns in the fate of production in plant communities. *The American Naturalist*, 154(4):449–468, 1999.
- [6] Xi Chen, Stephen B Baines, and Nicholas S Fisher. Can copepods be limited by the iron content of their food? *Limnology and Oceanography*, 56(2):451–460, 2011.
- [7] Nakul Chitnis, James M Hyman, and Jim M Cushing. Determining important parameters in the spread of malaria through the sensitivity analysis of a mathematical model. *Bulletin of Mathematical Biology*, 70(5):1272–1296, 2008.
- [8] Marie-Anne de Graaff, Kees-Jan van Groenigen, Johan Six, Bruce Hungate, and Chris van Kessel. Interactions between plant growth and soil nutrient cycling under elevated CO_2 : a meta-analysis. *Global Change Biology*, 12(11):2077–2091, 2006.

- [9] Martin G De Kauwe, Belinda E Medlyn, Sönke Zaehle, Anthony P Walker, Michael C Dietze, Thomas Hickler, Atul K Jain, Yiqi Luo, William J Parton, I Colin Prentice, et al. Forest water use and water use efficiency at elevated CO₂: a model-data intercomparison at two contrasting temperate forest FACE sites. *Global Change Biology*, 19(6):1759–1779, 2013.
- [10] Annick Dhooge, Willy Govaerts, Yu A Kuznetsov, Hil Gaétan Ellart Meijer, and Bart Sautois. New features of the software MatCont for bifurcation analysis of dynamical systems. *Mathematical and Computer Modelling of Dynamical Systems*, 14(2):147–175, 2008.
- [11] Sebastian Diehl. Paradoxes of enrichment: effects of increased light versus nutrient supply on pelagic producer–grazer systems. *The American Naturalist*, 169(6):E173–E191, 2007.
- [12] Bert G Drake, Miquel A González-Meler, and Steve P Long. More efficient plants: a consequence of rising atmospheric CO₂? *Annual Review of Plant Biology*, 48(1):609–639, 1997.
- [13] Chenjun Du, Xiaodan Wang, Mengyao Zhang, Jie Jing, and Yongheng Gao. Effects of elevated CO₂ on plant CNP stoichiometry in terrestrial ecosystems: a meta-analysis. *Science of the Total Environment*, 650:697–708, 2019.
- [14] Leah Edelstein-Keshet. *Mathematical Models in Biology*. SIAM, 2005.
- [15] James J Elser, William F Fagan, Andrew J Kerkhoff, Nathan G Swenson, and Brian J Enquist. Biological stoichiometry of plant production: metabolism, scaling and ecological response to global change. *New Phytologist*, 186(3):593–608, 2010.
- [16] James J Elser and Yang Kuang. Ecological stoichiometry. *Encyclopedia of Theoretical Ecology*, 84:718–722, 2002.
- [17] Willy Govaerts. Numerical bifurcation analysis for ODEs. *Journal of Computational and Applied Mathematics*, 125(1-2):57–68, 2000.
- [18] John Guckenheimer and Philip Holmes. *Nonlinear Oscillations, Dynamical Systems, and Bifurcations of Vector Fields*. Springer, 1983.
- [19] Michael R Guevara. Bifurcations involving fixed points and limit cycles in biological systems. In *Nonlinear Dynamics in Physiology and Medicine*, pages 41–85. Springer, 2003.

- [20] MPR Haaker and Peter JT Verheijen. Local and global sensitivity analysis for a reactor design with parameter uncertainty. *Chemical Engineering Research and Design*, 82(5):591–598, 2004.
- [21] Daniel A Herms and William J Mattson. The dilemma of plants: to grow or defend. *The Quarterly Review of Biology*, 67(3):283–335, 1992.
- [22] Dag O Hessen, James J Elser, Robert W Sterner, and Jotaro Urabe. Ecological stoichiometry: an elementary approach using basic principles. *Limnology and Oceanography*, 58(6):2219–2236, 2013.
- [23] Jude D Kong, Paul Salceanu, and Hao Wang. A stoichiometric organic matter decomposition model in a chemostat culture. *Journal of Mathematical Biology*, 76(3):609–644, 2018.
- [24] Christian Körner. Responses of humid tropical trees to rising CO₂. *Annual Review of Ecology, Evolution, and Systematics*, 40:61–79, 2009.
- [25] Andrew DB Leakey, Elizabeth A Ainsworth, Carl J Bernacchi, Alistair Rogers, Stephen P Long, and Donald R Ort. Elevated CO₂ effects on plant carbon, nitrogen, and water relations: six important lessons from FACE. *Journal of Experimental Botany*, 60(10):2859–2876, 2009.
- [26] Wai Leong and Joseph R Pawlik. Evidence of a resource trade-off between growth and chemical defenses among Caribbean coral reef sponges. *Marine Ecology Progress Series*, 406:71–78, 2010.
- [27] Xiong Li and Hao Wang. A stoichiometrically derived algal growth model and its global analysis. *Mathematical Biosciences and Engineering*, 7(4):825–836, 2010.
- [28] Xiong Li, Hao Wang, and Yang Kuang. Global analysis of a stoichiometric producer–grazer model with Holling Type functional responses. *Journal of Mathematical Biology*, 63(5):901–932, 2011.
- [29] Irakli Loladze, Yang Kuang, and James J Elser. Stoichiometry in producer-grazer systems: linking energy flow with element cycling. *Bulletin of Mathematical Biology*, 62(6):1137–1162, 2000.
- [30] Stephen P Long and Bert G Drake. Effect of the long-term elevation of CO₂ concentration in the field on the quantum yield of photosynthesis of the C₃ sedge, *Scirpus olneyi*. *Plant Physiology*, 96(1):221–226, 1991.

- [31] Catherine E Lovelock, D Kylo, and Klaus Winter. Growth responses to vesicular-arbuscular mycorrhizae and elevated CO₂ in seedlings of a tropical tree, *Beilschmiedia pendula*. *Functional Ecology*, 10(5):662–667, 1996.
- [32] Etienne Low-Décarie, Gregor F Fussmann, and Graham Bell. Aquatic primary production in a high-CO₂ world. *Trends in Ecology & Evolution*, 29(4):223–232, 2014.
- [33] Ivan A Nestorov. Sensitivity analysis of pharmacokinetic and pharmacodynamic systems: I. A structural approach to sensitivity analysis of physiologically based pharmacokinetic models. *Journal of Pharmacokinetics and Biopharmaceutics*, 27(6):577–596, 1999.
- [34] Rajendra K Pachauri, Myles R Allen, Vicente R Barros, John Broome, Wolfgang Cramer, Renate Christ, John A Church, Leon Clarke, Qin Dahe, Purnamita Dasgupta, et al. *Climate Change 2014: Synthesis Report. Contribution of Working Groups I, II and III to the Fifth Assessment Report of the Intergovernmental Panel on Climate Change*. IPCC, 2014.
- [35] Angela Peace and Hao Wang. Compensatory foraging in stoichiometric producer–grazer models. *Bulletin of Mathematical Biology*, 81(12):4932–4950, 2019.
- [36] Angela Peace, Hao Wang, and Yang Kuang. Dynamics of a producer–grazer model incorporating the effects of excess food nutrient content on grazer’s growth. *Bulletin of Mathematical Biology*, 76(9):2175–2197, 2014.
- [37] Angela Peace, Yuqin Zhao, Irakli Loladze, James J Elser, and Yang Kuang. A stoichiometric producer–grazer model incorporating the effects of excess food-nutrient content on consumer dynamics. *Mathematical Biosciences*, 244(2):107–115, 2013.
- [38] Robin A Pellew. The impacts of elephant, giraffe and fire upon the *Acacia tortilis* woodlands of the Serengeti. *African Journal of Ecology*, 21(1):41–74, 1983.
- [39] Robin A Pellew. Food consumption and energy budgets of the giraffe. *Journal of Applied Ecology*, 21(1):141–159, 1984.
- [40] Ralph H Petrucci, F Geoffrey Herring, Jeffrey D Madura, and Carey Bissonnette. *General Chemistry: Principles and Modern Applications*. Pearson Canada Inc., 10 edition, 2011.

- [41] TAM Pugh, Christoph Müller, Almuth Arneth, Vanessa Haverd, and Benjamin Smith. Key knowledge and data gaps in modelling the influence of CO₂ concentration on the terrestrial carbon sink. *Journal of Plant Physiology*, 203:3–15, 2016.
- [42] Jonathan B Shurin, Daniel S Gruner, and Helmut Hillebrand. All wet or dried up? Real differences between aquatic and terrestrial food webs. *Proceedings of the Royal Society B: Biological Sciences*, 273(1582):1–9, 2006.
- [43] Elly Spijkerman, Francisco de Castro, and Ursula Gaedke. Independent colimitation for carbon dioxide and inorganic phosphorus. *PLoS One*, 6(12), 2011.
- [44] Robert W Sterner and James J Elser. *Ecological stoichiometry: the biology of elements from molecules to the biosphere*. Princeton University Press, 2002.
- [45] Mark Stitt, John Lunn, and Björn Usadel. Arabidopsis and primary photosynthetic metabolism—more than the icing on the cake. *The Plant Journal*, 61(6):1067–1091, 2010.
- [46] Yukari Suzuki-Ohno, Masakado Kawata, and Jotaro Urabe. Optimal feeding under stoichiometric constraints: a model of compensatory feeding with functional response. *Oikos*, 121(4):569–578, 2012.
- [47] Tamás Turányi and Alison S Tomlin. Sensitivity and uncertainty analyses. In *Analysis of Kinetic Reaction Mechanisms*, pages 61–144. Springer, 2014.
- [48] Jotaro Urabe, James J Elser, Marcia Kyle, Takehito Yoshida, Tatsuki Sekino, and Zenichiro Kawabata. Herbivorous animals can mitigate unfavourable ratios of energy and material supplies by enhancing nutrient recycling. *Ecology Letters*, 5(2):177–185, 2002.
- [49] Jotaro Urabe, Jun Togari, and James J Elser. Stoichiometric impacts of increased carbon dioxide on a planktonic herbivore. *Global Change Biology*, 9(6):818–825, 2003.
- [50] Dedmer B van de Waal, Antonie M Verschoor, Jolanda MH Verspagen, Ellen van Donk, and Jef Huisman. Climate-driven changes in the ecological stoichiometry of aquatic ecosystems. *Frontiers in Ecology and the Environment*, 8(3):145–152, 2010.

- [51] Susanne von Caemmerer and W Paul Quick. Rubisco: physiology in vivo. In *Photosynthesis: Physiology and Metabolism*, pages 85–113. Springer, 2000.
- [52] Hao Wang, Katherine Dunning, James J Elser, and Yang Kuang. Daphnia species invasion, competitive exclusion, and chaotic coexistence. *Discrete and Continuous Dynamical Systems - Series B*, 12(2):481–493, 2009.
- [53] Hao Wang, Yang Kuang, and Irakli Loladze. Dynamics of a mechanistically derived stoichiometric producer–grazer model. *Journal of Biological Dynamics*, 2(3):286–296, 2008.
- [54] Hao Wang, Zexian Lu, and Aditya Raghavan. Weak dynamical threshold for the “strict homeostasis” assumption in ecological stoichiometry. *Ecological Modelling*, 384:233–240, 2018.
- [55] Hao Wang, Robert W Sterner, and James J Elser. On the “strict homeostasis” assumption in ecological stoichiometry. *Ecological Modelling*, 243:81–88, 2012.
- [56] Rik Wanninkhof. The impact of different gas exchange formulations and wind speed products on global air-sea CO₂ fluxes. In *Transport at the Air-Sea Interface*, pages 1–23. Springer, 2007.
- [57] MKR Würth, Klaus Winter, and Christian Körner. In situ responses to elevated CO₂ in tropical forest understorey plants. *Functional Ecology*, 12(6):886–895, 1998.
- [58] Tian Xie, Xianshan Yang, Xiong Li, and Hao Wang. Complete global and bifurcation analysis of a stoichiometric predator–prey model. *Journal of Dynamics and Differential Equations*, 30(2):447–472, 2018.
- [59] Masato Yamamichi, Cédric L Meunier, Angela Peace, Clay Prater, and Megan A Rúa. Rapid evolution of a consumer stoichiometric trait destabilizes consumer–producer dynamics. *Oikos*, 124(7):960–969, 2015.
- [60] Xianshan Yang, Xiong Li, Hao Wang, and Yang Kuang. Stability and bifurcation in a stoichiometric producer–grazer model with knife edge. *SIAM Journal on Applied Dynamical Systems*, 15(4):2051–2077, 2016.

Appendix A

Additional stability analysis for Chapter 2

Case 1: $\bar{p} < Kq$ and $\bar{p} < \theta\bar{x}$: $E_1 = (\bar{p}/q, 0, \bar{p})$.

Boundary equilibrium:

$$\left(\frac{dq(\hat{a} + T) - \hat{c}T}{q(dq - \hat{c})}, 0, \frac{dq(\hat{a} + T) - \hat{c}T}{dq - \hat{c}} \right).$$

Jacobian:

$$A_1 = \begin{bmatrix} -r & -\frac{c\bar{p}}{aq + \bar{p}} & \frac{r}{q} \\ 0 & \frac{c\hat{c}\bar{p}q}{\theta(aq + \bar{p})} - \hat{d} & 0 \\ \frac{\hat{c}(T - \bar{p})}{\hat{a} + T - \bar{p}} & -\frac{\hat{a}\hat{c}\theta\bar{p}}{q(\hat{a} + T - \bar{p})^2} - \frac{c\bar{p}q}{aq + \bar{p}} & -\frac{\hat{a}\hat{c}\bar{p}}{q(\hat{a} + T - \bar{p})^2} - d \end{bmatrix}.$$

Let the entries of matrix A_1 be labelled with a_{ij} , for the entry in row i , column j of matrix A_1 . Then we have

$$a_{11} = -r,$$

$$a_{12} = -\frac{c[dq(\hat{a} + T) - \hat{c}T]}{q[a(dq - \hat{c}) + d(\hat{a} + T)] - \hat{c}T},$$

$$a_{13} = \frac{r}{q},$$

$$a_{21} = 0,$$

$$a_{22} = \frac{c\hat{c}q[dq(\hat{a} + T) - \hat{c}T]}{\theta(aq(dq - \hat{c}) + dq(\hat{a} + T) - \hat{c}T)} - \hat{d},$$

$$a_{23} = 0,$$

$$\begin{aligned}
a_{31} &= dq, \\
a_{32} &= -\frac{\theta(dq(\hat{a} + T) - \hat{c}T)(dq - \hat{c})}{\hat{a}\hat{c}q} - \frac{cq[dq(\hat{a} + T) - \hat{c}T]}{\hat{a}dq + (aq + T)(dq - \hat{c})}, \\
a_{33} &= -\frac{d^2q^2(\hat{a} + T) + \hat{c}T(\hat{c} - 2dq)}{\hat{a}\hat{c}q}.
\end{aligned}$$

Then

$$\begin{aligned}
\text{tr}(A_1) &= a_{11} + a_{22} + a_{33} \\
&= -r + \frac{c\hat{c}q[dq(\hat{a} + T) - \hat{c}T]}{\theta(aq(dq - \hat{c}) + dq(\hat{a} + T) - \hat{c}T)} - \hat{d} - \frac{d^2q^2(\hat{a} + T) + \hat{c}T(\hat{c} - 2dq)}{\hat{a}\hat{c}q}. \\
\det(A_1) &= a_{22}(a_{11} * a_{33} - a_{13} * a_{31}) \\
&= \left(\frac{c\hat{c}q[dq(\hat{a} + T) - \hat{c}T]}{\theta(aq(dq - \hat{c}) + dq(\hat{a} + T) - \hat{c}T)} - \hat{d} \right) \\
&\quad \left(r \left(\frac{d^2q^2(\hat{a} + T) + \hat{c}T(\hat{c} - 2dq)}{\hat{a}\hat{c}q} \right) - dr \right). \\
A_1^{11} &= a_{22} * a_{33} \\
&= \left(\frac{c\hat{c}q[dq(\hat{a} + T) - \hat{c}T]}{\theta(aq(dq - \hat{c}) + dq(\hat{a} + T) - \hat{c}T)} - \hat{d} \right) \left(-\frac{d^2q^2(\hat{a} + T) + \hat{c}T(\hat{c} - 2dq)}{\hat{a}\hat{c}q} \right). \\
A_1^{22} &= a_{11} * a_{33} - a_{13} * a_{31} \\
&= r \left(\frac{d^2q^2(\hat{a} + T) + \hat{c}T(\hat{c} - 2dq)}{\hat{a}\hat{c}q} \right) - dr. \\
A_1^{33} &= a_{11} * a_{22} \\
&= -r * \left(\frac{c\hat{c}q[dq(\hat{a} + T) - \hat{c}T]}{\theta(aq(dq - \hat{c}) + dq(\hat{a} + T) - \hat{c}T)} - \hat{d} \right).
\end{aligned}$$

We observe that this matrix has the following eigenvalues (see App. B):

$$\begin{aligned}
\lambda_1 &= \frac{c\hat{c}q[dq(\hat{a} + T) - \hat{c}T]}{\theta(aq(dq - \hat{c}) + dq(\hat{a} + T) - \hat{c}T)} - \hat{d}, \\
\lambda_2 &= -\frac{1}{2} \sqrt{\left(-r + \frac{d^2q^2(\hat{a} + T) + \hat{c}T(\hat{c} - 2dq)}{\hat{a}\hat{c}q} \right)^2 + 4dr} \\
&\quad + \frac{1}{2} \left(-r - \frac{d^2q^2(\hat{a} + T) + \hat{c}T(\hat{c} - 2dq)}{\hat{a}\hat{c}q} \right),
\end{aligned}$$

$$\lambda_3 = \frac{1}{2} \sqrt{\left(-r + \frac{d^2 q^2 (\hat{a} + T) + \hat{c} T (\hat{c} - 2dq)}{\hat{a} \hat{c} q}\right)^2 + 4dr} + \frac{1}{2} \left(-r - \frac{d^2 q^2 (\hat{a} + T) + \hat{c} T (\hat{c} - 2dq)}{\hat{a} \hat{c} q}\right).$$

The WKL model with Holling type II functional responses has 12 parameters: $r, K, c, \hat{c}, a, \hat{a}, \hat{e}, \hat{d}, d, \theta, q,$ and T (see Table 2.1). The parameter that is not in these eigenvalues is K . Therefore, stability of this equilibrium does not depend on K .

Case 2: $\bar{p} < Kq$ and $\bar{p} > \theta\bar{x}$: $E_1 = (\bar{p}/q, 0, \bar{p})$.

Boundary equilibrium:

$$\left(\frac{dq(\hat{a} + T) - \hat{c}T}{q(dq - \hat{c})}, 0, \frac{dq(\hat{a} + T) - \hat{c}T}{dq - \hat{c}}\right).$$

Jacobian:

$$A_2 = \begin{bmatrix} -r & -\frac{c\bar{p}}{aq + \bar{p}} & \frac{r}{q} \\ 0 & \frac{c\hat{e}\bar{p}}{aq + \bar{p}} - \hat{d} & 0 \\ \frac{\hat{c}(T - \bar{p})}{\hat{a} + T - \bar{p}} & -\frac{\hat{a}\hat{c}\theta\bar{p}}{q(\hat{a} + T - \bar{p})^2} - \frac{c\bar{p}q}{aq + \bar{p}} & -\frac{\hat{a}\hat{c}\bar{p}}{q(\hat{a} + T - \bar{p})^2} - d \end{bmatrix}.$$

Let the entries of matrix A_2 be labelled with a_{ij} , for the entry in row i , column j of matrix A_2 . Then we have

$$a_{11} = -r,$$

$$a_{12} = -\frac{c[dq(\hat{a} + T) - \hat{c}T]}{q[a(dq - \hat{c}) + d(\hat{a} + T)] - \hat{c}T},$$

$$a_{13} = \frac{r}{q},$$

$$a_{21} = 0,$$

$$a_{22} = \frac{c\hat{e}[dq(\hat{a} + T) - \hat{c}T]}{aq(dq - \hat{c}) + dq(\hat{a} + T) - \hat{c}T} - \hat{d},$$

$$a_{23} = 0,$$

$$\begin{aligned}
a_{31} &= dq, \\
a_{32} &= -\frac{\theta(dq(\hat{a} + T) - \hat{c}T)(dq - \hat{c})}{\hat{a}\hat{c}q} - \frac{cq[dq(\hat{a} + T) - \hat{c}T]}{\hat{a}dq + (aq + T)(dq - \hat{c})}, \\
a_{33} &= -\frac{d^2q^2(\hat{a} + T) + \hat{c}T(\hat{c} - 2dq)}{\hat{a}\hat{c}q}.
\end{aligned}$$

Then

$$\begin{aligned}
\text{tr}(A_2) &= a_{11} + a_{22} + a_{33} \\
&= -r + \frac{c\hat{c}[dq(\hat{a} + T) - \hat{c}T]}{aq(dq - \hat{c}) + dq(\hat{a} + T) - \hat{c}T} - \hat{d} - \frac{d^2q^2(\hat{a} + T) + \hat{c}T(\hat{c} - 2dq)}{\hat{a}\hat{c}q}. \\
\det(A_2) &= a_{22}(a_{11} * a_{33} - a_{13} * a_{31}) \\
&= \left(\frac{c\hat{c}[dq(\hat{a} + T) - \hat{c}T]}{aq(dq - \hat{c}) + dq(\hat{a} + T) - \hat{c}T} - \hat{d} \right) \\
&\quad \left(r \left(\frac{d^2q^2(\hat{a} + T) + \hat{c}T(\hat{c} - 2dq)}{\hat{a}\hat{c}q} \right) - dr \right). \\
A_2^{11} &= a_{22} * a_{33} \\
&= \left(\frac{c\hat{c}[dq(\hat{a} + T) - \hat{c}T]}{aq(dq - \hat{c}) + dq(\hat{a} + T) - \hat{c}T} - \hat{d} \right) \left(-\frac{d^2q^2(\hat{a} + T) + \hat{c}T(\hat{c} - 2dq)}{\hat{a}\hat{c}q} \right). \\
A_2^{22} &= a_{11} * a_{33} - a_{13} * a_{31} \\
&= r \left(\frac{d^2q^2(\hat{a} + T) + \hat{c}T(\hat{c} - 2dq)}{\hat{a}\hat{c}q} \right) - dr. \\
A_2^{33} &= a_{11} * a_{22} \\
&= -r * \left(\frac{c\hat{c}[dq(\hat{a} + T) - \hat{c}T]}{aq(dq - \hat{c}) + dq(\hat{a} + T) - \hat{c}T} - \hat{d} \right).
\end{aligned}$$

We observe A_2 has the following eigenvalues (see App. B):

$$\begin{aligned}
\lambda_1 &= \frac{c\hat{c}[dq(\hat{a} + T) - \hat{c}T]}{aq(dq - \hat{c}) + dq(\hat{a} + T) - \hat{c}T} - \hat{d}, \\
\lambda_2 &= -\frac{1}{2} \sqrt{\left(-r + \frac{d^2q^2(\hat{a} + T) + \hat{c}T(\hat{c} - 2dq)}{\hat{a}\hat{c}q} \right)^2 + 4dr} \\
&\quad + \frac{1}{2} \left(-r - \frac{d^2q^2(\hat{a} + T) + \hat{c}T(\hat{c} - 2dq)}{\hat{a}\hat{c}q} \right),
\end{aligned}$$

$$\lambda_3 = \frac{1}{2} \sqrt{\left(-r + \frac{d^2 q^2 (\hat{a} + T) + \hat{c} T (\hat{c} - 2dq)}{\hat{a} \hat{c} q}\right)^2 + 4dr} + \frac{1}{2} \left(-r - \frac{d^2 q^2 (\hat{a} + T) + \hat{c} T (\hat{c} - 2dq)}{\hat{a} \hat{c} q}\right).$$

The WKL model with Holling type II functional responses has 12 parameters: r , K , c , \hat{c} , a , \hat{a} , \hat{e} , \hat{d} , d , θ , q , and T (see Table 2.1). The parameters that are not in these eigenvalues are K and θ . Therefore, stability of this equilibrium does not depend on these two parameters.

Additional stability analysis for Chapter 3

Holling type I

Case 1: $\bar{p}/q \leq \min\{K, \gamma(T_C - \bar{x} - \bar{y})\}$ and $\bar{p} < \theta \bar{x}$.

Boundary equilibrium: $(\bar{x}, \bar{y}, \bar{p})$, where

$$\begin{aligned}\bar{x} &= \frac{\hat{c} T_P (r - l_x) - dqr}{\hat{c} qr}, \\ \bar{y} &= 0, \\ \bar{p} &= \frac{\hat{c} T_P (r - l_x) - dqr}{\hat{c} (r - l_x)}.\end{aligned}$$

Jacobian:

$$A_1 = \begin{bmatrix} a_{11} & a_{12} & a_{13} \\ a_{21} & a_{22} & a_{23} \\ a_{31} & a_{32} & a_{33} \end{bmatrix},$$

where

$$\begin{aligned}a_{11} &= l_x - r, \\ a_{12} &= -\frac{c \hat{c} T_P (r - l_x) + cdqr}{\hat{c} qr}, \\ a_{13} &= \frac{(r - l_x)^2}{qr}, \\ a_{21} &= 0, \\ a_{22} &= \frac{c \hat{c} \hat{e} T_P (r - l_x) - cd \hat{e} qr}{\hat{c} \theta (r - l_x)} - \hat{d} - l_y, \\ a_{23} &= 0,\end{aligned}$$

$$\begin{aligned}
a_{31} &= \frac{dqr}{r - l_x}, \\
a_{32} &= -\frac{\hat{c}T_P\theta(r - l_x) - dqr\theta}{qr} - \frac{c\hat{c}T_P(r - l_x) - cdqr}{\hat{c}(r - l_x)}, \\
a_{33} &= -\frac{\hat{c}T_P(r - l_x)}{qr}.
\end{aligned}$$

We see

$$\begin{aligned}
\text{tr}(A_1) &= l_x - r + \frac{c\hat{c}\hat{e}T_P(r - l_x) - cd\hat{e}qr}{\hat{c}\theta(r - l_x)} - \hat{d} - l_y - \frac{\hat{c}T_P(r - l_x)}{qr}, \\
\det(A_1) &= \left(\frac{c\hat{c}\hat{e}T_P(r - l_x) - cd\hat{e}qr}{\hat{c}\theta(r - l_x)} - \hat{d} - l_y \right) \left(\left(\frac{\hat{c}T_P(r - l_x)^2}{qr} \right) - d(r - l_x) \right).
\end{aligned}$$

The eigenvalues are λ such that (see Appendix B for proof)

$$\begin{aligned}
0 &= \left(\frac{c\hat{c}\hat{e}T_P(r - l_x) - cd\hat{e}qr}{\hat{c}\theta(r - l_x)} - \hat{d} - l_y - \lambda \right) \\
&\quad \left((l_x - r - \lambda) \left(-\frac{\hat{c}T_P(r - l_x)}{qr} - \lambda \right) - d(r - l_x) \right).
\end{aligned}$$

Therefore, the three eigenvalues for A_1 are

$$\begin{aligned}
\lambda_1 &= \frac{c\hat{c}\hat{e}T_P(r - l_x) - cd\hat{e}qr}{\hat{c}\theta(r - l_x)} - \hat{d} - l_y, \\
\lambda_2 &= -\frac{1}{2} \sqrt{\left(l_x - r + \frac{\hat{c}T_P(r - l_x)}{qr} \right)^2 + 4d(r - l_x)} + \frac{1}{2} \left(l_x - r - \frac{\hat{c}T_P(r - l_x)}{qr} \right), \\
\lambda_3 &= \frac{1}{2} \sqrt{\left(l_x - r + \frac{\hat{c}T_P(r - l_x)}{qr} \right)^2 + 4d(r - l_x)} - \frac{1}{2} \left(l_x - r - \frac{\hat{c}T_P(r - l_x)}{qr} \right).
\end{aligned}$$

The local closed model with Holling type I functional responses has 14 parameters: r , K , c , \hat{c} , \hat{e} , d , θ , q , T_P , T_C , \hat{d} , l_x , l_y and γ . From the above equations for λ_1 , λ_2 and λ_3 , we see that the eigenvalues do not depend upon K , T_C , or γ . Therefore, stability of this equilibrium does not depend on these three parameters.

Case 2: $\bar{p}/q \leq \min\{K, \gamma(T_C - \bar{x} - \bar{y})\}$ and $\bar{p} > \theta\bar{x}$.

Boundary equilibrium: $(\bar{x}, \bar{y}, \bar{p})$, where

$$\begin{aligned}\bar{x} &= \frac{\hat{c}T_P(r - l_x) - dqr}{\hat{c}qr}, \\ \bar{y} &= 0, \\ \bar{p} &= \frac{\hat{c}T_P(r - l_x) - dqr}{\hat{c}(r - l_x)}.\end{aligned}$$

Jacobian:

$$A_2 = \begin{bmatrix} a_{11} & a_{12} & a_{13} \\ a_{21} & a_{22} & a_{23} \\ a_{31} & a_{32} & a_{33} \end{bmatrix},$$

where the entries are the same as in Case 1 (above), except

$$a_{22} = \frac{c\hat{c}\hat{e}T_P(r - l_x) - cd\hat{e}qr}{\hat{c}qr} - \hat{d} - l_y.$$

We know that the middle entry is an eigenvalue. Also,

$$\begin{aligned}\text{tr}(A_2) &= l_x - r + \frac{c\hat{c}\hat{e}T_P(r - l_x) - cd\hat{e}qr}{\hat{c}qr} - \hat{d} - l_y - \frac{\hat{c}T_P(r - l_x)}{qr}, \\ \det(A_2) &= \left(\frac{c\hat{c}\hat{e}T_P(r - l_x) - cd\hat{e}qr}{\hat{c}qr} - \hat{d} - l_y \right) \left(\left(\frac{\hat{c}T_P(r - l_x)^2}{qr} \right) - d(r - l_x) \right).\end{aligned}$$

We can solve for the eigenvalues, as in the Case 1 (see Appendix B):

$$\begin{aligned}\lambda_1 &= \frac{c\hat{c}\hat{e}T_P(r - l_x) - cd\hat{e}qr}{\hat{c}qr} - \hat{d} - l_y, \\ \lambda_2 &= -\frac{1}{2} \sqrt{\left(l_x - r + \frac{\hat{c}T_P(r - l_x)}{qr} \right)^2 + 4d(r - l_x)} + \frac{1}{2} \left(l_x - r - \frac{\hat{c}T_P(r - l_x)}{qr} \right), \\ \lambda_3 &= \frac{1}{2} \sqrt{\left(l_x - r + \frac{\hat{c}T_P(r - l_x)}{qr} \right)^2 + 4d(r - l_x)} - \frac{1}{2} \left(l_x - r - \frac{\hat{c}T_P(r - l_x)}{qr} \right).\end{aligned}$$

The local closed model with Holling type I functional responses has 14 parameters: $r, K, c, \hat{c}, \hat{e}, d, \theta, q, T_P, T_C, \hat{d}, l_x, l_y$ and γ . We see that stability does not depend on K, T_C, γ , or θ , since these parameters are not in the equations for the eigenvalues.

Holling type II

Case 1: $\bar{p}/q \leq \min\{K, \gamma(T_C - \bar{x} - \bar{y})\}$ and $\bar{p} < \theta\bar{x}$.

Boundary equilibrium: $(\bar{x}, \bar{y}, \bar{p})$, where

$$\begin{aligned}\bar{x} &= \frac{\bar{p}}{q} \left[1 - \frac{l_x}{r} \right] = \frac{dq r (\hat{a} + T_P)(r - l_x) - \hat{c} T_P (r - l_x)^2}{dq^2 r^2 - \hat{c} q r (r - l_x)}, \\ \bar{y} &= 0, \\ \bar{p} &= \frac{dq(\hat{a} + T_P) - \hat{c} T_P \left(1 - \frac{l_x}{r}\right)}{dq - \hat{c} \left(1 - \frac{l_x}{r}\right)} = \frac{dq r (\hat{a} + T_P) - \hat{c} T_P (r - l_x)}{dq r - \hat{c} (r - l_x)}.\end{aligned}$$

Jacobian:

$$B_1 = \begin{bmatrix} l_x - r & -\frac{c\bar{p}(r - l_x)}{aqr + \bar{p}(r - l_x)} & \frac{(r - l_x)^2}{qr} \\ 0 & \frac{c\hat{e}q r \bar{p}}{\theta(aqr + \bar{p}(r - l_x))} - \hat{d} - l_y & 0 \\ \frac{dq r}{r - l_x} & -\frac{\hat{a}\hat{c}\bar{p}(r - l_x)}{qr(\hat{a} + T_P - \bar{p})^2} - \frac{cqr\bar{p}}{aqr + \bar{p}(r - l_x)} & -\frac{\hat{a}\hat{c}\bar{p}(r - l_x)}{qr(\hat{a} + T_P - \bar{p})^2} - d \end{bmatrix}.$$

The eigenvalues are (see Appendix B for proof)

$$\begin{aligned}\lambda_1 &= \frac{c\hat{e}q r \bar{p}}{\theta(aqr + \bar{p}(r - l_x))} - \hat{d} - l_y, \\ \lambda_2 &= -\frac{1}{2} \sqrt{\left(l_x - r + \frac{\hat{a}\hat{c}\bar{p}(r - l_x)}{qr(\hat{a} + T_P - \bar{p})^2} + d \right)^2 + 4d(r - l_x)} \\ &\quad + \frac{1}{2} \left(l_x - r - \frac{\hat{a}\hat{c}\bar{p}(r - l_x)}{qr(\hat{a} + T_P - \bar{p})^2} - d \right), \\ \lambda_3 &= \frac{1}{2} \sqrt{\left(l_x - r + \frac{\hat{a}\hat{c}\bar{p}(r - l_x)}{qr(\hat{a} + T_P - \bar{p})^2} + d \right)^2 + 4d(r - l_x)} \\ &\quad + \frac{1}{2} \left(l_x - r - \frac{\hat{a}\hat{c}\bar{p}(r - l_x)}{qr(\hat{a} + T_P - \bar{p})^2} - d \right),\end{aligned}$$

where $\hat{a} + T_P - \bar{p} = -\frac{\hat{a}\hat{c}(r - l_x)}{dq r - \hat{c}(r - l_x)}$.

Note that these eigenvalues do not have \bar{p} substituted in. The local closed model with Holling type II functional responses has 16 parameters: $r, K, c, \hat{c}, a, \hat{a}, \hat{e}, d, \theta, q, T_P, T_C, \hat{d}, l_x, l_y$ and γ . Similar to Case 1 for the Holling type I functional responses, the eigenvalues do not depend on K, T_C or γ .

Case 2: $\bar{p}/q \leq \min\{K, \gamma(T_C - \bar{x} - \bar{y})\}$ and $\bar{p} > \theta\bar{x}$.

Boundary equilibrium: $(\bar{x}, \bar{y}, \bar{p})$, where

$$\begin{aligned}\bar{x} &= \frac{\bar{p}}{q} \left[1 - \frac{l_x}{r} \right] = \frac{dqr(\hat{a} + T_P)(r - l_x) - \hat{c}T_P(r - l_x)^2}{dq^2r^2 - \hat{c}qr(r - l_x)}, \\ \bar{y} &= 0, \\ \bar{p} &= \frac{dq(\hat{a} + T_P) - \hat{c}T_P \left(1 - \frac{l_x}{r}\right)}{dq - \hat{c} \left(1 - \frac{l_x}{r}\right)} = \frac{dqr(\hat{a} + T_P) - \hat{c}T_P(r - l_x)}{dqr - \hat{c}(r - l_x)}.\end{aligned}$$

Jacobian:

$$B_2 = \begin{bmatrix} l_x - r & -\frac{c\bar{p}(r - l_x)}{arq + \bar{p}(r - l_x)} & \frac{(r - l_x)^2}{qr} \\ 0 & \frac{c\hat{e}\bar{p}(r - l_x)}{aqr + \bar{p}(r - l_x)} - \hat{d} - l_y & 0 \\ \frac{dqr}{r - l_x} & -\frac{\hat{a}\hat{c}\theta\bar{p}(r - l_x)}{qr(\hat{a} + T_P - \bar{p})^2} - \frac{cqr\bar{p}}{aqr + \bar{p}(r - l_x)} & -\frac{\hat{a}\hat{c}\bar{p}(r - l_x)}{qr(\hat{a} + T_P - \bar{p})^2} - d \end{bmatrix}.$$

The eigenvalues are (see Appendix B for proof)

$$\begin{aligned}\lambda_1 &= \frac{c\hat{e}\bar{p}(r - l_x)}{aqr + \bar{p}(r - l_x)} - \hat{d} - l_y, \\ \lambda_2 &= -\frac{1}{2} \sqrt{\left(l_x - r + \frac{\hat{a}\hat{c}\bar{p}(r - l_x)}{qr(\hat{a} + T_P - \bar{p})^2} + d \right)^2 + 4d(r - l_x)} \\ &\quad + \frac{1}{2} \left(l_x - r - \frac{\hat{a}\hat{c}\bar{p}(r - l_x)}{qr(\hat{a} + T_P - \bar{p})^2} - d \right), \\ \lambda_3 &= \frac{1}{2} \sqrt{\left(l_x - r + \frac{\hat{a}\hat{c}\bar{p}(r - l_x)}{qr(\hat{a} + T_P - \bar{p})^2} + d \right)^2 + 4d(r - l_x)} \\ &\quad + \frac{1}{2} \left(l_x - r - \frac{\hat{a}\hat{c}\bar{p}(r - l_x)}{qr(\hat{a} + T_P - \bar{p})^2} - d \right).\end{aligned}$$

The local closed model with Holling type II functional responses has 16 parameters: $r, K, c, \hat{c}, a, \hat{a}, \hat{e}, d, \theta, q, T_P, T_C, \hat{d}, l_x, l_y$ and γ . Similar to Case 2 for the Holling type I functional responses, the eigenvalues do not depend on K, T_C, γ , or θ .

Appendix B

Claim: For a matrix of the form

$$A = \begin{bmatrix} a & b & c \\ 0 & d & 0 \\ f & g & h \end{bmatrix}$$

where all entries are real numbers, the eigenvalues are

$$\begin{aligned} \lambda_1 &= d, \\ \lambda_2 &= \frac{1}{2} \left(-\sqrt{(a-h)^2 + 4cf} + a + h \right), \\ \lambda_3 &= \frac{1}{2} \left(\sqrt{(a-h)^2 + 4cf} + a + h \right). \end{aligned}$$

Proof: We know an eigenvalue λ of matrix A satisfies $\det(A - \lambda I) = 0$. Hence, we solve this equation for λ .

We see that

$$\det(A - \lambda I) = \det \left(\begin{bmatrix} a - \lambda & b & c \\ 0 & d - \lambda & 0 \\ f & g & h - \lambda \end{bmatrix} \right).$$

Using a cofactor expansion along the second row, we see

$$\begin{aligned} \det(A - \lambda I) &= (d - \lambda) \det \left(\begin{bmatrix} a - \lambda & c \\ f & h - \lambda \end{bmatrix} \right) \\ &= (d - \lambda) ((a - \lambda)(h - \lambda) - cf) \\ &= (d - \lambda) (ah - (a + h)\lambda + \lambda^2 - cf) \\ &= (d - \lambda) (\lambda^2 - (a + h)\lambda + (ah - cf)). \end{aligned}$$

We can find solutions to the following using the quadratic formula:

$$(d - \lambda)(\lambda^2 - (a + h)\lambda + (ah - cf)) = 0.$$

The resulting solutions are

$$\begin{aligned}\lambda_1 &= d, \\ \lambda_2 &= \frac{1}{2}(\sqrt{(a+h)^2 - 4(ah - cf)} + a + h), \\ \lambda_3 &= \frac{1}{2}(-\sqrt{(a+h)^2 - 4(ah - cf)} + a + h).\end{aligned}$$

Clearly

$$(a+h)^2 - 4(ah - cf) = a^2 + 2ah + h^2 - 4ah + 4cf = a^2 - 2ah + h^2 + 4cf = (a-h)^2 + 4cf,$$

and this proves the claim.